AD-773 026

ANALYTICAL INVESTIGATION OF THE AERO-
DYNAMIC STABILITY OF HELICAL VORTICES
SHED FROM A HOVERiNG ROTOR

Bharat P. Gupta, et al

Rochester University

AD 773026

DOCUMENT CONTROL DATA - R & D

(Security classification of title, body of abstract and indexing annotation must be entered when the overall report is classified)

1. ORIGINATING ACTIVITY *(Corporate author)*	2a. REPORT SECURITY CLASSIFICATION
University of Rochester, Rochester, New York	Unclassified
	2b. GROUP

3. REPORT TITLE

ANALYTICAL INVESTIGATION OF THE AERODYNAMIC STABILITY OF HELICAL VORTICES SHED FROM A HOVERING ROTOR

4. DESCRIPTIVE NOTES *(Type of report and inclusive dates)*

Final Report

5. AUTHOR(S) *(First name, middle initial, last name)*

Bharat P. Gupta
Robert G. Loewy

6. REPORT DATE	7a. TOTAL NO. OF PAGES	7b. NO. OF REFS
October 1973	146 /5 (	30

8a. CONTRACT OR GRANT NO	9a. ORIGINATOR'S REPORT NUMBER(S)
DAAJ02-72-C-0042	
b. PROJECT NO	USAAMRDL Technical Report 73-84
Task 1F162204AA4201	
c.	9b. OTHER REPORT NO(S) *(Any other numbers that may be assigned this report)*
d.	

10. DISTRIBUTION STATEMENT

Approved for public release; distribution unlimited.

11. SUPPLEMENTARY NOTES	12. SPONSORING MILITARY ACTIVITY
	Eustis Directorate U.S. Army Air Mobility R&D Laboratory Fort Eustis, Virginia

13. ABSTRACT

A small-perturbation stability analysis of a doubly infinite array of interdigitated, right circular helical vortices has been formulated. This array corresponds to the vortices trailed from the tips of the blades of a helicopter rotor or propeller in static thrust or axial flight condition and at great distance from the plane of rotation of the blades. The analysis makes use of the Biot-Savart law of induction and the Vorticity Transport Theorem. The singularities in the Biot-Savart integration for self-induction have been eliminated by substituting appropriate approximate functions. Near-singular behavior in other integrals has been minimized by adding and subtracting functions with similar near-singular behavior and which have exact, closed-form integrals. The calculations of induced perturbation velocities and those required for the stability analysis have been programmed for digital computer.

Numerical results have been obtained for two-, three-, four-, five-, six-helix arrays representing the vortices trailing from the same number of blades. The special case of a single helix has been run and the results compared with those presently available from studies by Levy and Forsdyke and by Widnall. A continuum of instability modes has been found associated with all values of wave numbers; only modes with wave number 0 and 1 are so much as neutrally stable, and only for the case of a single helix. The most unstable modes involve the most axial motion of adjacent vortex segments relative to each other. By "adjacent segments" is meant vortex segments above and below each other (i.e., at the same azimuthal location on adjacent coils of the same or neighboring helices). Furthermore, the larger the percentage of the helical arc length involved in such motion, the more rapidly the distortion will diverge. Maximum divergence rates in the unstable modes increase as the helix pitch decreases, increase as the number of helices increase, and decrease as the number of cycles of deformations in one turn of the helix (i.e., wave number) increases. The larger the helix filament core diameter, the more sensitive the analysis is to the means by which the singularities in the self-induction integrals are eliminated. Increasing core diameters, however, reduces the maximum divergence rates.

DD ,FORM,.1473 REPLACES DD FORM 1473, 1 JAN 64 WHICH IS OBSOLETE FOR ARMY USE.

14. KEY WORDS	LINK A		LINK B		LINK C	
	ROLE	WT	ROLE	WT	ROLE	WT
Helicopter Rotors						
Helicopter Rotor Wake						
Wake Geometry						
Far Wake Stability						
Aerodynamic Stability						
Interdigitated Helical Vortices						

DISCLAIMERS

This report has been reviewed by the Eustis Directorate, U. S. Army Air Mobility Research and Development Laboratory and is considered to be technically sound. The purpose of this program was to analytically investigate the aerodynamic stability of helical vortex arrays as shed from a hovering rotor of two, three, four, five, and six blades.

The program was conducted under the technical management of Donald J. Merkley of the Technology Applications Division of this Directorate.

ANALYTICAL INVESTIGATION OF THE AERODYNAMIC STABILITY OF HELICAL VORTICES SHED FROM A HOVERING ROTOR

By

B. Gupta
R. Loewy

Prepared by

University of Rochester
Rochester, New York

for

ABSTRACT

A small-perturbation stability analysis of a doubly infinite array of interdigitated, right circular helical vortices has been formulated. This array corresponds to the vortices trailed from the tips of the blades of a helicopter rotor or propeller in static thrust or axial flight condition and at great distance from the plane of rotation of the blades. The analysis makes use of the Biot-Savart law of induction and the Vorticity Transport Theorem. The singularities in the Biot-Savart integration for self-induction have been eliminated by substituting appropriate approximate functions. Near-singular behavior in other integrals has been minimized by adding and subtracting functions with similar near-singular behavior and which have exact, closed-form integrals. The calculations of induced perturbation velocities and those required for the stability analysis have been programmed for digital computer.

Numerical results have been obtained for two-, three-, four-, five-, six-helix arrays representing the vortices trailing from the same number of blades. The special case of a single helix has been run and the results compared with those presently available from studies by Levy and Forsdyke and by Widnall. A continuum of instability modes has been found associated with all values of wave numbers; only modes with wave number 0 and 1 are so much as neutrally stable, and only for the case of a single helix. The most unstable modes involve the most axial motion of adjacent vortex segments relative to each other. By "adjacent segments" is meant vortex segments above and below each other (i.e., at the same azimuthal location) on adjacent coils of the same or neighboring helices. Furthermore, the larger the percentage of the helical arc length involved in such motion, the more rapidly the distortion will diverge. Maximum divergence rates in the unstable modes increase as the helix pitch decreases, increase as the number of helices increase, and decrease as the number of cycles of deformations in one turn of the helix (i.e., wave number) increases. The larger the helix filament core diameter, the more sensitive the analysis is to the means by which the singularities in the self-induction integrals are eliminated. Increasing core diameters, however, reduces the maximum divergence rates.

TABLE OF CONTENTS

LIST OF ILLUSTRATIONS

LIST OF TABLES

LIST OF SYMBOLS

a	constant defined as $\sqrt{\frac{\varepsilon^2}{(1+k^2)}}$
a_o	lower limit in Gaussian Quadrature Formula
$A_k^{(n)}$	coefficients in the series expansion of the integral in the Gaussian Quadrature Formula
$\underline{A}_{mm}$	3x3 matrix of complex elements representing self-induction for the mth vortex
$\underline{A}_{mn}$	3x3 matrix of complex elements representing mutual-inductance of mth vortex on nth vortex
b	distance between two trailing vortices from the aircraft
b_o	upper limit in the Gaussian Quadrature Formula
d	axial distance between two parallel elements which are closest to each other on two neighboring coils at the same circumferential position, nondimensionalized by r
d_c	cutoff arc length used in Crow's work
dx_m, dy_m, dz_m	differentials in x, y, z Cartesian coordinate directions along mth vortex
$\vec{dL}_m$	elemental length vector on mth vortex, feet
$\vec{dL}_m(\vec{r}_m + \delta\vec{r}_m)$	elemental length vector at the point $\vec{r}_m + \delta\vec{r}_m$ on mth vortex due to the modified system of vortex helices, feet
D/L	disc loading, lb/ft^2
$\vec{e}_x, \vec{e}_y, \vec{e}_z$	unit vectors in Cartesian coordinate system
$\vec{e}_r, \vec{e}_\phi, \vec{e}_z$	unit vectors in cylindrical polar coordinate system
i	index describing ith eigenvector
I	perturbation integrand
I_1 to I_8	analytically defined integrals for removal of numerical singularities from self-induction integrals

J_{mp} square of the scalar distance between points on m^{th} and p^{th} vortex, modified to $|\vec{R}_{mp}|^2 + \epsilon_o^2$ for self-induction

k pitch of the helix; axial displacement in one turn of helix is $2\pi k r$, dimensionless

k_s wave number for S. C. Crow's case of the stability of aircraft trailing vortices

K parameter used in computer program to identify the set of calculations corresponding to possible combinations of p and m as in the table on page 36

K_{mp} first order quantity defined as
$(x_m - x_p)(\delta x_m - \delta x_p) + (y_m - y_p)(\delta y_m - \delta y_p) + (z_m - z_p)(\delta z_m - \delta z_p)$

$L1$ parameter in the main computer program used for preselecting the two separate sets of integration subroutines

$LL1$ parameter in the main computer program which stops modifying the singular integrals beyond an upper limit of $xU = 2\pi$

m index describing m^{th} vortex

M parameter in the main computer program used for selecting the overall integration limits on perturbation integrals

n number of blades in the rotor

p index describing p^{th} vortex

q_{kp} set of scalars which could be used for transformation from x_k to y_p

$\underline{Q}$ unitary matrix in decomposition of $\underline{A}$ into the product $\underline{Q}\underline{U}$

r radius of circular helix, feet

$\vec{r}_m$ position vector of point (x_m , y_m , z_m), nondimensionalized by r

$\dot{r}_p , (r\dot{\phi}_p), \dot{z}_p$ steady induced velocities at a point on p^{th} helix in (r , ϕ , z) cylindrical polar directions; where $\dot{r}_p = \frac{d}{dt}(r_p)$, etc.

r_m, ϕ_m, z_m	cylindrical polar coordinate description of points on m^{th} vortex as functions of parameter θ_m and constants ψ_m and k
$\vec{R}_{mp}$	relative position vector of point on p^{th} vortex relative to point on m^{th} vortex, feet
t	time variable, seconds
$t_k^{(n)}$	nodes, roots of Legendre polynomials of degree n
T	period for one complete rotor revolution, seconds
$\vec{U}_p$	induced velocity on p^{th} vortex, ft/sec
$\vec{U}_p(\vec{r}_p + \delta\vec{r}_p)$	velocity at the point $\vec{r}_p + \delta\vec{r}_p$ on p^{th} vortex due to the modified system of vortex helices, ft/sec
$\underline{U}$	upper triangular matrix in decomposition of $\underline{A}$ into the product $\underline{Q}\,\underline{U}$
U_{xp}, U_{yp}, U_{zp}	x, y and z components of zeroth order induced velocities respectively, ft/sec
v_i	induced velocity or increase in velocity at the actuator disc, ft/sec
V_c	climb velocity in vertical flight, ft/sec
V_*	downward axial velocity in the fully developed slipstream, ft/sec
$\underline{x}$	eigenvector of the system of interdigitated vortex helices, nondimensionalized by r
x_*	axial coordinate in case of aircraft trailing vortices
$\underline{x}_k$	perturbation vector for k^{th} vortex; $\underline{x}_k = \underline{x}_k$
$\underline{x}_m$	eigenvector for m^{th} vortex having $\delta\hat{r}_m$, $r\delta\hat{\phi}_m$ and $\delta\hat{z}_m$ as its components
$\mathbf{x}_{mp}$	nondimensional quantity defined as the difference $(\theta_m - \theta_p)$ for all m and p
$\mathbf{x}$	special case of $\mathbf{x}_{mp}$ where m = p; ie $(\theta_p' - \theta_p)$. See Figures 4, 5 and 6.

x_m, y_m, z_m	Cartesian coordinate description of points on m^{th} vortex as functions of parameter θ_m and constants ψ_m and k
x_U	upper limit on analytically defined integrals for removal of numerical singularities from self-induction integrals
y_j	j^{th} left eigenvector
$\underset{\sim}{y}_P$	new perturbation vector as a result of an attempt toward simplifying the eigenmatrix equation
y_{mp}	defined as the difference ($x_{mp} - \psi_{mp}$)
z	constant defined as $\sinh^{-1}(\frac{x_U}{a})$
α	exponential growth rate factor, complex, sec^{-1}
β_s	nondimensional wave number
$\delta\theta_m$	first-order perturbation of the helical coordinate θ_m along the mth vortex
$\vec{\delta r_m}$	displacement perturbation vector of the point (x_m, y_m, z_m)
$\delta x_m, \delta y_m, \delta z_m$	first-order displacement perturbations of the point (x_m, y_m, z_m) in Cartesian coordinate directions
$\delta r_m, \delta\phi_m, \delta z_m$	first-order displacement perturbations of the point on m^{th} vortex in cylindrical polar coordinate directions
$\delta\dot{r}_m, \delta\dot{\phi}_m, \delta\dot{z}_m$	total time derivatives of quantities δr_m, $\delta\phi_m$, δz_m respectively
$\delta\hat{r}_m, \delta\hat{\phi}_m, \delta\hat{z}_m$	amplitude of displacement perturbations in r, ϕ and z directions respectively
$\delta\hat{r}_{i\lambda}, \delta\hat{\phi}_{i\lambda}, \delta\hat{z}_{i\lambda}$	i^{th} eigenvector components in r, ϕ and z directions corresponding to an eigenvalue λ
$\delta U_{xP}, \delta U_{yP}, \delta U_{zP}$	x, y and z components of first-order induced velocities respectively

ϵ	perturbation in d in radial or axial directions, nondimensionalized by r
ϵ_o	radius of finite core vortex, feet
ϵ	nondimensionalized 'core size' defined as ϵ_o/r
Γ_m	circulation strength of mth vortex
θ	helical coordinate parameter used for describing a circular helix, dimensionless
Θ_m	helical coordinate describing the circumferential position of mth vortex
λ	set of complex eigenvalues for the perturbations of the system of interdigitated helices
ρ	mass density of air, slugs/ft^3
$\Phi(\tau)$	function to be integrated as a function of the variable τ
Φ	phase difference between eigenvectors $\underline{x}_1$ and $\underline{x}_2$ for system of two interdigitated helices
Ψ_m	phase difference angle for m^{th} vortex
Ψ_{mp}	nondimensional quantity defined as the difference ($\Psi_m - \Psi_p$) for all m and p
τ	normalized variable of integration used on page 32
ω	wave number of the perturbations, assigned real, dimensionless
$\dot{\xi}_p, \dot{\eta}_p, \dot{\zeta}_p$	induced velocity component at a point on p^{th} vortex in r, ϕ and z directions respectively due to perturbed system of vortex helices, ft/sec
$(\ )'$	prime on a variable corresponds to the position of the general point involved in the space integration as contrasted to the specific point at which induced velocity is being evaluated in self-induction integration
$(\ )_o$	zero-order quantities
$(\ )_1$	first-order quantities

CHAPTER 1

INTRODUCTION

1.1   IMPORTANCE OF AN ACCURATE KNOWLEDGE OF WAKE GEOMETRY

The geometry of the wake beneath a helicopter rotor is impor-
tant to the accurate prediction of the airloads acting on the
blades. Determination of such airloads is prerequisite to
nearly every area of rotary-wing design including performance,
vibrations, acoustics and structural integrity. An accurate
knowledge of the wake-induced velocity field is also impor-
tant for determining (1) interference effects between rotors,
(2) positioning and effectiveness of auxiliary surfaces,
(3) interference with the fuselage and other non-lifting
bodies, etc.

The impact of wake geometry is felt directly in attempts to
predict wake-induced velocity fields. Inability to do so with
acceptable accuracy has limited the state of the art of heli-
copter rotor designs for perhaps a decade. This is a problem
on which considerable emphasis has been and is still being
placed. Some of the reasons for this emphasis include the
following: (1) The desirability of attaining peak lift system
performance is greater with helicopters than with conventional
aircraft because of generally less favorable payload and power
to gross weight ratios. (2) The distinctive acoustic signature
of a lifting rotor can be troublesome, and this imposes re-
quirements on the induced velocity field that have no counter-
parts in fixed-wing aircraft design. (3) Not only is the
geometry of the rotor's vortex system considerably more compli-
cated than that of a fixed-wing aircraft, but it is of greater
influence, since rotation causes the wake vorticity to remain
longer in the vicinity of the blades. (4) Unsteady effects
must almost always be considered since velocity at the blade
element varies with time even when the helicopter is in steady
flight. (5) Aeroelastic effects are always a factor since
rotor blades are relatively more flexible than conventional
fixed wings.

1.2   CLASSICAL METHODS OF COMPUTING WAKE-INDUCED FIELDS

The simplest hovering theory is the so-called actuator disc
analysis, where the induced velocities are calculated in terms
of momentum and energy changes as the flow crosses an "actuator

disc". See, for example, Glauert [Reference 1], Shapiro [Reference 2] and Gessow and Meyers [Reference 3]. Refinements of this approach accounting for nonuniformities around the azimuth have been made by Mangler [Reference 4] and Loewy and Joglekar [Reference 5]. The next step taken in developing an analytical model of the hovering rotor was to consider the individual blade elements. The rotor disc was divided into elemental annuli through each of which the momentum change was equated to the blade element lift for a given blade pitch. This method was first introduced by S. Goldstein [Reference 6]. It has most recently been developed to account for experimental airfoil characteristics and labeled 'nonlinear strip theory" by Jenny, Olson and Landgrebe [Reference 7].

1.3   VORTEX TUBE REPRESENTATION OF HELICAL WAKE AND DISTORTED WAKE GEOMETRIES

Considerable research has been and is being done to develop a rotary-wing equivalent to the classical lifting-line type of inflow analysis employed with success for fixed-wing aircraft. Among advances made in the last decade are methods of wake analysis which deal with the three-dimensional array of vorticity in the wake "shed and trailed"* from the finite number of blades in a lifting rotor. Such analyses [Miller, Reference 8; DuWaldt, Reference 9, etc.] have the following classical bases: (1) Making use of Prandtl's theory of airfoils, the wing is represented by a "lifting line" with a circulating flow around it. This circulating flow in turn gives rise to circulation, Γ, which is related to both the aerodynamic forces and the strength of a vortex called the "bound vortex" which is, essentially, the lifting line. (2) The aerodynamic forces are also related to the induced velocities at the lifting line through the angle of attack, on which dimensional analysis shows lift to be dependent. (3) A fundamental law of the mechanics of perfect fluids (Kelvin's theorem or the Helmholtz theorem) is involved; namely, that a vortex can not end in the middle of a fluid, so the bound vortex continues in the fluid beyond the extent of the blade, as a "free" vortex trailing from the wing tips. (4) Experience has shown that when a sheet of free vortices trails in a distributed manner from some significant spanwise length of a blade's trailing edge, it then rolls up into a pair of vortex tubes of equal strength and opposite directions and is "transported" away from the blade which trailed it by the rotational velocity and the downward

---

* "Shed" vorticity arises from time-wise variations in lift, "trailed" vorticity from spanwise variations. Only the latter kind is considered in this report.

2

axial induced velocity generated by the rotor. (5) The velocity induced at the airfoil by both bound and trailing vorticity is given by the Biot-Savart law of induction.

The classical wake is generally considered in two distinct parts: near wake and far wake. The near wake is defined as a set of circular helices of finite length trailing from the blade tips and near the blade roots, together with the "lifting line" or bound vortex representation of the rotor blades. The length of this set of trailing vortices is usually in terms of some number of rotations below the "lifting lines". The far wake, on the other hand, can be treated as consisting of an array of infinitely long, interdigitated circular helices as generated by the blade tip only.

The wake-induced field of a hovering rotor, therefore, can be inferred from proper consideration of trailing vorticity, i.e., a set of interdigitated circular vortex helices generated by the tip of each blade in the rotor. The question is, "How can this vortex helix representation be used to deal more fundamentally with rotor-induced flows?"

Although most of the recent methods of blade airload analysis represent a considerable improvement in the state of the art, they still do not permit accurate calculation of blade airloads and associated bending moments. The fact that wake geometry is prescribed in advance imposes a fundamental limit to such methods. Optimum rotor design is not likely to be achieved until a distorted wake geometry can be accounted for rather than prescribing a rigid helical geometry. Tarrarine [Reference 10], Landgrebe [Reference 11] and others have shown, using flow visualization techniques, that the actual rotor wake geometry differs significantly from the pure helix. Relatively recent efforts, therefore, have concentrated on the development of analytical methods for predicting the distorted helical geometry of the actual rotor wake. In one approach [Reference 5], the nonuniform velocity fields predicted by momentum theory have been used to calculate the distortion of a canted, but otherwise pure, helix. In others [References 12, 13], the self-induced distortions of a rotor wake represented by numerous discrete vortex elements are computed by application of the classical Biot-Savart law involving both numerical integration and iteration techniques.

1.4   MOTIVATION FOR THE PRESENT WORK AND DESCRIPTION OF THE
       GENERAL APPROACH ADOPTED

The determination and use of a distorted wake geometry, free

from the constraint of conforming with a pure helix, would be
expected to provide a more accurate means for computing the
instantaneous rotor flow field and the associated blade air-
loads. It seems significant to this objective that, in tests
and wake geometry analyses, evidence of apparent instabilities
in the tip vortex patterns was discerned; in experiments, rapid
deviations from the helical geometry were observed [Reference
10], and during numerical integrations, the numbers seemed to
diverge in successive iterations [Reference 11]. In either
case, distorted rotor wakes were obtained. In Reference 11 it
was noted that the portion of the wake in the immediate vicini-
ty of the rotor plane (extremely near wake) did converge in the
calculations, with the degree of convergence improving with in-
creasing proximity to the rotor. This, presumably, is due to
the fact that one end of the wake is tied to a blade whose
position is prescribed. Close examination of the computed re-
sults, however, indicated that the wake did become unstable at
moderate distances from the rotor. It therefore appears that
to gain insight as to the completeness needed for acceptable
theoretical rotor blade analysis methods, stability of the wake
should be studied. Further, it seems prudent to examine the
far wake first, both because of its greater simplicity and be-
cause of its apparently greater tendencies toward instability.

Two-dimensional flow fields behind a circular cylinder were
found by Kármán [Reference 14] to be stable only when vortices
were in the staggered formation, which has come to be known as
the "Kármán Vortex Street". A "Kármán Vortex Street" might be
thought of as the cross section of a right circular helical
vortex on a plane through its axis. Such an analogy suggested
that the interdigitated vortex helix system associated with two
or more blades would, by extension of Karman's analysis, be
more unstable than a single helical vortex. A literature sur-
vey revealed no analyses of the stability of an interdigitated
vortex helix array such as might represent the wake of a multi-
bladed rotor. An early stability analysis of a single helical
vortex, however, was carried out by Levy and Forsdyke [Refer-
ence 15]. This work was prompted by flow visualization experi-
ments in the wind tunnel with a stationary, circular disc with
its polar axis parallel to the flow. At high values of Rey-
nolds numbers, it was found that its wake consisted of a ro-
tating helical vortex filament.

The Levy and Forsdyke analysis, while basically like that of
Kármán, involved numerical techniques which, without modern
computing, led to some erroneous results. Nevertheless, the
approach adopted here for the stability analysis of interdigi-
tated helical vortex systems follows the same general line. A
system of helical vortices is postulated. Perturbation dis-
placements are assumed, and the self-induced and mutual-induced

4

perturbation velocities at the perturbed vortices are calcu-
lated. Subsequently their growth rate is determined using the
vorticity transport theorem. As was found in an independent
study of the stability of a single helical vortex, published
after the initiation of the research reported here [Widnall,
Reference 16], the vortex system is unstable under most situa-
tions. The results of the analysis reported here, however,
show that stability and growth rate of perturbations depend
very strongly on the number of blades in the multi-bladed case.

CHAPTER 2

THEORETICAL ANALYSIS

2.1   BACKGROUND

Where instabilities exist, iterative techniques will not
converge, and direct numerical integrations with respect to
time will be greatly enhanced by a prior knowledge of the
unstable modes and their rates of divergence. As noted in the
preceding chapter, Levy and Forsdyke [Reference 15] considered
a single, doubly infinite, constant-diameter, helical vortex.
They found it to be unstable for disturbance modes with no
distortion for vortex helix pitch angles less than 0.3 radian.
Their analysis, however, suffered from several shortcomings.
The numerical integration was performed using a planimeter,
which is understandable, considering the early date of their
work (1928), but nevertheless the loss in accuracy contributed
to errors in their results, and the approximations used in
evaluating the singular integrals were quite crude.

Widnall [Reference 16] recently investigated the stability of a
single helical vortex filament with a finite core, using the
method of matched asymptotic expansions. The results of that
work, except for certain differences in evaluating the singular
integrals encountered in the analysis, were obtained as a
special case in the present investigation. In another relative-
ly recent study, S. C. Crow [Reference 17] dealt with the
stability of a pair of linear, parallel infinite vortices of
constant strength, as trailed from the tips of the wings of
fixed-wing aircraft. In theory, such a pair of trailing
vortices could be given as a special case of the family of
interdigitated, helical vortices considered here; specifically,
a set of two interdigitated helical vortices as trailed from
the tips of a two-bladed rotor, but with infinite pitch. In
practice, the approximations used in performing the numerical
integrations over space precluded such a quantitative comparison.
However, Crow's study did provide insight into ways of looking
into the mutual inductance effects of the two vortices in the
present investigation.

2.2   CAPSULE STATEMENT OF THE WORK DONE

The present work deals with the stability of interdigitated

6

helical vortices, representing the part of the far wake trailed from the tips of multibladed helicopter rotors in hovering or vertical flight. A review of the literature revealed that only References 15 and 16, which are limited to single helices contained pertinent work. The analysis in this report involves the following steps: (1) An n-bladed, hovering rotor is represented by interdigitated, doubly infinite, right circular helical vortices of constant diameter. (2) The system of n vortices is perturbed from its normal helical configuration and position in radial, circumferential, and axial directions. (3) Application of the Biot-Savart law and the requirement that the time rate of perturbation displacements be compatible with the resulting induced velocities yields a system of eigenvalue equations for the admissible characteristics of these perturbations.

2.3   DEVELOPMENT

2.3.1 Mathematical Definition of Infinite Helical Vortices

Referring to Figure 1, which makes use of a left-handed Cartesian coordinate system, the parametric equation of a circular helix of radius r and pitch k is

$$x = r \cos \theta \quad , \quad y = r \sin \theta \quad , \quad z = k r \theta \quad ; \quad -\infty < \theta < \infty$$

To mathematically define n coaxial vortices of radius r and pitch k, one can define an azimuthal separation angle between the first helix and successive helices (see Figure 1) as

$$\psi_m = \frac{(m-1) \cdot 2\pi}{n} \quad ; \quad m = 1, 2, ---, n$$

If θ_m represents the parameter for the mth vortex, the parametric equation for the mth vortex can then be written as

$$x_m = r \cos(\theta_m + \psi_m)$$

$$y_m = r \sin(\theta_m + \psi_m)$$

$$z_m = k r \theta_m$$

7

2.3.2   Calculations of the Induced Velocities

The kinematic relation between vorticity and velocity in an incompressible fluid is given by the well-known Biot-Savart law. This equation can be applied to the system of n vortices and results in the expression

$$\vec{U}_p = \sum_{m=1}^{n} \frac{\Gamma_m}{4\pi} \int \frac{\vec{R}_{mp} \times d\vec{L}_m}{|\vec{R}_{mp}|^3} \qquad (1)$$

where $\vec{U}_p$ = induced velocity on p^{th} vortex.

Γ_m = circulation strength of mth vortex.

$d\vec{L}_m$ = elemental length vector on m^{th} vortex.

$\vec{R}_{mp}$ = relative position vector of point on p^{th} vortex relative to points on m^{th} vortex.

Referring to Figure 1, a vector representing an element of length along the mth vortex can be written as

$$d\vec{L}_m = [dx'_m, dy'_m, dz'_m]$$

and

$$\vec{R}_{mp} = [(x'_m - x_p), (y'_m - y_p), (z'_m - z_p)]$$

Note that the integration in equation (1) must be performed for all values of m, including the case where $m=p$, to account for the fact that the pth vortex induces velocity on itself. Primes have, therefore, been used to identify the general points involved in the space integration, as contrasted to the specific point at which the induced velocities are evaluated.

Rewriting the Cartesian coordinate description for the mth and p^{th} vortex,

$$x'_m = r\cos(\theta'_m + \psi_m)$$
$$y'_m = r\sin(\theta'_m + \psi_m)$$
$$z'_m = k r \theta'_m$$

and

$$x_p = r\cos(\theta_p + \psi_p)$$
$$y_p = r\sin(\theta_p + \psi_p)$$
$$z_p = k r \theta_p$$

8

Therefore, $d\vec{L}_m = [-r\sin(\theta'_m+\psi_m), r\cos(\theta'_m+\psi_m), kr]\, d\theta'_m$

$\vec{R}_{mp} = [\{r\cos(\theta'_m+\psi_m) - r\cos(\theta_p+\psi_p)\}, \{r\sin(\theta'_m+\psi_m) - r\sin(\theta_p+\psi_p)\}$
$$, \{kr(\theta'_m-\theta_p)\}]$$

In determinantal form, $\vec{R}_{mp} \times d\vec{L}_m$ can be written as

$$\vec{R}_{mp} \times d\vec{L}_m = d\theta'_m \begin{vmatrix} \vec{e}_x & \vec{e}_y & \vec{e}_z \\ \{r\cos(\theta'_m+\psi_m) & \{r\sin(\theta'_m+\psi_m) & kr(\theta'_m-\theta_p) \\ -r\cos(\theta_p+\psi_p)\} & -r\sin(\theta_p+\psi_p)\} & \\ -r\sin(\theta'_m+\psi_m) & r\cos(\theta'_m+\psi_m) & kr \end{vmatrix}$$

where $\vec{e}_x$, $\vec{e}_y$, $\vec{e}_z$ are unit vectors in the Cartesian x, y and z directions, respectively.

Therefore, the expressions for the induced velocities are

$$\vec{U}_p \cdot \vec{e}_x = \sum_{m=1}^{n} \frac{\Gamma_m}{4\pi} \int_{\theta'_m=-\infty}^{\theta'_m=+\infty} \frac{kr^2[\sin(\theta'_m+\psi_m) - \sin(\theta_p+\psi_p) - (\theta'_m-\theta_p)\cos(\theta'_m+\psi_m)]}{[2r^2 - 2r^2\cos(\theta'_m-\theta_p+\psi_m-\psi_p) + k^2r^2(\theta'_m-\theta_p)^2]^{3/2}}\, d\theta'_m$$

$$\vec{U}_p \cdot \vec{e}_y = \sum_{m=1}^{n} \frac{\Gamma_m}{4\pi} \int_{\theta'_m=-\infty}^{\theta'_m=+\infty} \frac{kr^2[\cos(\theta_p+\psi_p) - \cos(\theta'_m+\psi_m) - (\theta'_m-\theta_p)\sin(\theta'_m+\psi_m)]}{[2r^2 - 2r^2\cos(\theta'_m-\theta_p+\psi_m-\psi_p) + k^2r^2(\theta'_m-\theta_p)^2]^{3/2}}\, d\theta'_m$$

$$\vec{U}_p \cdot \vec{e}_z = \sum_{m=1}^{n} \frac{\Gamma_m}{4\pi} \int_{\theta'_m=-\infty}^{\theta'_m=+\infty} \frac{r^2[1 - \cos(\theta'_m-\theta_p+\psi_m-\psi_p)]}{[2r^2 - 2r^2\cos(\theta'_m-\theta_p+\psi_m-\psi_p) + k^2r^2(\theta'_m-\theta_p)^2]^{3/2}}\, d\theta'_m$$

The following simple transformation can be used to transform the Cartesian (x, y, z) velocities into cylindrical-polar (r, ϕ, z) velocities:

$$[\vec{U}_p \cdot \vec{e}_r] = [\vec{U}_p \cdot \vec{e}_x]\cos(\theta_p+\psi_p) + [\vec{U}_p \cdot \vec{e}_y]\sin(\theta_p+\psi_p)$$

$$[\vec{U}_p \cdot \vec{e}_\phi] = -[\vec{U}_p \cdot \vec{e}_x]\sin(\theta_p+\psi_p) + [\vec{U}_p \cdot \vec{e}_y]\cos(\theta_p+\psi_p)$$

The cylindrical-polar (r, ϕ, z) velocity components thus can

9

be written as

$$[\vec{U}_p \cdot \vec{e}_r] = \sum_{m=1}^{n} \frac{\Gamma_m}{4\pi} \int_{\theta_m' = -\infty}^{\theta_m' = +\infty} \frac{kr^2[\sin(\theta_m' - \theta_p + \psi_m - \psi_p) - (\theta_m' - \theta_p)\cos(\theta_m' - \theta_p + \psi_m - \psi_p)]}{[2r^2 - 2r^2\cos(\theta_m' - \theta_p + \psi_m - \psi_p) + k^2 r^2(\theta_m' - \theta_p)^2]^{3/2}} d\theta_m'$$

$$[\vec{U}_p \cdot \vec{e}_\phi] = \sum_{m=1}^{n} \frac{\Gamma_m}{4\pi} \int_{\theta_m' = -\infty}^{\theta_m' = +\infty} \frac{kr^2[1 - \cos(\theta_m' - \theta_p + \psi_m - \psi_p) - (\theta_m' - \theta_p)\sin(\theta_m' - \theta_p + \psi_m - \psi_p)]}{[2r^2 - 2r^2\cos(\theta_m' - \theta_p + \psi_m - \psi_p) + k^2 r^2(\theta_m' - \theta_p)^2]^{3/2}} d\theta_m'$$

$$[\vec{U}_p \cdot \vec{e}_z] = \sum_{m=1}^{n} \frac{\Gamma_m}{4\pi} \int_{\theta_m' = -\infty}^{\theta_m' = +\infty} \frac{r^2[1 - \cos(\theta_m' - \theta_p + \psi_m - \psi_p)]}{[2r^2 - 2r^2\cos(\theta_m' - \theta_p + \psi_m - \psi_p) + k^2 r^2(\theta_m' - \theta_p)^2]^{3/2}} d\theta_m'$$

If, now, we define $\quad x_{mp} \triangleq (\theta_m' - \theta_p)$

and $\quad \psi_{mp} \triangleq (\psi_m - \psi_p)$

and transform the variable of integration, remembering that θ_p is constant, there results

$$[\vec{U}_p \cdot \vec{e}_r] = \sum_{m=1}^{n} \frac{\Gamma_m}{4\pi} \int_{-\infty}^{\infty} \frac{kr^2[\sin(x_{mp} + \psi_{mp}) - x_{mp}\cos(x_{mp} + \psi_{mp})]}{[2r^2 - 2r^2\cos(x_{mp} + \psi_{mp}) + k^2 r^2 x_{mp}^2]^{3/2}} dx_{mp}$$

$$[\vec{U}_p \cdot \vec{e}_\phi] = \sum_{m=1}^{n} \frac{\Gamma_m}{4\pi} \int_{-\infty}^{+\infty} \frac{kr^2[1 - \cos(x_{mp} + \psi_{mp}) - x_{mp}\sin(x_{mp} + \psi_{mp})]}{[2r^2 - 2r^2\cos(x_{mp} + \psi_{mp}) + k^2 r^2 x_{mp}^2]^{3/2}} dx_{mp}$$

$$[\vec{U}_p \cdot \vec{e}_z] = \sum_{m=1}^{n} \frac{\Gamma_m}{4\pi} \int_{-\infty}^{+\infty} \frac{r^2[1 - \cos(x_{mp} + \psi_{mp})]}{[2r^2 - 2r^2\cos(x_{mp} + \psi_{mp}) + k^2 r^2 x_{mp}^2]^{3/2}} dx_{mp}$$

Self Induction

Induced velocity components on any vortex, p , result from the sum of the induced velocities due to all n vortices. In each of the three expressions immediately above there is a term on the right-hand side corresponding to $m = p$. This term gives the self-induced velocity components for the pth vortex. However, for $m = p$,

$$\psi_{pp} = \psi_p - \psi_p = 0$$

and at $x_{mp} = 0$ the denominator becomes a zero of higher order than

10

the numerator, resulting in a singularity in the line integral.
The difficulty is fundamental in that the Biot-Savart law
is invalid in a vortex core, i.e., where viscous forces
predominate.

Removal of the Singularity

If we assume that the vortex has a finite core of radius ε,
the singularity in the Biot-Savart integral can be removed in
several possible ways developed to a considerable extent in the
literature. S. C. Crow [Reference 17] in his work with fixed
wing trailing vortices eliminated the singularity by cutting
the integral off at some arc length α_c on either side of the
point where $|\vec{R}_{mp}| = 0$. He then subsequently determined α by
taking it proportional to the radius ε of the vortex core and
evaluating the constant of proportionality by reference to two
similar problems whose solutions are known by other means. A
similar technique has been used by Hama [References 18 and 19]
for determining the progressive deformation of vortex filaments
with initial curvature without and with, respectively, several
kinds of initial perturbations. More recently, Widnall [Refer-
ence 16] used the method of matched asymptotic expansions to
remove the singularity in the self-induction integrals by re-
lating the problem for helices to that for two-dimensional
circular vortex rings. Yet another method is to replace the
denominator $[|\vec{R}_{pp}|^2]^{3/2}$ by $[|\vec{R}_{pp}|^2 + \varepsilon^2]^{3/2}$; this approach was used
by Levy and Forsdyke [Reference 15] in their early work and
more recently by P. C. Parks [Reference 20].

For this study a procedure similar to that of P. C. Parks was
selected because a comparison with the Widnall results would
provide some insights into the equivalence of different ap-
proaches and because complications are avoided in this approach
when multiple interdigitated helices are considered. Thus,
$[|\vec{R}_{pp}|^2]^{3/2}$ will be replaced by $[|\vec{R}_{pp}|^2 + \varepsilon^2]^{3/2}$ when self-induced
velocities are calculated and subsequently in the perturbation
equations.

Even with the treatment of singularities described above,
another problem remains in the process of numerical integra-
tion, because the integrals behave almost as though they are
singular so far as numerical evaluation is concerned. The
evaluation and interpretation of integrals are therefore done
by rewriting the integrand, adding and subtracting functions
which have the same singularities numerically but which can be
more easily treated analytically. This procedure will be dis-
cussed further in chapter 3 in connection with integration of
the perturbation equations.

11

2.4   VORTICITY TRANSPORT THEOREM

In this analysis we have assumed a fluid of uniform density and zero viscosity and that elements of the vortex line move with fluid particles. If $\vec{r}$ denotes the position of points on a vortex line, the total derivative (Eulerian) of $\vec{r}$ is equal to the fluid velocity at that point.

If one is considering only those fluid velocities induced by the presence of vortices, then, mathematically, the vorticity transport theorem can be expressed as $\frac{d}{dt}(\vec{r}) = \vec{U}$ for points $\vec{r}$ on the vortex filaments.

A description of vorticity transport theorem can be found, for example, in the fluid dynamics book by G. K. Batchelor [Reference 21].

2.5   PERTURBATION EQUATIONS

Let the point (x_m, y_m, z_m) on the mth vortex helix be perturbed to the positions $x_m + \delta x_m,\ y_m + \delta y_m,\ z_m + \delta z_m$. Here $\delta x_m,\ \delta y_m$ and δz_m are considered to be first-order perturbations; i.e., their products, squares and higher powers can be neglected. The functional relationships for these perturbations can be written as

$$\delta x_m = \delta x_m(\theta_m, t)$$

$$\delta y_m = \delta y_m(\theta_m, t)$$

$$\delta z_m = \delta z_m(\theta_m, t)$$

where t is the time variable.

Now writing $\qquad\qquad \vec{r}_m = (x_m, y_m, z_m)$

and $\qquad\qquad \delta\vec{r}_m = (\delta x_m, \delta y_m, \delta z_m)$

the vorticity transport theorem thus gives, for the perturbed

p^{th} vortex, $\qquad \frac{d}{dt}(\vec{r}_p + \delta\vec{r}_p) = \vec{U}_p(\vec{r}_p + \delta\vec{r}_p)$

where $\vec{U}_p(\vec{r}_p + \delta\vec{r}_p)$ is the induced velocity at point $\vec{r}_p + \delta\vec{r}_p$ on

the perturbed p^{th} vortex.

12

The induced velocity, $\vec{U_p}$, is obtained by using the Biot-Savart
law at the point $\vec{r_p} + \delta\vec{r_p}$ due to the system of vortex helices
as modified by the perturbation displacements.

$$\vec{U_p}(\vec{r_p} + \delta\vec{r_p}) = \sum_{m=1}^{n} \frac{\Gamma_m}{4\pi} \int \frac{\vec{R_{mp}} \times d\vec{L_m}(\vec{r_m} + \delta\vec{r_m})}{|\vec{R_{mp}}|^3}$$

where $\qquad \vec{R_{mp}} = \vec{r_m'} - \vec{r_p'} + \delta\vec{r_m'} - \delta\vec{r_p'}$

$$d\vec{L_m} = d\vec{L_m}(\vec{r_m} + \delta\vec{r_m})$$
$$= [dx_m' + d(\delta x_m'), \ dy_m' + d(\delta y_m'), \ dz_m' + d(\delta z_m')]$$

The zero[th] and first-order cross products are

$$[\vec{R_{mp}} \times d\vec{L_m}]_o = (\vec{r_m'} - \vec{r_p}) \times \frac{\partial}{\partial\theta_m'}(\vec{r_m'}) d\theta_m'$$

$$[\vec{R_{mp}} \times d\vec{L_m}]_1 = (\vec{r_m'} - \vec{r_p}) \times \frac{\partial}{\partial\theta_m'}(\delta\vec{r_m'}) d\theta_m'$$
$$+ (\delta\vec{r_m'} - \delta\vec{r_p}) \times \frac{\partial}{\partial\theta_m'}(\vec{r_m'}) d\theta_m'$$

We may now write

$$|\vec{R_{mp}}|^{-3} = [(x_m' - x_p + \delta x_m' - \delta x_p)^2 + (y_m' - y_p + \delta y_m' - \delta y_p)^2$$
$$+ (z_m' - z_p + \delta z_m' - \delta z_p)^2]^{-3/2}$$

Defining the zero[th]-order term expression as

$$|\vec{R_{mp}}|_o^{-3} = [(x_m' - x_p)^2 + (y_m' - y_p)^2 + (z_m' - z_p)^2]^{-3/2}$$
$$\triangleq J_{mp}^{-3/2}$$

and the first order term expression as

$$|\vec{R_{mp}}|_1^{-3} \triangleq J_{mp}^{-3/2} [1 + 2 J_{mp}^{-1} \{(x_m' - x_p)(\delta x_m' - \delta x_p)$$
$$+ (y_m' - y_p)(\delta y_m' - \delta y_p) + (z_m' - z_p)(\delta z_m' - \delta z_p)\}]^{-3/2}$$

13

and expanding, retaining only first-order terms, yields

$$\left| \vec{R}_{mp} \right|_1^{-3} = -3 J_{mp}^{-5/2} K_{mp}$$

where K_{mp} is defined as

$$K_{mp} \triangleq (x_m' - x_p)(\delta x_m' - \delta x_p) + (y_m' - y_p)(\delta y_m' - \delta y_p)$$

$$+ (z_m' - z_p)(\delta z_m' - \delta z_p)$$

The corresponding zero and first-order induced velocity vectors(denoted by 0 and 1 subscripts) can be written as

$$\left[\vec{U}_p \right]_0 = \sum_{m=1}^{n} \frac{\Gamma_m}{4\pi} \int_{\theta_m' = -\infty}^{\theta_m' = +\infty} J_{mp}^{-3/2} \left[(\vec{r}_m' - \vec{r}_p) \times \frac{\partial}{\partial \theta_m'} (\vec{r}_m') \right] d\theta_m'$$

$$\left[\vec{U}_p \right]_1 = \sum_{m=1}^{n} \frac{\Gamma_m}{4\pi} \int_{\theta_m' = -\infty}^{\theta_m' = +\infty} J_{mp}^{-3/2} \left[(\vec{r}_m' - \vec{r}_p) \times \frac{\partial}{\partial \theta_m'} (\delta \vec{r}_m') + (\delta \vec{r}_m' - \delta \vec{r}_p) \times \frac{\partial}{\partial \theta_m'} (\vec{r}_m') \right] d\theta_m'$$

$$+ \sum_{m=1}^{n} \frac{\Gamma_m}{4\pi} \int_{\theta_m' = -\infty}^{\theta_m' = +\infty} -3 K_{mp} J_{mp}^{-5/2} \left[(\vec{r}_m' - \vec{r}_p) \times \frac{\partial}{\partial \theta_m'} (\vec{r}_m') \right] d\theta_m'$$

It will be convenient to carry out the calculations in terms of the helical coordinates, r and θ. Since the parametric equation for the mth vortex helix is

$$x_m' = r \cos(\theta_m' + \psi_m)$$

$$y_m' = r \sin(\theta_m' + \psi_m)$$

$$z_m' = k r \theta_m'$$

the first-order displacement perturbation expressions can be written as

$$\delta x_m' = \delta r_m \cos(\theta_m' + \psi_m) - r \sin(\theta_m' + \psi_m) \delta \phi_m$$

$$\delta y_m' = \delta r_m \sin(\theta_m' + \psi_m) + r \cos(\theta_m' + \psi_m) \delta \phi_m$$

14

$$\delta z_m' = \delta z_m$$

The zeroth and first order terms of the numerator of the integrand in the x, y and z directions also can be written as

Zeroth order terms in the x direction

$$(y_m' - y_p)\frac{\partial}{\partial\theta_m'}(z_m') - (z_m' - z_p)\frac{\partial}{\partial\theta_m'}(y_m') = \{r\sin(\theta_m' + \psi_m) - r\sin(\theta_p + \psi_p)\}\cdot kr$$

$$- kr^2(\theta_m' - \theta_p)\cos(\theta_m' + \psi_m)$$

First order terms in the x direction

$$(\delta y_m' - \delta y_p)\frac{\partial}{\partial\theta_m'}(z_m') - (\delta z_m' - \delta z_p)\frac{\partial}{\partial\theta_m'}(y_m') =$$

$$kr[\delta r_m \sin(\theta_m' + \psi_m) - \delta r_p \sin(\theta_p + \psi_p) + r\delta\phi_m \cos(\theta_m' + \psi_m) - r\delta\phi_p \cos(\theta_p + \psi_p)]$$

$$- (\delta z_m - \delta z_p)\cdot r\cos(\theta_m' + \psi_m)$$

$$(y_m' - y_p)\frac{\partial}{\partial\theta_m'}(\delta z_m') - (z_m' - z_p)\frac{\partial}{\partial\theta_m'}(\delta y_m') =$$

$$r\frac{\partial}{\partial\theta_m'}(\delta z_m)[\sin(\theta_m' + \psi_m) - \sin(\theta_p + \psi_p)] - kr(\theta_m' - \theta_p)\left[\frac{\partial}{\partial\theta_m'}(\delta r_m)\sin(\theta_m' + \psi_m)\right.$$

$$\left. + \delta r_m \cos(\theta_m' + \psi_m) + r\cos(\theta_m' + \psi_m)\frac{\partial}{\partial\theta_m'}(\delta\phi_m) - r\delta\phi_m \sin(\theta_m' + \psi_m)\right]$$

Zeroth order terms in the y direction

$$(z_m' - z_p)\frac{\partial}{\partial\theta_m'}(x_m') - (x_m' - x_p)\frac{\partial}{\partial\theta_m'}(z_m') =$$

$$- kr^2(\theta_m' - \theta_p)\sin(\theta_m' + \psi_m) - kr^2\{\cos(\theta_m' + \psi_m) - \cos(\theta_p + \psi_p)\}$$

15

First-order terms in the y direction

$$(\delta z_m' - \delta z_p)\frac{\partial}{\partial\theta_m'}(x_m') - (\delta x_m' - \delta x_p)\frac{\partial}{\partial\theta_m'}(z_m') =$$

$$-r(\delta z_m - \delta z_p)\sin(\theta_m' + \psi_m) - Rr[\delta r_m \cos(\theta_m' + \psi_m) - \delta r_p \cos(\theta_p + \psi_p)$$

$$-r\delta\phi_m \sin(\theta_m' + \psi_m) + r\delta\phi_p \sin(\theta_p + \psi_p)]$$

$$(z_m' - z_p)\frac{\partial}{\partial\theta_m'}(\delta x_m') - (x_m' - x_p)\frac{\partial}{\partial\theta_m'}(\delta z_m') =$$

$$Rr(\theta_m' - \theta_p)\left[\frac{\partial}{\partial\theta_m'}(\delta r_m)\cos(\theta_m' + \psi_m) - \delta r_m \sin(\theta_m' + \psi_m) - r\delta\phi_m \cos(\theta_m' + \psi_m)\right.$$

$$\left. - r\sin(\theta_m' + \psi_m)\frac{\partial}{\partial\theta_m'}(\delta\phi_m)\right] - r\frac{\partial}{\partial\theta_m'}(\delta z_m)\left[\cos(\theta_m' + \psi_m) - \cos(\theta_p + \psi_p)\right]$$

Zeroth-order terms in the z direction

$$(x_m' - x_p)\frac{\partial}{\partial\theta_m'}(y_m') - (y_m' - y_p)\frac{\partial}{\partial\theta_m'}(x_m') =$$

$$r^2\cos(\theta_m' + \psi_m)\{\cos(\theta_m' + \psi_m) - \cos(\theta_p + \psi_p)\} - r^2\sin(\theta_m' + \psi_m)\{\sin(\theta_m' + \psi_m) - \sin(\theta_p + \psi_p)\}$$

First-order terms in the z direction

$$(\delta x_m' - \delta x_p)\frac{\partial}{\partial\theta_m'}(y_m') - (\delta y_m' - \delta y_p)\frac{\partial}{\partial\theta_m'}(x_m') =$$

$$r\cos(\theta_m' + \psi_m)\left[\delta r_m \cos(\theta_m' + \psi_m) - \delta r_p \cos(\theta_p + \psi_p) - r\delta\phi_m \sin(\theta_m' + \psi_m)\right.$$

$$\left. + r\delta\phi_p \sin(\theta_p + \psi_p)\right] + r\sin(\theta_m' + \psi_m)\left[\delta r_m \sin(\theta_m' + \psi_m)\right.$$

$$\left. - \delta r_p \sin(\theta_p + \psi_p) + r\delta\phi_m \cos(\theta_m' + \psi_m) - r\delta\phi_p \sin(\theta_p + \psi_p)\right]$$

16

$$(x'_m - x_p)\frac{\partial}{\partial\theta'_m}(\delta y'_m) - (y'_m - y_p)\frac{\partial}{\partial\theta'_m}(\delta x'_m) =$$

$$r[\cos(\theta'_m + \psi_m) - \cos(\theta_p + \psi_p)]\cdot\left[\frac{\partial}{\partial\theta'_m}(\delta r_m)\sin(\theta'_m + \psi_m) + \delta r_m \cos(\theta'_m + \psi_m)\right.$$

$$\left. - r\delta\phi_m \sin(\theta'_m + \psi_m) + r\cos(\theta'_m + \psi_m)\frac{\partial}{\partial\theta'_m}(\delta\phi_m)\right] - r[\sin(\theta'_m + \psi_m) - \sin(\theta_p + \psi_p)]$$

$$\left[\frac{\partial}{\partial\theta'_m}(\delta r_m)\cos(\theta'_m + \psi_m) - \delta r_m \sin(\theta'_m + \psi_m) - r\delta\phi_m\cos(\theta'_m + \psi_m) - r\sin(\theta'_m + \psi_m)\frac{\partial}{\partial\theta'_m}(\delta\phi_m)\right]$$

$$J_{mp}^2 = 2r^2 - 2r^2\cos(\theta'_m - \theta_p + \psi_m - \psi_p) + k^2 r^2(\theta'_m - \theta_p)^2$$

$$K_{mp} = r\delta r_m\{1 - \cos(x_{mp} + \psi_{mp})\} + r\delta r_p\{1 - \cos(x_{mp} + \psi_{mp})\}$$

$$+ r^2\delta\phi_m \sin(x_{mp} + \psi_{mp}) - r^2\delta\phi_p\sin(x_{mp} + \psi_{mp})$$

$$+ krx_{mp}\delta\dot{z}_m - krx_{mp}\delta\dot{z}_p$$

Calculation of Terms on the Left Side of the Vortex Transport Perturbation Equation

$$x_p + \delta x_p = r\cos(\theta_p + \psi_p) + \delta r_p\cos(\theta_p + \psi_p) - r\sin(\theta_p + \psi_p)\delta\phi_p$$

$$\frac{d}{dt}(x_p + \delta x_p) = \dot{r}_p\cos(\theta_p + \psi_p) - r\dot{\phi}_p\sin(\theta_p + \psi_p) + \delta\dot{r}_p\cos(\theta_p + \psi_p)$$

$$- \delta r_p\dot{\phi}_p\sin(\theta_p + \psi_p) - \dot{r}_p\delta\phi_p\sin(\theta_p + \psi_p)$$

$$- r\dot{\phi}_p\delta\phi_p\cos(\theta_p + \psi_p) - r\delta\dot{\phi}_p\sin(\theta_p + \psi_p) \tag{2}$$

$$y_p + \delta y_p = r\sin(\theta_p + \psi_p) + \delta r_p\sin(\theta_p + \psi_p) + r\delta\phi_p\cos(\theta_p + \psi_p)$$

17

$$\frac{d}{dt}(y_p + \delta y_p) = \dot{r}_p \sin(\theta_p + \psi_p) + r\dot{\phi}_p \cos(\theta_p + \psi_p) + \delta\dot{r}_p \sin(\theta_p + \psi_p)$$

$$+ \delta r_p \dot{\phi}_p \cos(\theta_p + \psi_p) + \dot{r}_p \delta\phi_p \cos(\theta_p + \psi_p)$$

$$+ r\delta\dot{\phi}_p \cos(\theta_p + \psi_p) - r\dot{\phi}_p \delta\phi_p \sin(\theta_p + \psi_p) \qquad (3)$$

$$\frac{d}{dt}(z_p + \delta z_p) = \frac{dz_p}{dt} + \delta\dot{z}_p \qquad (4)$$

We now resolve the velocity radially, circumferentially, and axially (i.e., in r, ϕ and z directions); these components will be defined as ξ_p, η_p and ζ_p respectively.

Multiplying equation (2) by $\cos(\theta_p + \psi_p + \delta\phi_p)$ and equation (3) by $\sin(\theta_p + \psi_p + \delta\phi_p)$ and remembering that

$$\cos(\theta_p + \psi_p + \delta\phi_p) = \cos(\theta_p + \psi_p) - \delta\phi_p \sin(\theta_p + \psi_p)$$

$$\sin(\theta_p + \psi_p + \delta\phi_p) = \sin(\theta_p + \psi_p) + \delta\phi_p \cos(\theta_p + \psi_p)$$

we obtain the total radial velocity of the perturbed helix at P; thus:

$$\dot{\xi}_p = \dot{r}_p + \delta\dot{r}_p - r\dot{\phi}_p \delta\phi_p + r\dot{\phi}_p \delta\phi_p = \dot{r}_p + \delta\dot{r}_p$$

where $\dot{r}_p$ = zeroth-order radial velocity at P.

$\delta\dot{r}_p$ = first-order radial velocity at P.

Similarly, multiplying equation (2) by $-\sin(\theta_p + \psi_p + \delta\phi_p)$ and equation (3) by $\cos(\theta_p + \psi_p + \delta\phi_p)$, we obtain

$$\dot{\eta}_p = r\dot{\phi}_p - \dot{r}_p \delta\phi_p + \delta r_p \dot{\phi}_p + \dot{r}_p \delta\phi_p + r\delta\dot{\phi}_p$$

$$= r\dot{\phi}_p + \delta r_p \dot{\phi}_p + r\delta\dot{\phi}_p$$

18

where $r\dot{\phi}_p$ is the zero[th]-order velocity and the remaining terms

on the right-hand side represent first-order circumferential velocity.

Finally, $\qquad \dot{\zeta}_p = \dot{z}_p + \delta\dot{z}_p$

where $\qquad \dot{z}_p =$ zero[th]-order axial velocity.

$\qquad\qquad \delta\dot{z}_p =$ first-order axial velocity.

Transformation of the Induced Velocities to Polar Form

The zero[th]-order velocity in the x, y and z directions which result when the right side of equation (1) is expanded will be called U_{xp}, U_{yp} and U_{zp}, respectively, and the

corresponding first-order velocity terms will be called $\delta U_{xp}, \delta U_{yp}$

and δU_{zp}. Expressing the induced velocities also in terms of radial, circumferential, and axial components, and equating the left sides and right sides of equation (1) component by component yields

$$\dot{\xi}_p = \dot{r}_p + \delta\dot{r}_p = (U_{xp} + \delta U_{xp})\, \cos(\theta_p + \psi_p + \delta\phi_p)$$
$$+ (U_{yp} + \delta U_{yp})\, \sin(\theta_p + \psi_p + \delta\phi_p)$$

$$\dot{\eta}_p = r\dot{\phi}_p + \delta r_p\dot{\phi}_p + r\delta\dot{\phi}_p = -(U_{xp} + \delta U_{xp})\, \sin(\theta_p + \psi_p + \delta\phi_p)$$
$$+ (U_{yp} + \delta U_{yp})\, \cos(\theta_p + \psi_p + \delta\phi_p)$$

$$\dot{\zeta}_p = \dot{z}_p + \delta\dot{z}_p = U_{zp} + \delta U_{zp}$$

Now, separating zero[th]-order and first-order terms, the vortex transport equations are obtained in terms of helical coordinates for unperturbed and first-order perturbed motion, as follows:

Zero[th]-order (unperturbed) transport relations

$$\dot{r}_p = U_{xp}\cos(\theta_p + \psi_p) + U_{yp}\sin(\theta_p + \psi_p)$$

19

$$r\dot{\phi}_p = -U_{xp}\sin(\theta_p+\psi_p) + U_{yp}\cos(\theta_p+\psi_p)$$

$$\dot{z}_p = U_{zp}$$

First-order perturbation transport equations

$$\delta\dot{r}_p = -U_{xp}\,\delta\phi_p\,\sin(\theta_p+\psi_p) + U_{yp}\,\delta\phi_p\,\cos(\theta_p+\psi_p)$$

$$+ \delta U_{xp}\,\cos(\theta_p+\psi_p) + \delta U_{yp}\,\sin(\theta_p+\psi_p)$$

$$= r\dot{\phi}_p\,\delta\phi_p + \delta U_{xp}\cos(\theta_p+\psi_p) + \delta U_{yp}\sin(\theta_p+\psi_p)$$

$$\delta r_p\dot{\phi}_p + r\,\delta\dot{\phi}_p = -U_{xp}\,\delta\phi_p\,\cos(\theta_p+\psi_p) - U_{yp}\,\delta\phi_p\,\sin(\theta_p+\psi_p)$$

$$- \delta U_{xp}\sin(\theta_p+\psi_p) + \delta U_{yp}\cos(\theta_p+\psi_p)$$

$$= -\dot{r}_p\,\delta\phi_p - \delta U_{xp}\sin(\theta_p+\psi_p) + \delta U_{yp}\cos(\theta_p+\psi_p)$$

or

$$\delta\dot{r}_p = r\dot{\phi}_p\,\delta\phi_p + \delta U_{xp}\cos(\theta_p+\psi_p) + \delta U_{yp}\sin(\theta_p+\psi_p) \tag{5}$$

$$r\,\delta\dot{\phi}_p = -\delta r_p\dot{\phi}_p - \dot{r}_p\,\delta\phi_p - \delta U_{xp}\sin(\theta_p+\psi_p) + \delta U_{yp}\cos(\theta_p+\psi_p) \tag{6}$$

$$\delta\dot{z}_p = \delta U_{zp} \tag{7}$$

Substituting for induced velocities and time rates of displacement, the unperturbed relations become

$$\dot{r}_p = \sum_{m=1}^{n} \frac{\Gamma_m}{4\pi}\int_{-\infty}^{\infty} kr^2\{\sin(x_{mp}+\psi_{mp}) - x_{mp}\cos(x_{mp}+\psi_{mp})\}\,J_{mp}^{-3/2}\,dx_{mp}$$

$$r\dot{\phi}_p = \sum_{m=1}^{n} \frac{\Gamma_m}{4\pi}\int_{-\infty}^{\infty} kr^2\{1-\cos(x_{mp}+\psi_{mp}) - x_{mp}\sin(x_{mp}+\psi_{mp})\}\,J_{mp}^{-3/2}\,dx_{mp}$$

$$\dot{z}_p = \sum_{m=1}^{n} \frac{\Gamma_m}{4\pi}\int_{-\infty}^{\infty} r^2\{1-\cos(x_{mp}+\psi_{mp})\}\,J_{mp}^{-3/2}\,dx_{mp}$$

20

Similarly, the first-order perturbation equations can be written as

$$
\delta \dot{r}_p = \sum_{m=1}^{n} \frac{\Gamma_m}{4\pi} \int_{-\infty}^{\infty} J_{mp}^{-3/2} \Big[\{ -kr \, x_{mp} \sin(x_{mp} + \psi_{mp}) \frac{\partial}{\partial \theta'_m} (\delta r_m)
$$

$$
- kr \, x_{mp} \, \delta r_m \cos(x_{mp} + \psi_{mp}) + kr \, \delta r_m \sin(x_{mp} + \psi_{mp}) \}
$$

$$
+ kr^2 \{ \delta \phi_m \cos(x_{mp} + \psi_{mp}) + x_{mp} \, \delta \phi_m \sin(x_{mp} + \psi_{mp})
$$

$$
- x_{mp} \frac{\partial}{\partial \theta'_m} (\delta \phi_m) \cos(x_{mp} + \psi_{mp}) - \delta \phi_p \cos(x_{mp} + \psi_{mp}) \}
$$

$$
+ r \{ -\delta z_m \cos(x_{mp} + \psi_{mp}) + \delta z_p \cos(x_{mp} + \psi_{mp})
$$

$$
+ \frac{\partial}{\partial \theta'_m} (\delta z_m) \sin(x_{mp} + \psi_{mp}) \} \Big] dx_{mp}
$$

$$
- 3 \sum_{m=1}^{n} \frac{\Gamma_m}{4\pi} \int_{-\infty}^{\infty} J_{mp}^{-5/2} \, kr^2 \{ \sin(x_{mp} + \psi_{mp}) - x_{mp} \cos(x_{mp} + \psi_{mp}) \} K_{mp} \, dx_{mp}
$$

$$
\text{(8)}
$$

$$
r \, \delta \dot{\phi}_p = \sum_{m=1}^{n} \frac{\Gamma_m}{4\pi} \int_{-\infty}^{\infty} J_{mp}^{-3/2} \Big[kr \{ x_{mp} \frac{\partial}{\partial \theta'_m} (\delta r_m) \cos(x_{mp} + \psi_{mp}) - \delta r_m \cos(x_{mp} + \psi_{mp})
$$

$$
- x_{mp} \, \delta r_m \sin(x_{mp} + \psi_{mp}) + \delta r_p \cos(x_{mp} + \psi_{mp})
$$

$$
+ x_{mp} \, \delta r_p \sin(x_{mp} + \psi_{mp}) \} + kr^2 \{ -x_{mp} \frac{\partial}{\partial \theta'_m} (\delta \phi'_m) \sin(x_{mp} + \psi_{mp})
$$

$$
- x_{mp} \, \delta \phi_m \cos(x_{mp} + \psi_{mp}) + \delta \phi_m \sin(x_{mp} + \psi_{mp}) - \delta \phi_p \sin(x_{mp} + \psi_{mp})
$$

$$
+ x_{mp} \, \delta \phi_p \cos(x_{mp} + \psi_{mp}) \} + r \{ -\delta z_m \sin(x_{mp} + \psi_{mp})
$$

$$
+ \delta z_p \sin(x_{mp} + \psi_{mp}) - \frac{\partial}{\partial \theta'_m} (\delta z_m) \cos(x_{mp} + \psi_{mp}) + \frac{\partial}{\partial \theta'_m} (\delta z_m) \} \Big] dx_{mp}
$$

$$
- 3 \sum_{m=1}^{n} \frac{\Gamma_m}{4\pi} \int_{-\infty}^{\infty} kr^2 J_{mp}^{-5/2} \cdot K_{mp} \big[1 - \cos(x_{mp} + \psi_{mp} - x_{mp} \sin(x_{mp} + \psi_{mp}) \big] dx_{mp}
$$

$$
\text{(9)}
$$

21

$$\delta \dot{z}_p = \sum_{m=1}^{n} \frac{\Gamma_m}{4\pi} \int_{-\infty}^{\infty} J_{mp}^{-3/2} \left[r \left\{ \frac{\partial}{\partial \theta_m'} (\delta r_m) \sin(x_{mp} + \psi_{mp}) + 2\delta r_m \right. \right.$$

$$- \delta r_m \cos(x_{mp} + \psi_{mp}) - \delta r_p \cos(x_{mp} + \psi_{mp}) \}$$

$$+ r^2 \left\{ \frac{\partial}{\partial \theta_m'} (\delta\phi_m) + \delta\phi_m \sin(x_{mp} + \psi_{mp}) - \cos(x_{mp} + \psi_{mp}) \frac{\partial}{\partial \theta_m'} (\delta\phi_m) \right.$$

$$- \delta\phi_p \sin(x_{mp} + \psi_{mp}) \} \Big] dx_{mp}$$

$$- \sum_{m=1}^{n} \frac{\Gamma_m}{4\pi} \int_{-\infty}^{\infty} J_{mp}^{-5/2} r^2 \{ 1 - \cos(x_{mp} + \psi_{mp}) \} K_{mp} \, dx_{mp} \qquad (10)$$

Removal of Singularities

As explained in Section 2.3.2, the integrand that provides the self-induced contribution to induced velocity becomes singular at $x_{mp} = 0$. This singularity is eliminated by changing the

expression for J_{mp} from $\{ 2r^2 - 2r^2\cos(x_{mp} + \psi_{mp}) + R^2 r^2 x_{mp}^2 \}^{1/2}$

to $\{ 2r^2 - 2r^2\cos(x_{mp} + \psi_{mp}) + R^2 r^2 x_{mp}^2 + \varepsilon_0^2 \}^{1/2}$

when $m = p$. Here ε_0 is the vortex core radius and is small compared to the radius r of the helix. Note, however, that when $m \neq p$, the expression for J_{mp} remains unmodified.

2.6   TYPE OF PERTURBATIONS AND EIGENVALUE EQUATIONS

The integro-differential perturbation equations derived in Section 2.5 admit solutions of the exponential type, for perturbations δr_m ; that is,

22

$$\vec{\delta r_m} = \hat{\vec{\delta r_m}} e^{\alpha t + i\omega\theta_m'} \tag{11}$$

or in component form

$$\delta r_m = \hat{\delta r_m} e^{\alpha t + i\omega\theta_m'}$$

$$\delta\phi_m = \hat{\delta\phi_m} e^{\alpha t + i\omega\theta_m'}$$

$$\delta z_m = \hat{\delta z_m} e^{\alpha t + i\omega\theta_m'}$$

where $\vec{\delta r_m}$ = vector perturbation of the mth vortex having δr_m,

$\delta\phi_m$ and δz_m as its components in the r, ϕ and z

directions.

α = exponential growth rate factor, complex.

ω = wave number* of the perturbation.

In principle, no generality is lost in considering such solutions, since an arbitrary perturbation can be synthesized from these by Fourier Integration. In practice, the numerical work will, of course, deal with a limited number of wavelengths. The exponential form assumed in the solutions of perturbation equations (8), (9), and (10) allows this set of integro-differential equations to be written as a set of linear algebraic equations in the amplitudes of the perturbation components $\hat{\delta r_m}$,

$\hat{\delta\phi_m}$, $\hat{\delta z_m}$. The spatial derivatives of the solution forms are

given by

$$\frac{\partial}{\partial\theta_m'}(\delta r_m) = \frac{\partial}{\partial\theta_m'}[\hat{\delta r_m} e^{\alpha t + i\omega\theta_m'}] = i\omega\,\delta r_m$$

---

* The inverse of the wavelength, i.e., number of waves per
  helix turn.

23

and

$$\frac{\partial}{\partial \theta_m'}(\delta \phi_m) = i \omega \, \delta \phi_m$$

$$\frac{\partial}{\partial \theta_m'}(\delta z_m) = i \omega \, \delta z_m$$

Also, the first-order displacement perturbation components can be rewritten as

$$\delta r_m = \hat{\delta r}_m \, e^{\alpha t + i \omega \theta_m'} = \hat{\delta r}_m \, e^{\alpha t + i \omega \theta_m' - i \omega \theta_p + i \omega \theta_p}$$

$$= \hat{\delta r}_m \, e^{\alpha t + i \omega \theta_p} \, e^{i \omega x_{mp}}$$

$$\delta \phi_m = \hat{\delta \phi}_m \, e^{\alpha t + i \omega \theta_p} \, e^{i \omega x_{mp}}$$

$$\delta z_m = \hat{\delta z}_m \, e^{\alpha t + i \omega \theta_p} \, e^{i \omega x_{mp}} \tag{12}$$

Substituting equations (12) into the perturbation equations (8), (9) and (10) and defining $y_{mp} \triangleq x_{mp} + \psi_{mp}$ yields the following eigenvalue equations:

$$\frac{4 \pi \alpha \hat{\delta r}_p}{\Gamma} = \sum_{m=1}^{n} \int_{-\infty}^{\infty} J_{mp}^{-3/2} \left[kr \hat{\delta r}_m \left\{ \omega x_{mp} \sin y_{mp} \sin \omega x_{mp} \right. \right.$$

$$- x_{mp} \cos y_{mp} \cos \omega x_{mp} + \sin y_{mp} \cos \omega x_{mp} \} + i kr \hat{\delta r}_m$$

$$\{ -\omega x_{mp} \sin y_{mp} \cos \omega x_{mp} - x_{mp} \cos y_{mp} \sin \omega x_{mp}$$

$$+ \sin y_{mp} \sin \omega x_{mp} \} + kr^2 \hat{\delta \phi}_m \{ \cos y_{mp} \cos \omega x_{mp}$$

$$+ x_{mp} \sin y_{mp} \cos \omega x_{mp} + \omega x_{mp} \cos y_{mp} \sin \omega x_{mp} \}$$

$$+ i kr^2 \hat{\delta \phi}_m \{ \cos y_{mp} \sin \omega x_{mp} + x_{mp} \sin y_{mp} \sin \omega x_{mp}$$

$$- \omega x_{mp} \cos y_{mp} \cos \omega x_{mp} \} + r \hat{\delta z}_m \{ -\cos y_{mp} \cos \omega x_{mp}$$

$$- \omega \sin y_{mp} \sin \omega x_{mp} \} + i r \hat{\delta z}_m \{ -\cos y_{mp} \sin \omega x_{mp}$$

$$+ \omega \sin y_{mp} \cos \omega x_{mp} \} + kr^2 \hat{\delta \phi}_p \{ -\cos y_{mp} - x_{mp} \sin y_{mp} \}$$

$$+ r \delta \hat{z}_p \cos x_{mp} \big] \, dx_{mp}$$

$$-3 \sum_{m=1}^{n} \int_{-\infty}^{\infty} J_{mp}^{-5/2} \big[k r^2 \{ \sin y_{mp} - x_{mp} \cos y_{mp} \} \big] \cdot \big[r \delta r_m$$

$$\{ (1 - \cos y_{mp}) \cos \omega x_{mp} + i (1 - \cos y_{mp}) \sin \omega x_{mp} \}$$

$$+ r^2 \delta \hat{\phi}_m \{ \sin y_{mp} \cos \omega x_{mp} + i \sin y_{mp} \sin \omega x_{mp} \}$$

$$+ k r \delta \hat{z}_m \{ + x_{mp} \cos \omega x_{mp} + i x_{mp} \sin \omega x_{mp} \}$$

$$+ r \delta \hat{r}_p \{ 1 - \cos y_{mp} \} - r^2 \delta \hat{\phi}_p \{ \sin y_{mp} \} - k r \delta \hat{z}_p x_{mp} \big] \, dx_{mp}$$

$$\qquad\qquad\qquad\qquad\qquad\qquad\qquad\qquad - \qquad (13)$$

Similarly,

$$\frac{4 \pi r \alpha \, \delta \hat{\phi}_p}{\Gamma} = \sum_{m=1}^{n} \int_{-\infty}^{\infty} J_{mp}^{-3/2} \big[k r \delta \hat{r}_m \{ - \omega x_{mp} \cos y_{mp} \sin \omega x_{mp}$$

$$- \cos y_{mp} \cos \omega x_{mp} - x_{mp} \sin y_{mp} \cos \omega x_{mp} \}$$

$$+ i k r \delta \hat{r}_m \{ \omega x_{mp} \cos y_{mp} \cos \omega x_{mp} - \cos y_{mp} \sin \omega x_{mp}$$

$$- x_{mp} \sin y_{mp} \sin \omega x_{mp} \} + k r \delta \hat{r}_p \{ \cos y_{mp} + x_{mp} \sin y_{mp} \}$$

$$+ k r^2 \delta \hat{\phi}_m \{ \omega x_{mp} \sin y_{mp} \sin \omega x_{mp} - x_{mp} \cos y_{mp} \cos \omega x_{mp}$$

$$+ \sin y_{mp} \cos \omega x_{mp} \} + i k r^2 \delta \hat{\phi}_m \{ - \omega x_{mp} \sin y_{mp} \cos \omega x_{mp}$$

$$- x_{mp} \cos y_{mp} \sin \omega x_{mp} + \sin y_{mp} \sin \omega x_{mp} \}$$

$$- k r^2 \delta \hat{\phi}_p \{ \sin y_{mp} - x_{mp} \cos y_{mp} \} + r \delta \hat{z}_m \{ - \sin y_{mp} \cos \omega x_{mp}$$

$$+ \omega \cos y_{mp} \sin \omega x_{mp} - \omega \sin \omega x_{mp} \} + i r \delta \hat{z}_m$$

$$\{ - \sin y_{mp} \sin \omega x_{mp} - \omega \cos y_{mp} \cos \omega x_{mp} + \omega \cos \omega x_{mp} \}$$

$$+ r \delta \hat{z}_p \sin y_{mp} \big] \, dx_{mp}$$

$$-3 \sum_{m=1}^{n} \int_{-\infty}^{\infty} J_{mp}^{-5/2} \big[k r^2 \{ 1 - \cos y_{mp} - x_{mp} \sin y_{mp} \} \big] \cdot \big[r \delta \hat{r}_m$$

$$\{ + (1 - \cos y_{mp}) \cos \omega x_{mp} + i (1 - \cos y_{mp}) \sin \omega x_{mp} \} + r^2 \delta \hat{\phi}_m$$

$$\{ + \sin y_{mp} \cos \omega x_{mp} + i \sin y_{mp} \sin \omega x_{mp} \} + k r \delta \hat{z}_m$$

$$\{ + x_{mp} \cos \omega x_{mp} + i x_{mp} \sin \omega x_{mp} \} + r \delta \hat{r}_p$$

$$\{ + 1 - \cos y_{mp} \} + r^2 \delta \hat{\phi}_p \{ \sin y_{mp} \} - k r \delta \hat{z}_p x_{mp} \big] \, dx_{mp} \quad - \quad (14)$$

25

$$\frac{4\pi\alpha\delta\hat{z}_p}{\Gamma} = \sum_{m=1}^{n}\int_{-\infty}^{\infty}\Big[r\delta\hat{r}_m\{\omega\sin y_{mp}\sin\omega x_{mp} + 2\cos\omega x_{mp} - \cos y_{mp}\cos\omega x_{mp}\}$$

$$+ ir\delta\hat{r}_m\{-\omega\sin y_{mp}\cos\omega x_{mp} + 2\sin\omega x_{mp} - \cos y_{mp}\sin\omega x_{mp}\}$$

$$- r\delta\hat{r}_p\cos y_{mp} + r^2\delta\hat{\phi}_m\{-\omega\sin\omega x_{mp} + \sin y_{mp}\cos\omega x_{mp}$$

$$+ \omega\cos y_{mp}\sin\omega x_{mp}\} + ir^2\delta\hat{\phi}_m\{\omega\cos\omega x_{mp}$$

$$+ \sin y_{mp}\sin\omega x_{mp} - \omega\cos y_{mp}\cos\omega x_{mp}\}$$

$$+ r^2\delta\hat{\phi}_p\{-\sin y_{mp}\}\Big]\,dx_{mp}\cdot J_{mp}^{-3/2}$$

$$-3\sum_{m=1}^{n}\int_{-\infty}^{\infty}J_{mp}^{-5/2}\big[r^2(1-\cos y_{mp})\big]\cdot\Big[r\delta r_m\{(1-\cos y_{mp})\cos\omega x_{mp}$$

$$+ i(1-\cos y_{mp})\sin\omega x_{mp}\} + r^2\delta\hat{\phi}_m\{$$

$$+ \sin y_{mp}\cos\omega x_{mp} + i\sin y_{mp}\sin\omega x_{mp}\}$$

$$+ Rr\delta\hat{z}_m\{x_{mp}\cos\omega x_{mp} + ix_{mp}\sin\omega x_{mp}\} + r\delta\hat{r}_p$$

$$\{1-\cos y_{mp}\} - r^2\delta\hat{\phi}_p\{\sin y_{mp}\}$$

$$- Rr\delta\hat{z}_p\,x_{mp}\Big]\,dx_{mp} \qquad\qquad (15)$$

2.7   STABILITY ANALYSIS

Equations (13) through (15) can be written for integer values of p ranging from 1 to n , where n corresponds to the number of interdigitated helices. After numerically evaluating the set of self and mutual induction integrals, a system of $3n$ eigenvalue equations is obtained. The limits of integration are from $-\infty$ to $+\infty$. The integrals in the perturbation equations are convergent, since both $J_{mp}^{-3/2}$ and $J_{mp}^{-5/2}$ vary as x_{mp}^{-3} and x_{mp}^{-5} , respectively, in the limit as x_{mp} approaches infinity.

26

Nevertheless, these integrals must be calculated numerically with some care and with proper treatment of the singularities. These techniques are discussed in the next chapter in more detail.

2.8   SYMMETRY CONSIDERATIONS FOR $n = 2$

For two-bladed rotors, it is possible to separate symmetric and antisymmetric perturbation modes since the resulting eigenmatrix is symmetric. No such simple reduction in the order of the problem can be made for rotors with more than two blades, as the symmetry of the eigenmatrix is lost. The procedure is as follows: define x_1 and x_2 as the perturbation vectors for the first and second helix, respectively;

$$\text{that is,} \quad \underline{x}_1 \triangleq \begin{bmatrix} \delta \hat{r}_1 \\ r \delta \hat{\phi}_1 \\ \delta \hat{z}_1 \end{bmatrix} \qquad \text{and} \qquad \underline{x}_2 \triangleq \begin{bmatrix} \delta \hat{r}_2 \\ r \delta \hat{\phi}_2 \\ \delta \hat{z}_2 \end{bmatrix}$$

and $\quad \underline{x} \triangleq \begin{bmatrix} x_1 \\ x_2 \end{bmatrix}$ as the perturbation vector of the matrix

equation $\quad \lambda \underline{x} = \underline{\underline{A}} \, \underline{x}.$ Equations 13, 14, and 15 show

that $\quad \lambda \triangleq \frac{2\pi \alpha r^2}{\Gamma}.$

The eigenmatrix $\underline{\underline{A}}$ can be written in the form

$$\underline{\underline{A}} = \begin{bmatrix} \underline{\underline{A}}_{11} & \underline{\underline{A}}_{12} \\ \underline{\underline{A}}_{21} & \underline{\underline{A}}_{22} \end{bmatrix}$$

where $\underline{\underline{A}}_{11}$ and $\underline{\underline{A}}_{22}$ are 3x3 matrices and represent self induction for the first and second helix, respectively. $\underline{\underline{A}}_{12}$ and $\underline{\underline{A}}_{21}$ are the 3x3 matrices representing the mutual-inductance effects.

27

The eigenvalue equations can be expanded in the form

$$\lambda \underline{x}_1 = \underline{\underline{A}}_{11} \underline{x}_1 + \underline{\underline{A}}_{12} \underline{x}_2$$

$$\lambda \underline{x}_2 = \underline{\underline{A}}_{21} \underline{x}_1 + \underline{\underline{A}}_{22} \underline{x}_2$$

Consider a class of perturbations in which disturbance motions in one helix are repeated on another, but not necessarily at the same time. This kind of disturbance can be investigated by imposing the relationship $\underline{x}_1 = e^{i\Phi} \underline{x}_2$. In these circumstances, the above two equations remain compatible, since $\underline{\underline{A}}_{11} = \underline{\underline{A}}_{22}$ and $\underline{\underline{A}}_{12} = \underline{\underline{A}}_{21}$. Three eigenvalues can then be solved

from

$$\lambda \underline{x}_2 = e^{i\Phi} \underline{\underline{A}}_{21} \underline{x}_2 + \underline{\underline{A}}_{22} \underline{x}_2 = (e^{i\Phi} \underline{\underline{A}}_{21} + \underline{\underline{A}}_{22}) \underline{x}_2$$

These eigenvalues will give maximum and minimum amplification rates for certain values of Φ. In Figure 2, divergence rates are plotted against the phase difference Φ. For $\Phi = 0$ or 2π, $\underline{x}_1 = \underline{x}_2$; for $\Phi = \pi$, $\underline{x}_1 = -\underline{x}_2$. Thus, these are cases of

special symmetry: in the first case, perturbations in the two helices are of same magnitude and occur in same direction simultaneously; in the second case, they are of the same magnitude but occur in opposite directions at the same time.

These special cases have been incorporated in the computer program for the increased efficiency afforded by that option. The full eigenmatrix, which does not involve the special symmetry combinations described above, has also been calculated for the two helix cases, and the results are identical.

CHAPTER 3

COMPUTER PROGRAM

3.1 GENERAL DESCRIPTION

The computer program for the stability analysis consists of a
main program and integration and eigenvalue-analysis subrou-
tines. The main program has three significant subparts, which
can be described as follows. The first part deals with treat-
ment of singularities for the self-induction integrals. The
second part deals with integration and with obtaining the per-
turbation equations. The third part is that used for eigen-
value and eigenfunction determination and printout. The three
subparts of the main program and the subroutines will be des-
cribed separately in more detail in subsequent sections.

The program is written in FORTRAN IV language and has been run
on an IBM360/65 computer. Double precision, i.e., operation
with 16 significant digits, has been used in the integration
and in the portion of the program eliminating the singularity.
The rest of the program and subroutines are in single preci-
sion, i.e., operations in which 8 significant digits are car-
ried. Wherever a "substitute function" approximation has been
made, numerical checks have been made to insure that a more
complete approximation would not change the eigenvalues to
within the last 5 significant digits. A block diagram for the
computer program is shown in Figure 3.

3.2 TREATMENT OF SINGULARITIES IN THE SELF-INDUCTION INTEGRALS

As explained in Section 2.3.2, the singularities in self-induc-
tion integrals have been eliminated by considering that the
vortex cores have a finite size. That is, the term

$$J_{pp}^{-3/2} = \left[2r^2 - 2r^2 \cos(x_{pp} + \psi_{pp}) + k^2 r^2 x_{pp}^2 \right]^{-3/2}$$

has been changed to $J_{pp}^{-3/2} = \left[2r^2 - 2r^2 \cos(x_{pp} + \psi_{pp}) + k^2 r^2 x_{pp}^2 + \varepsilon_o^2 \right]^{-3/2}$.

Although classical singular behavior of the integral has been
eliminated by this modification, the integral is still quite
sensitive to numerical evaluation. Figures 4 and 5 show some
of the integrands which occur in the perturbation equations.
The former exhibits near singular behavior at $x_{mp} = 0$.

29

As noted earlier, numerical evaluation of the integrals has been accomplished by adding or subtracting functions which can eliminate the troublesome near-singular behavior of the integrands and which can themselves be integrated in closed form. The following are eight such integrals which have been found useful in dealing with numerical difficulties, together with their analytically integrated values.

Denote
$$a^2 \triangleq \frac{\varepsilon^2}{(1+k^2)}$$

and
$$z \triangleq \sinh^{-1}\left(\frac{xU}{a}\right)$$

where xU = some upper limit to be chosen.

$$I_1 = (1+k^2)^{-3/2} \int_0^{xU} \frac{dx}{(x^2+a^2)^{3/2}} = \frac{(1+k^2)^{-3/2}}{a^2}\tanh z = \frac{1}{\varepsilon^2\sqrt{1+k^2}}\tanh z$$

$$I_2 = (1+k^2)^{-3/2} \int_0^{xU} \frac{x\,dx}{(x^2+a^2)^{3/2}} = \frac{1}{(1+k^2)}\left[\frac{1}{\varepsilon} - \frac{1}{\{(1+k^2)(xU)^2+\varepsilon^2\}^{1/2}}\right]$$

$$I_3 = (1+k^2)^{-3/2} \int_0^{xU} \frac{x^2\,dx}{(x^2+a^2)^{3/2}} = (1+k^2)^{-3/2}\left[z - \tanh z\right]$$

$$I_4 = (1+k^2)^{-5/2} \int_c^{xU} \frac{dx}{(x^2+a^2)^{5/2}} = \frac{1}{\varepsilon^4(1+k^2)^{1/2}}\left[\tanh z - \frac{1}{3}\tanh^3 z\right]$$

$$I_5 = (1+k^2)^{-5/2} \int_0^{xU} \frac{x\,dx}{(x^2+a^2)^{5/2}} = \frac{1}{3(1+k^2)}\left[\frac{1}{\varepsilon^3} - \frac{1}{\{(1+k^2)(xU)^2+\varepsilon^2\}^{3/2}}\right]$$

$$I_6 = (1+k^2)^{-5/2} \int_0^{xU} \frac{x^2\,dx}{(x^2+a^2)^{5/2}} = \frac{1}{3a^2}\left[\tanh^3 z\right]$$

$$I_7 = (1+k^2)^{-5/2} \int_0^{xU} \frac{x^3\,dx}{(x^2+a^2)^{5/2}} = \frac{1}{(1+k^2)^2}\left[\frac{2}{3\varepsilon} - \frac{1}{\{(1+k^2)(xU)^2+\varepsilon^2\}^{3/2}} + \frac{\varepsilon^2}{3\{(1+k^2)(xU)^2+\varepsilon^2\}^{3/2}}\right]$$

$$I_8 = (1+k^2)^{-5/2} \int_0^{xU} \frac{x^4\,dx}{(x^2+a^2)^{5/2}} = \frac{1}{(1+k^2)^2}\left[z - \tanh z - \frac{1}{3}\tanh^3 z\right]$$

30

In Figure 6, the dashed curve II shows the plot of one of the singular integrals plotted after subtracting these analytical functions in the range 0 to 2π. Since x_u is an arbitrary upper limit on the above integrals, it is chosen such that the addition and subtraction mentioned above will be carried out only in the region where the original integrand is nearly singular.

It can be seen that, for small values of x_{pp}, the modified function

$$J_{pp} \cong [2r^2 - 2r^2(1 - \tfrac{1}{2}x_{pp}^2) + k^2 r^2 x_{pp}^2 + \varepsilon_o^2]$$

$$\cong [(1+k^2)r^2 x_{pp}^2 + \varepsilon_o^2] = (1+k^2)[r^2 x_{pp}^2 + \frac{\varepsilon_o^2}{(1+k^2)}]$$

Similarly, if in the numerator one makes the approximation $\cos x_{pp} \cong 1$ and $\sin x_{pp} \cong x_{pp}$, the perturbation integrals take the form of one of the integrals I_1 to I_8. Therefore, the perturbation integrals behave like integrals I_1 to I_8 in the neighborhood of $x_{pp} = 0$. Some idea of the errors involved in this approximation is gained by the comparison of perturbation integrand and modified perturbation integrand plotted in Figure 6.

The analytical integrals used to remove near-singular behavior labeled I_1 to I_8 and mentioned in the previous section have been denoted by symbols $co(1)$ to $co(8)$ in the computer program. The integrand of the perturbation integrals is thus modified by subtracting $co(1)$ to $co(8)$ from the appropriate integrands. The upper limit, x_u, on the integrals I_1 to I_8 has been chosen to be 2π; beyond this, the perturbation integrals behave sufficiently smoothly to be amenable to standard numerical techniques.

M is the parameter which selects the overall integration limits on the perturbation integrals; $M = 1$ corresponds to semi-infinite integration limits, while $M = 2$ corresponds to doubly infinite integration limits.

The process of integrating the modified nonsingular expressions was tested by calculating some sample integrands against increasing x_{mp}, to determine a reasonable cutoff upper limit for infinite integrals. This limit is dependent upon the pitch of the helix. For a pitch of less than 0.2 radian, the integration has been performed up to $100\pi \simeq 314$ radians. For pitch values between 0.2 and 0.4 radian, the cutoff upper limit was set at 70π. Finally, the cutoff limit for values of pitch ranging between 0.4 and 1.0 is 50π. Increasing the cutoff limit beyond the values specified above does not change eigenvalues to within five digits.

A combination of two numerical integration methods has been

31

used to balance accuracy and computer time. Since the major contributions to the integral are made when x_{mp} is small, a double precision Simpson's rule [see, for example, Hildebrand, Reference 22] has been used with an interval size limit of 14π. Between 14π and the appropriate cutoff upper limit, a double precision quadrature integration has been used. The quadrature integration technique is much faster, although less accurate. Parameter $L1$ of the main program preselects between the two separate sets of integration subroutines. Also, the parameter $LL1$ of the main program stops modifying the singular integrals beyond an upper limit of $xv = 2\pi$.

A short note regarding the quadrature integration technique is perhaps of some value. To compute

$$y = \int_{a_0}^{b_0} f(x)\, dx$$

by Gaussian quadrature formula, an n point expansion in terms of Legendre polynomials is used. First, transforming the range $x = a_0$ to b_0 into $\tau = -1$ to $+1$ by defining

$$\tau \triangleq \frac{2x - (a_0 + b_0)}{(b_0 - a_0)} \qquad \text{or} \qquad x = \frac{b_0 - a_0}{2}\tau + \frac{b_0 + a_0}{2}$$

there results

$$y = \frac{b_0 - a_0}{2} \int_{-1}^{+1} \phi(\tau)\, d\tau \qquad \text{with} \qquad \phi(\tau) = f\left(\frac{b_0 - a_0}{2}\tau + \frac{b_0 + a_0}{2}\right)$$

Using

$$\int_{-1}^{1} \phi(\tau)\, d\tau = \sum_{k=1}^{n} \left[A_k^{(n)} \phi(t_k^{(n)}) \right]$$

for some given n with coefficients $A_k^{(n)}$ and nodes $t_k^{(n)}$ (note that $t_k^{(n)}$ are the roots of Legendre polynomials of degree n), the result is the approximation

$$y_n = (b_0 - a_0) \sum_{k=1}^{n} \left\{ \frac{A_k^{(n)}}{2} f\left[(b_0 - a_0)\frac{t_k^{(n)}}{2} + \frac{b_0 + a_0}{2}\right] \right\}$$

which is exact whenever $f(x)$ is a polynomial up to the degree $2n-1$.

32

In the present program the subroutine QG9 evaluates the integrals by means of a 12-point Gaussian quadrature formula which integrates polynomials up to degree 23 exactly. This subroutine is based on DQG12 taken from IBM publication System/360 Scientific Subroutine Package, Version III, Programmer's Manual. The nodes $t_k^{(n)}$ and coefficients $A_k^{(n)}$ used in QG9 are listed in Krylov [Reference 23]. IBM-supplied Scientific Subroutine Package DQG12 has been modified to collaborate with subroutine INTG, which supplies the integrand functions.

Test programs were run to check the convergence of integrated values. The upper limit on Simpson's rule, integration, the range of integration in one step of the Gaussian quadrature formula, the interval size in Simpson's rule, and the upper cut-off limits for the infinite integrals were all varied till the eigenvalues converged to five-digit accuracy for the range of parameters in the program.

3.3   FORMULATION OF EIGENVALUE EQUATIONS

The perturbation equations of Section 2.6 are a set of eigenvalue equations consisting of the growth rate terms on some p^{th} vortex. These growth rate terms are dependent upon the self-induced velocities due to perturbations in the position of the pth vortex and the velocities induced by the remaining $(n-1)$ vortices. Note that mutual-inductance terms influence the pth vortex in two ways: first, by affecting the growth rate of perturbations on the pth vortex due to velocity changes induced by deformations of the vortices other than the pth vortex; and second, by inducing zeroth-order velocities on the pth vortex which affects growth rate terms involving perturbations of the pth vortex itself.

The terms associated with the mth vortices and contributing to the growth rate of the pth vortex differ from each other through the constant $\Psi_{mp} = \Psi_m - \Psi_p$; values of this constant are

33

tabulated for each p and m in Table I. Each value of p and m corresponds to contributions of the perturbations of the

m^{th} vortex to the growth rate of the pth vortex. This contribution is accounted for in terms of a 3x3 matrix. It will not, however, be necessary to obtain, numerically, all $n \times n$ sets of 3x3 matrices.

Since the effect of some m^{th} vortex on the pth vortex is dependent only upon the difference $\Psi_m - \Psi_p = \Psi_{mp}$ rather than either

Ψ_m or Ψ_p, the resulting symmetry considerations reduced the

numerical work considerably. All the diagonal elements in Table I correspond to $\Psi_{mp} = 0$; therefore, there is one

such 3x3 matrix, representing self-induction effects in the three coordinate directions. All the super-diagonal elements correspond to the mutual inductance terms [$p=1$, $m=2$; $p=2$, $m=3$; . . .; $p = n-1$, $m = n$] and have $\Psi_{mp} = \frac{2\pi}{n}$. These also need only be evaluated once instead of $(n-1)$ times. It follows that in order to obtain the complete system of eigenvalue equations, only $(2n-1)$ set of separate calculations need be made.

All of these reductions in the number of additional evaluations of eigenmatrix elements occur whether semi-infinite or doubly infinite vortices are considered. Further reductions in the number of calculations which must be performed are possible for the doubly infinite case, i.e., where $M = 2$, and such simplifications have been taken advantage of in the present investigation. Where the integration is from $-\infty$ to $+\infty$, all <u>odd terms*</u> drop out. Thus, for the $M=2$ case, calculations for $-\Psi_{mp}$ and result in the same 3x3 matrix. In all the analyses in this report, therefore, the eigenvalue matrices are psuedosymmetric; that is, they are symmetric if one considers that the 3x3 submatrices are the eigenvalue matrix elements.

This set of n calculations is carried out by the computer program in terms of n values of the parameter K, as shown in Table II; the value of K corresponds to the number of matrix elements that must be calculated.

---

* Here "odd terms" refer to those which change sign in crossing zero on the axis of integration.

	m=1	m=2	m=3	- - -	m=n-1	m=n

TABLE I. VALUES OF $\Psi_{mp} = \Psi_m - \Psi_p$, THE PHASE DIFFERENCE CONSTANT FOR n-BLADED ROTOR

	m=1	m=2	m=3	- - -	m=n-1	m=n
p=1	0	$2\pi/n$	$4\pi/n$	- - -	$\dfrac{2\pi(n-2)}{n}$	$\dfrac{2\pi(n-1)}{n}$
p=2	$-2\pi/n$	0	$2\pi/n$	- - -	$\dfrac{2\pi(n-3)}{n}$	$\dfrac{2\pi(n-2)}{n}$
p=3	$-4\pi/n$	$-2\pi/n$	0	- - -	$\dfrac{2\pi(n-4)}{n}$	$\dfrac{2\pi(n-3)}{n}$
$\vdots$	$\vdots$	$\vdots$	$\vdots$	0	$\vdots$	$\vdots$
p=n-1	$-\dfrac{2\pi(n-2)}{n}$	$-\dfrac{2\pi(n-3)}{n}$	$-\dfrac{2\pi(n-4)}{n}$	- - -	0	$2\pi/n$
p=n	$-\dfrac{2\pi(n-1)}{n}$	$-\dfrac{2\pi(n-2)}{n}$	$-\dfrac{2\pi(n-3)}{n}$	- - -	$-2\pi/n$	0

$\Psi_m = \dfrac{2\pi(m-1)}{n}$; m = 1 to n

$\Psi_p = \dfrac{2\pi(p-1)}{n}$; p = 1 to n and $\Psi_{mp} = \Psi_m - \Psi_p$

TABLE II. NO. OF MATRIX ELEMENTS RESULTING FROM EACH CALCULATION K				
K	ψ_{mp}	p	m	No. of matrix elements resulting from this set of calculations
1	$\dfrac{2\pi(n-1)}{n}$	1	n	1
2	$\dfrac{2\pi(n-2)}{n}$	1 2	n-1 n	2
n-1	$\dfrac{2\pi}{n}$	1 2 . . n-1	2 3 . . n	n-1
n	0	1 2 . . n	1 2 . . n	n

3.4   EIGENVALUE ANALYSIS

For a set of n vortex helices, the perturbation equations are a set of $n \times n$ self- and mutual-inductance effects. Each of these $n \times n$ components in turn is a 3x3 matrix involving perturbations in the r, ϕ and z directions. The resulting perturbation equations, therefore, constitute a $3n \times 3n$ eigenmatrix, which must be solved to conduct the stability analysis. Each 3x3 matrix has complex elements. As suggested by use of the term "psuedo-symmetric" in the previous section, although the $n \times n$ array of matrix elements is symmetric, when the 3x3 matrix elements are inserted, the $3n \times 3n$ stability matrix is not symmetric.

The eigenmatrix equation which expresses the conditions for solution of admissible perturbation growth rates can be written as

$$\lambda \underline{x} = \underline{\underline{A}} \, \underline{x}$$

where $\underline{x}$ = $3n \times 1$ vector corresponding to the $3n$ perturbation displacement components.

36

$\underline{A}$ = nonsymmetric 3nx3n matrix with complex elements.

λ = eigenvalues of the above matrix equation; a set of 3n complex quantities, related to the dimensional growth rates and wave velocities of the perturbations, i.e., the complex quantity, α , by $\lambda = \frac{2\pi\alpha r^2}{\Gamma}$.

Solving this perturbation equation is a substantial task even with the help of a digital computer. $\underline{A}$ is nonsymmetric, has complex elements, and has the order 18x18 for a six-bladed rotor.

Considerable effort was expended in attempts to simplify the above matrix equation. Section 2.8 describes one such simplification for a two-bladed rotor. This, however, cannot be generalized for three-, four-, five-, and six-bladed rotors, since the structure of the eigenvalue matrix, $\underline{A}$, does not permit a transformation of the type

$$\underline{y}_p = \sum_{k=1}^{n} q_{kp} \underline{x}_k$$

where $\underline{y}_p$ = a new perturbation vector ($\delta r_p, r\delta\phi_p, \delta z_p$) for the vortex.

$\underline{x}_k$ = a perturbation vector ($\delta r_k, r\delta\phi_k, \delta z_k$) for the vortex.

q_{kp} = a set of scalars.

The subroutine labled 'ALLMAT' has been used to determine eigenvalues and eigenvectors. 'ALLMAT' is a FORTRAN IV subprogram that calculates the right eigenvalues* and/or eigenvectors of arbitrary complex matrices, using the QR algorithm and the Wielandt inverse power method for vectors.

Some discussion concerning the suitability of this subroutine, the technique used for calculations, and its numerical stability seems pertinent. The theoretical background for the QR algorithm may be found in numerical analysis texts, for example, Ralston [Reference 24] and Acton [Reference 25]. The function of the QR algorithm is to decompose an arbitrary, nonsymmetric complex matrix $\underline{A}$ into a product $\underline{Q}\underline{U}$, where $\underline{Q}$ is unitary and $\underline{U}$ is upper triangular. Since this method utilizes unitary

---

* If $\underline{A}$ is a nonsymmetric complex matrix and $\underline{A}^H$ denotes its Hermitian transpose, right eigenvectors $\underline{x}_i$ and left eigenvectors $\underline{y}_j$ are defined by relations $\underline{A}\underline{x}_i = \lambda_i \underline{x}_i$ and $\underline{y}_j^H \underline{A} = \lambda_j \underline{y}_j^H$ respectively.

transformations, as opposed to triangular decomposition, it tends to be numerically stable. An alternate approach to treating the complex matrix eigenvalue problem is to reduce the problem to one involving real matrices. This technique, however, doubles the order of the matrix, and for large-order matrices it is generally preferable to treat a complex matrix directly.

The complex subroutine 'ALLMAT' calculates the full set of eigenvalues ($3n$ in number), after the eigenmatrix elements have been evaluated for the specified values of the parameters k (pitch), ω (wave number of the perturbations) and ε (vortex core size specified as a fraction of helix diameter or radius) for an n-bladed rotor. These eigenvalues, in general, are complex. The real part of the eigenvalues determines the decay or the growth rates of the perturbations, thereby showing stability or instability, respectively. Positive real eigenvalues are, of course, unstable while negative real eigenvalues are stable. Eigenvalues with zero real parts are "neutrally stable". It is sufficient, therefore, to examine the eigenvalue with maximum real part to determine stability. The imaginary parts of the eigenvalues define the direction of propagation of the disturbances. An eigenvalue with a negative imaginary part corresponds to disturbances propagating in the positive θ direction.

The stability analysis results obtained in this study indicate that there are in all cases disturbances travelling in several directions with positive, negative and zero growth rates. In a linear stability analysis such as this, the unstable modes with the largest divergence rates very quickly dominate the disturbance shapes and determine the shape of the resulting distorted helices.

CHAPTER 4

RESULTS

4.1   GENERAL

This chapter presents three distinct kinds of material. The
first consists of a discussion of the selection of cases and a
physical description of the modal deflections. These are
contained in Sections 4.2 and 4.3. The second
consists of the results for special cases which were selected
to help verify the theory and increase confidence in the
numerical methods used in the present investigation. This
material is contained in Sections 4.4 through 4.6. The third
kind of material is comprised of results for two-, three-,
four-, five-, and six-bladed rotors for various specific values
of parameters of interest, such as the pitch of the helix,
the wave number of perturbations, and core size. These results
are presented in Sections 4.7 and 4.8 .

There is very little experimental evidence against which to
check the predictions carried out in the present investigation
of wake stability. However, some qualitative experimental
results have been reported by Landgrebe [Reference 11] using a
rotor model hover test facility. The object of Landgrebe's
experiment was to measure the effect of parameters such as
number of blades, blade linear twist, blade aspect ratio,
rotor tip speed and collective pitch on rotor hover performance
and the associated wake geometry characteristics. Flow visual-
ization data were obtained by injecting smoke, and wake
photographs and high-frame-speed movies were taken. Examination
of the photographic results leads to the qualitative conclusion
that the far-wake region of a hovering rotor is unstable or,
at best, neutrally stable. These conclusions do not, at least,
contradict the results of the present investigation.

4.2   SELECTION OF CASES TO BE RUN

In this section representative values of the pitch of the
helix have been calculated under hovering conditions. Glauert,
for example [Reference 1], and Payne [Reference 26] give the
following equation for the induced velocity at the rotor in
vertical flight.

$$(V_c + \upsilon_i)\,\upsilon_i = \frac{D/L}{2\rho}$$

where V_c = climb velocity.

v_i = increase in velocity at the actuator disc (induced velocity).

D_L = disc loading.

ρ = mass density of air = 0.0023 slug/ft^3 (sea level, std. day).

In hover, V_c = 0; therefore, $v_i = \sqrt{\frac{D_L}{2\rho}}$. The downward axial velocity in a fully developed slipstream V_z is given by

$$V_z = 2v_i = \sqrt{\frac{2\,D/L}{\rho}}$$

Typical helicopter disc loadings vary from 2 to 10 lb/ft^2, and typical tip speeds range from 500 to 700 ft/sec.

Thus, since average axial downwash velocity is given by

$$V_z = \sqrt{\frac{2(D_L)}{\rho}}$$

typical values vary from 40 ft/sec to 95 ft/sec.

A period for one rotor revolution is $T = \frac{2\pi}{\Omega}$, and axial displacement for one turn of the helix is $z = kr\theta = kr(2\pi)$.

Therefore,

$$\frac{2\pi}{\Omega} V_z = kr\,2\pi$$

or

$$k = \frac{V_z}{\Omega r} = \frac{\text{axial downwash speed}}{\text{tip speed of rotor}}$$

Thus values of pitch of the wake helix corresponding to typical disc loadings and tip speeds will vary from

$$\frac{40}{700} \approx 0.05 \quad \text{to} \quad \frac{95}{500} \approx 0.20$$

40

Although, as shown above, the pitch of the vortex helices corresponding to the normal extremes of hovering rotor operating conditions lies approximately between 0.05 and 0.20, the majority of results obtained here are for pitch equal to 0.1 radian. The ratio of vortex core diameter to the helix diameter, labeled in the tables given in this report as " core size", is, however, considerably more difficult to relate to reality. A paucity of experimental results or other evidence exists regarding actual vortex core size of the helices in the wake of a hovering rotor. The ratio of core radius to helix radius has been chosen here to be 0.1, following Widnall, and some cases have also been for this nondimensional core size equal to 0.33 to investigate the effect of core size on vortex stability. Perturbation wave numbers have been examined from 0.25 (long wavelengths) to 8.0 (short wavelengths), including the wave number of 0.0. Perturbation wavelengths which are very short compared to the helix diameter are likely to occur if the disturbances are concentrated and would seem to involve changes of vortex core cross section in the plane perpendicular to the helical filament centerline. Thomson [Reference 27], however, has shown that so long as the radius of the cross section of the core in the plane perpendicular to the filament centerline is small compared with the radius of curvature of that centerline, the cross section will remain approximately circular under the self-influence of the whole vortex. This same observation has been made by Widnall in her study of short wave perturbation instability modes of planar circular vortex rings [Reference 28]; however, a cutoff at rather large wave numbers was used to limit the extent of the stability curves in Reference 16. The core diameter ratio of 0.10 satisfies the assumption that the core size is small compared to helix radius; 0.33 does not. For the highest wave numbers, i.e., 8.0, even a core which is 0.1 helix diameter is hardly small compared to a wavelength of 0.393 helix diameter. Thus, in Figures 14 through 19 a wave number limit of about 8.0 is arbitrarily shown.

4.3   PHYSICAL DESCRIPTION OF MODAL DEFLECTIONS

A clear picture of modal perturbations will provide increased insight into instability mechanisms. The type of vector perturbations introduced in Section 2.6 is represented by

$$\vec{\delta r}_m = \vec{\hat{\delta r}}_m \, e^{\alpha t + i \omega \theta_m'}$$

This deflection, of course, has components in r, ϕ and z directions. To visualize the deflections associated with certain wave numbers, consider a deformation of the type $\delta r = \hat{\delta r} \cos(\omega \theta) \cdot e^{\alpha t}$

41

where δr = perturbation in r direction.

$\hat{\delta r}$ = amplitude of the perturbation.

ω = the wave number.

The real parts of distortion modes in axial and circumferential directions can similarly be written as

$$\delta\phi = \hat{\delta\phi} \; [\cos \omega \theta] \; e^{\alpha t}$$

and

$$\delta z = \hat{\delta z} \; [\cos \omega \theta] \; e^{\alpha t}$$

Once the eigenfunctions $\hat{\delta\phi}$ and $\hat{\delta z}$ are known, the distorted shapes of the helices in these directions can be calculated for the corresponding wave number, ω .

Dilatational Mode, $\omega = 0$

For $\omega = 0$,

$$\delta r = \hat{\delta r} \; e^{\alpha t}$$
$$\delta\phi = \hat{\delta\phi} \; e^{\alpha t}$$
$$\delta z = \hat{\delta z} \; e^{\alpha t}$$

Since this perturbation is independent of θ, it is uniform throughout space. Whereas the z and ϕ coordinates simply change the position of given helix with respect to coordinate axes, the radial perturbations expand or contract the diameter of the vortex helix uniformly. The unperturbed helix is shown in Figure 1, and a dilatational mode disturbance is shown in Figure 7. Note that to simplify sketches of distorted wake shapes, in all cases, perturbations will be shown in only one direction in any one sketch. This can be done without sacrificing generality, so long as the reader keeps in mind that reference to more than one figure will generally be required to visualize a given modal deflection. Since this dilatational mode distorts the helix from its initial configuration only by uniform diameter changes, it is a disturbance which,

42

in a nondimensional sense, changes the helix pitch angle
without changing the basic helical shape.

Deformation Mode for $\omega = 1$

For $\omega = 1$, the deformation shape can be pictured by noting that
at

$$\theta = 0 \quad ; \quad \delta r = \delta \hat{r} e^{\alpha t}, \quad \delta z = \delta \hat{z} e^{\alpha t}, \quad \delta \phi = \delta \hat{\phi} e^{\alpha t}$$

$$\theta = \frac{\pi}{2} \quad ; \quad \delta r = 0 \quad , \quad \delta z = 0 \quad , \quad \delta \phi = 0$$

$$\theta = \pi \quad ; \quad \delta r = -\delta \hat{r} e^{\alpha t}, \quad \delta z = -\delta \hat{z} e^{\alpha t}, \quad \delta \phi = -\delta \hat{\phi} e^{\alpha t}$$

$$\theta = \frac{3\pi}{2} \quad ; \quad \delta r = 0 \quad , \quad \delta z = 0 \quad , \quad \delta \phi = 0$$

These deformations are sketched in Figures 8 and 9.
As shown in the top and side views, there is some deformation
of the initial circular shape of the helix as a result of
perturbations in r direction, but in the main, it represents
a relatively undistorted translation in a direction normal to
the centerline axis of the helix. In the z- direction, however,
these deformations amount to a tilting of the coils relative
to the axis of the helix. This point has been elaborated
in Section 4.4. Deformations in the ϕ or circumferential sense
mainly stretch or compress the helical vortex line, and since
in this analysis the cross section of the vortex core (i.e.,
normal to the helical axis) has been assumed to be constant,
deformations in the circumferential sense can largely be
ignored.

Distortion Mode   Values of ω Other Than 0 or 1

Consider, for example, $\omega = 2$
at

$$\theta = 0 \quad ; \quad \delta r = \delta \hat{r} e^{\alpha t}, \quad \delta z = \delta \hat{z} e^{\alpha t} \quad , \quad \delta \phi = \delta \hat{\phi} e^{\alpha t}$$

$$\theta = \pi/2 \quad ; \quad \delta r = -\delta \hat{r} e^{\alpha t}, \quad \delta z = -\delta \hat{z} e^{\alpha t} \quad , \quad \delta \phi = -\delta \hat{\phi} e^{\alpha t}$$

$$\theta = \pi \quad ; \quad \delta r = \delta \hat{r} e^{\alpha t}, \quad \delta z = \delta \hat{z} e^{\alpha t} \quad , \quad \delta \phi = \delta \hat{\phi} e^{\alpha t}$$

$$\theta = 3\pi/2 \quad ; \quad \delta r = -\delta \hat{r} e^{\alpha t}, \quad \delta z = -\delta \hat{z} e^{\alpha t} \quad , \quad \delta \phi = -\delta \hat{\phi} e^{\alpha t}$$

The plan and side views of the helix distorted by radial and axial deformations in this mode are shown, respectively, in Figures 10 and 11. In Figure 10, the helix is shown to be distorted from circular to elliptic. In Figure 11, the distortions change the projections of the helical turns from straight lines to sickle-shaped curves, which are all either concave upward or concave downward, depending upon the sign of the deformation in the z direction.

Other Possible Distortion Modes

Distortion forms corresponding to higher integer and noninteger wave numbers can be similarly visualized. For example, the distorted shapes of two successive coils are quite different when $\omega = 1/2$, but such distortions are repeated after traversing every two coils of the helix. Similarly, for $\omega = 1.5$, three coils of the helix must be examined before one would expect to find a complete cycle. On the other hand, for $\omega = 3$, there will be three maximum and three minimum distortion points in one turn of helix. The $\omega = 1/2$ mode for r and z perturbations is shown in Figures 12 and 13a.

Extension of Modal Perturbation Modes to Multiple Interdigitated Helices

Each vortex helix in the array trailed by multibladed rotors can undergo the modal deformations discussed in the previous sections. In addition, however, the temporal phase relationship among the deformations in different helices provides three more possibilities of combinations of motions, one for each coordinate direction, for each additional helix. The actual phase and magnitude are determined by the eigen-solution. In the simplest possible example, two interdigitated helices may be undergoing a dilatational (i.e., $\omega = 0$) deformation, but with opposite sign, so that when one helix is expanding the other is contracting, and vice versa. Similarly, in a no-radial-deformation (i.e., $\omega = 1$) mode, the modal deformations for each helix of a two-bladed rotor may have the same sign, in which case the two helices would translate in the same direction, and the change in pitch angle would also be occurring in the same direction. In this case there would be no change in the relative positions of the two helices, one to the other. By contrast, if, in an $\omega = 1$ mode, the modal deformations of the two helices had opposite signs and equal magnitude, then the translation of each helix would be in opposite

directions and the effective pitch change of these helices would also be such as to reduce the axial distance between corresponding segments of the helices.

4.4   LEVY AND FORSDYKE CASE

The early Levy and Forsdyke analysis [Reference 15] cited earlier in this report concluded that a doubly infinite, constant-diameter helical vortex is unstable for the wave number = 1 mode when the helix pitch angle is less than 0.3 radian and is stable for pitch angles greater than 0.3 radian. Stability analyses for the same single helix case have also been carried out in the present study and have shown such a vortex to be stable in the wave number = 1 perturbation mode for all helix pitch angles. Some insight is gained by reference to the distortion shapes in this mode.

The ω =1 perturbation comes close to translating the whole helix to right, left,up,or down without much radial distortion. Such motion clearly is approximated by a change in the arbitrary choice of a coordinate axis system, and it cannot reasonably be expected to influence the tendency of the helix to distort. Such motion is depicted in Figure 8. However, deformations in the direction presented in Figure 9 for this mode are shown to be equivalent to tilting the coils relative to the axis of the helix. In this distortion, segments at any point on the helix always remain at the same distance from those segments in preceding or subsequent turns directly above and below them. With respect to their separation from vortex segments at different azimuthal stations on the helix, any given segment gets a bit closer to those on one "turn" and that same amount farther away from the corresponding segment on the next "turn". Thus, it is intuitively satisfying to find that such deformation modes are predicted to be stable.

Secondly, beyond those discrepancies in the Levy and Forsdyke results associated with the use of a planimeter, referred to earlier in this report, their evaluation of singular integrals expanded $\cos\omega$ and $\sin(x)$ terms in power series. Terms up to

x^6 were retained in the numerators and terms up to x^2 were retained in the denominators. Since the upper and lower limits of integration are 0 to $\pi/6$ and the integrands are near singular in their behavior, considerable error is introduced by this

approximation. Table III lists cases run under the present
investigation which may be compared with the results of Levy
and Forsdyke [Reference 15]. In addition, selected integrals
were calculated; most of the integrated values checked out,
but errors as high as an order of magnitude were noted in
others.

4.5   WIDNALL CASE OF SINGLE HELIX

The results recently published by Widnall [Reference 16] repre-
sent the stability of a single vortex filament of finite core
for small sinusoidal displacements of its (helical) center-
line. The singularity resulting from the self-induced motion
of the element has been removed in Reference 16 by cutting off
the integration in the region of the singularity and using a
method of matched asymtotic expansions in this region. The
solution in this region has been matched with the solution for
a plane, circular vortex ring of the same radius of curvature.
This mathematically sophisticated approach succesfully dupli-
cated the results of Betchov [Reference 29] for the case of a
vortex filament whose cross-sectional radius is very small
compared to its radius of curvature. Numerical results for
various pitch angles, core sizes and perturbation wave numbers
have been reported by Widnall.

The special case of a single helix in the present study deals
with the same physical situation as the work reported in Ref-
erence 16 but differs significantly in the treatment of
singularities, as has been mentioned in chapter 2.

The results of the single helix cases run under the present
study are plotted in Figure 14 and tabulated in Table IV
along with the corresponding results obtained by Widnall. The
table facilitates a direct comparison of the numerical results
of this analysis with those of Widnall. One observes that the
results are qualitatively similar, but that the numerical
values of maximum divergence rates differ. In a typical case,
for example, pitch = 0.1, wave number = 0.5 and core size =
0.33, Widnall predicts a divergence rate of 24.8   The corres-
ponding value in the present analysis is 7.90. Note, however,
that in the present investigation divergence rate is defined as
$\frac{r^2 2\pi\alpha}{r}$, while in the Widnall study divergence rate is taken to
be $\frac{r^2 4\pi\alpha}{r}$. Thus, for a comparison, the present value of 7.90
must be compared with (1/2)24.8 = 12.4.   Thus, to faci-
litate comparisons on the same nondimensionalized basis, the
divergence rates taken from the Widnall graphs have been divided

46

TABLE III. LEVY AND FORSDYKE CASE, COMPARISON WITH THE PRESENT STUDY				
			Stable or Unstable	
Wave Number	Core Size	Pitch	Levy/Forsdyke Study	Present Study
1.00	0.10	0.10	Unstable	Stable
1.00	0.10	0.20	Unstable	Stable
1.00	0.10	0.25	Unstable	Stable
1.00	0.10	0.30	Stable or Unstable	Stable
1.00	0.10	0.40	Stable	Stable
1.00	0.10	0.60	Stable	Stable
1.00	0.10	0.80	Stable	Stable
1.00	0.10	1.00	Stable	Stable

| TABLE IV. | CASE OF SINGLE-BLADE, DIVERGENCE RATES OBTAINED IN THE PRESENT STUDY COMPARED WITH THE VALUES OBTAINED BY WIDNALL (Ref. 16*) | | | | |

Pitch of Helix (rad)	Wave Number	Core Size = 0.1		Core Size = 0.33	
		Max. Divergence Rates in Present Study	Max. Divergence Rates Reported by Widnall	Max. Divergence Rates in Present Study	Max. Divergence Rates Reported by Widnall
0.1	0.00	~0.00	0.0 (0.0)	0.0	0.0 (0.0)
0.1	0.25	8.75	19.0 (9.5)	6.35	17.6 (8.8)
0.1	0.50	11.84	25.2 (12.6)	7.90	24.8 (12.4)
0.1	0.75	9.01	18.8 (9.4)	6.56	17.4 (8.7)
0.1	1.00	0.00	0.0 (0.0)	0.00	0.0 (0.0)
0.1	1.25	8.33	18.0 (9.0)	6.17	16.4 (8.2)
0.1	1.50	11.43	24.0 (12.0)	7.66	23.2 (11.6)
0.1	1.75	8.80	16.6 (8.3)	6.50	16.4 (8.2)
0.1	2.00	0.00	0.0 (0.0)	2.74	0.0 (0.0)
0.1	2.50	10.61	21.4 (10.7)	7.26	22.6 (11.3)
0.1	3.00	0.26	0.0 (0.0)	4.15	7.6 (3.8)
0.1	3.50	9.47	0.0 (0.0)	6.78	20.6 (10.3)
0.1	4.00	0.99	0.0 (0.0)	4.93	12.0 (6.0)
0.1	4.50	8.23	0.0 (0.0)	6.27	19.6 (9.8)
0.1	5.00	1.99	0.0 (0.0)	5.17	14.0 (7.0)
0.1	5.50	7.18	0.0 (0.0)	5.70	17.4 (8.7)
0.1	6.00	3.21	0.0 (0.0)	4.98	11.6 (5.8)
0.1	7.00	4.51	0.0 (0.0)	4.40	0.0 (0.0)
0.1	8.00	5.79	0.0 (0.0)	3.42	0.0 (0.0)

* The approximate divergence rates used in the above comparison were taken from the graphs in Ref. 16.

by a factor of 2 and written within the brackets in the same columns in Table IV. As pointed out in the previous paragraph, the results are significantly different for core size 0.33; the divergence rates compare quite closely, however, for core size 0.1. It has been noted that estimates of the core size of vortex helices in the wake of a hovering rotor are not known with any confidence, but a core diameter ratio of 0.1 would seem closer to reality than 0.33. Note that Landgrebe [Reference 11] assumed the core radius of 0.005, while Crimi [Reference 12] has used a value of 0.05 to 0.08 .

Some estimates of core size are, however, available for the vortices trailed by fixed-wing aircraft. Spreiter and Sacks [Reference 30] estimated the core diameter of vortices trailed behind elliptically loaded aircraft wings as 0.197 times the separation between the trailing vortices. The effect of curvature probably modifies the core size, but this estimate of core size falls somewhat closer to the 0.1 value used for helical vortices in the present study than it does to 0.33. For the smaller, more realistic core sizes, the present study with its different approach toward treatment of singularities in the Biot-Savart integration, appears to predict divergence rates quite comparable to the method used in the Widnall study.

4.6   S. C. CROW'S CASE (TRAILING VORTICES FROM FIXED-WING AIRCRAFT WINGS)

S. C. Crow [Reference 17] presents an analysis of the stability of a pair of straight, parallel vortices as trailed from a fixed-wing aircraft. This analysis also gives rise to an eigenvalue problem for the growth rate of sinusoidal perturbations.

If the pitch is allowed to approach infinity in the present study for the case of a two-bladed rotor, the wake should correspond to two straight, parallel infinite vortices. It is shown in Appendix I that the perturbation equations used here, taken to this limit, yield the same expressions as S. C. Crow's case, except for the differences associated with the cutoff technique to remove singularities. Incidentally, P. C. Parks [Reference 20] has duplicated S. C. Crow's results by modifying the self-induction integrals in lieu of "cutting off". Parks' integration to eliminate the effects of singular integrals yields the same expressions obtained in the present study, after the proper limits are taken, and has confirmed the essential features of Crow's theory with small numerical changes. Since the singularities in the self-induction integral have been removed in the present study by an approach similar to that used by P. C. Parks, it is reassuring that limiting expressions which are

49

approaching the case of trailing fixed-wing vortices do, in fact, duplicate those used by Parks.

It is a more difficult matter to attempt to duplicate S. C. Crow's quantitative results using the computer program developed in the present study, since the integration techniques used here are tailored for low values of pitch. In limiting cases where pitch is taken to be very large, the sine and cosine terms in the perturbation equations oscillate very rapidly, and the integrated values using the current numerical techniques are inappropriate for obtaining accurate results. Two cases, however, have been run, and the results are tabulated in Table V.

4.7   DISCUSSION OF RESULTS

Single Helix

The single-blade case was run primarily to check the present work against the results of Levy and Forsdyke [Reference 15] and Widnall [Reference 16]. The comparisons have been discussed in the preceding sections. Further consideration of the single helix case will be limited here to a discussion of the perturbation deflection shapes and their influence on helix stability. As shown in Figure 14, the single helix has no instabilities for wave numbers $\omega = 0$ and $\omega = 1$. Figures 7, 8, 9 and 13d show that radial and axial deflections for these two deformation modes have two characteristics in common: first, the circular cross section seen in the plan views is largely preserved, and second, axial separation between vortex segments at corresponding circumferential positions is preserved in the deformations. In terms of the Biot-Savart law of induction, it is clear that changes of the helix diameter, so long as they are uniform around the circumference, will cause uniform changes of induced effects. Further, if such deformations are repeated without change on every helix coil, then induced effects associated with changes in helix diameter will not distort the helix, but will simply cause the entire helix to translate axially. Since the choice of coordinate axes and their velocities in inertial space is completely arbitrary, it is not surprising that neither translation of the entire helix, such as exists in the plan view for $\omega = 1$, nor uniform change of the helix radius, as shown in the plan view of Figure 7 for $\omega = 0$, has any influence on the stability. Changes in the relative axial position of helix segments, however, will influence induced effects in the radial direction. For these two modes, however, there is no such change in relative position, at least among the

50

TABLE V. RESULTS OF THIS ANALYSIS FOR S. C. CROW'S CASE

Point 1				Point 2			
Eigenmatrix				Eigenmatrix			
0	0.92263	0	-0.91889	0	0.85992	0	-0.85935
-3.5407	0	-1.6991	0	-3.4780	0	-1.7587	0
0	+0.91889	0	-0.92263	0	0.85935	0	-0.85992
+1.6991	0	+3.5407	0	-1.7587	0	+3.4780	0

$\alpha_s = [(-0.92263+0.91889)(3.5407-1.6991)]^{1/2}$

$= [-ve]^{1/2}$ Stable.

$\alpha_s = [(-0.92263-0.91889)(3.5407-1.6991)]^{1/2}$

$= [-ve]^{1/2}$ Stable.

$\alpha_s = [(-0.85992+0.85935)(3.4780-1.7587)]^{1/2}$

$\cong 0$ Neutrally Stable.

$\alpha_s = [(-0.85992-0.85935)(3.4780+1.7587)]^{1/2}$

$= [-ve]^{1/2}$ Stable.

Point 1: Parameters in S. C. Crow's paper: $\beta = 2$, $\epsilon/\beta = 0.1$
Point 2: Parameters: $\beta = 0.5$, $\epsilon/\beta = 0.1$

corresponding parameters in present study

Point 1: Pitch = 1000, wave number = 1000, $\epsilon = 0.311$
Point 2: Pitch = 1000, wave number = 250, $\epsilon = 0.311$

Remarks: Numerical comparison of divergence rates with Crow's
results for these points has not been shown here
since the current program is not designed for such
large values of pitch and wave numbers; as a result,
the calculated values are not expected to be
accurate. The purpose of the above run is to demon-
strate the limiting behavior in the present study,
which has otherwise been shown theoretically.

vortex segments closest to one another, that is, in the same circumferential position from one coil to the next. For $\omega = 1/2$, on the other hand, as shown in the side view of Figure 12, the relative axial displacements of vortex segments at the same circumferential position do, in fact, approach each other or separate from one another. Induced effects of some importance do, therefore, exist, and any initial tendency for adjacent segments to come together will be amplified still more by the increased proximity. One would certainly expect such modes to be unstable, and they are, as shown in Figure 14.

For the $\omega = 2$ mode, the plan view changes as shown in Figure 10 from circle to ellipse. Such changes induce axial velocities which are not uniform around the circumference. Furthermore, they will be such as to cause roughly the same displacement changes as seen in the side view of modal perturbations shown in Figure 10. These are not very strong effects, however, since for every pair of opposite segments which come together in the sense seen in the plan view (and thereby increase their mutually induced effects), there are two other segments which are farther apart, not just from each other, but from the first pair. Since the induced effects of the latter pair on the first pair are reduced, there are tendencies toward compensation. The separation distance is in the denominator of the Biot-Savart law, however, so that such effects are not linear. This possibly explains why the divergence rate in the $\omega = 2$ mode is less stable for the single helix whose vortex core diameter ratio is .33 than it is for the case where this parameter is .1, as shown in Figure 14.

Finally, Figure 11 shows that the modal perturbation for $\omega = 2$ preserves the axial separation between points at corresponding circumferential locations on the single helix.

Multiple-Bladed Rotors

It is important to note that the solution method for multiple-bladed rotors is identical to that for a single helix; namely, a wave number, ω, is selected, and the eigenmatrix is solved numerically for the values of λ which determine the divergence rates corresponding to the perturbation modes associated with that value of ω. There is, of course, an eigen deformation mode associated with each eigenvalue, λ. Components of the eigen mode for the single helix are the complex values of $\delta \hat{r}$, $\delta \hat{\phi}$ and $\delta \hat{z}$. Since the multibladed rotor introduces additional degrees of freedom, for the case of a rotor with n blades there are n sets of eigenvectors, $\delta \hat{r}_{i\lambda}$, $\delta \hat{\phi}_{i\lambda}$ and $\delta \hat{z}_{i\lambda}$, where $i = 1, 2, \ldots n$, for every eigenvalue, λ. The phase relationship between motions of the blades i = 1 and i = 2 is

52

embodied in the complex values, say, of $\delta \hat{t}_{1\lambda}$ and $\hat{\delta z}_{2\lambda}$; this
phase relationship will determine whether the helix trailed
from the number 1 blade will move toward or away from the
helix trailed from the number 2 blade in the deformation eigen-
mode corresponding to λ . This phase relationship, between
motions in the same coordinate direction at corresponding
points on two different helices, cannot be known prior to solv-
ing the eigenvalue matrix. This contrasts with the case of a
single helix, for which phase relations among segments at
corresponding positions are known as soon as a value of ω is
chosen.

Numerical results for multiple-bladed rotors are tabulated in
Tables VI through X and are plotted in Figures 15 through
19. Most of these results are obtained with pitch = 0.1 and
core size = 0.1. A few cases were run for pitch = 0.15 and
core size = 0.33; these are also shown in the figures, although
the curves vs wave number are largely extrapolated, using the
curves for pitch = 0.1 and core size = 0.1 as guides.

For the case of a two-bladed rotor, the divergence rate, λ , is
plotted vs wave number, ω , in Figure 15. It is noted that
the maxima of the continuum of the divergence rate points de-
crease rather smoothly as wave number increases. Similarly the
minima of the curves increase slightly and then decrease rather
smoothly. For larger integer wave numbers, i.e., short wave-
length perturbations, the difference between minimum and
maximum divergence rates decreases as wave number increases.
Figures 20 and 21 suggest that maximum divergence rates occur
at integer wave numbers, because at these wave numbers the
segments adjacent to each other on the two helices approach
each other to the maximum extent. Minimum relative motion of
this sort seems to occur with half-integer wave numbers.
Imagining a helix from a second blade in Figure 13a with the
most favorable phase angle possible shows how little of the
vortices approach each other in such motion.

Figures 16 through 19, for three-, four-, five-, and six-bladed
rotors, respectively, exhibit similar divergence rate - wave
number relationships; i.e., the maximum and minimum divergence
rates occur at wave numbers equal to 1/2 times even-integer
multiples and 1/4 times odd-integer multiples, respectively,
times the number of blades. For example, a five-bladed rotor
exhibits maximum divergence rates at the wave numbers 2.5, 5.0
and 7.5, etc., which are 1/2, 1, and 3/2 times 5. Similarly,
minimum divergence rates for a five-bladed rotor occur at
wave numbers 1.25, 3.75 and 6.25, etc., which is 1/4, 3/4
and 5/4 times the number of blades in the rotor, namely, 5.
For three-, four-, five- and six-bladed rotors, the excursion from
the mean divergence rate also decreases with increasing wave
numbers.

53

TABLE VI. MAXIMUM DIVERGENCE RATES FOR TWO-BLADED ROTOR			
Pitch of Helix (rad)	Wave Number	Core Size	Max Divergence Rate
0.10	0.25	0.10	46.65
0.10	0.50	0.10	37.05
0.10	0.75	0.10	46.26
0.10	1.00	0.10	49.80
0.10	1.25	0.10	46.57
0.10	1.50	0.10	37.16
0.10	1.75	0.10	45.42
0.10	2.00	0.10	49.06
0.10	2.50	0.10	36.95
0.10	3.00	0.10	47.93
0.10	3.50	0.10	36.56
0.10	4.00	0.10	46.52
0.10	4.50	0.10	36.12
0.10	5.00	0.10	44.94
0.10	5.50	0.10	35.74
0.10	6.00	0.10	43.48
0.10	7.00	0.10	41.86
0.10	8.00	0.10	40.47
0.15	0.50	0.10	16.70
0.15	1.00	0.10	22.10
0.15	1.50	0.10	16.83
0.15	2.00	0.10	21.40
0.15	3.00	0.10	20.36
0.15	4.00	0.10	19.14
0.10	0.50	0.33	33.23
0.10	1.00	0.33	49.34
0.10	1.50	0.33	33.50
0.10	2.00	0.33	48.30
0.10	3.00	0.33	46.73
0.10	4.00	0.33	44.87

TABLE VII. MAXIMUM DIVERGENCE RATES FOR THREE-BLADED ROTOR			
Pitch of Helix (rad)	Wave Number	Core Size	Max Divergence Rate
0.10	0.25	0.10	113.97
0.10	0.50	0.10	100.98
0.10	0.75	0.10	78.83
0.10	1.00	0.10	94.00
0.10	1.25	0.10	115.57
0.10	1.50	0.10	123.71
0.10	1.75	0.10	116.57
0.10	2.00	0.10	96.52
0.10	2.25	0.10	79.65
0.10	2.50	0.10	96.85
0.10	3.00	0.10	115.37
0.10	3.50	0.10	99.41
0.10	3.75	0.10	79.28
0.10	4.00	0.10	90.88
0.10	4.50	0.10	114.81
0.10	5.00	0.10	95.85
0.10	5.25	0.10	79.47
0.10	5.50	0.10	89.97
0.10	6.00	0.10	108.00
0.15	0.50	0.10	45.38
0.15	1.00	0.10	41.62
0.15	1.50	0.10	54.67
0.15	2.00	0.10	43.79
0.15	3.00	0.10	50.17
0.15	4.00	0.10	38.36
0.10	0.50	0.33	97.19
0.10	1.00	0.33	93.55
0.10	1.50	0.33	120.01
0.10	2.00	0.33	95.78
0.10	3.00	0.33	114.16
0.10	4.00	0.33	89.40

55

TABLE VIII.	MAXIMUM DIVERGENCE RATES FOR FOUR-BLADED ROTOR		
Pitch of Helix (rad)	Wave Number	Core Size	Max Divergence Rate
0.1	0.25	0.1	209.37
0.1	0.50	0.1	194.22
0.1	0.75	0.1	168.98
0.1	1.00	0.1	135.16
0.1	1.25	0.1	165.99
0.1	1.50	0.1	191.69
0.1	1.75	0.1	207.28
0.1	2.00	0.1	212.87
0.1	2.50	0.1	193.32
0.1	3.00	0.1	138.17
0.1	3.50	0.1	186.24
0.1	4.00	0.1	208.16
0.1	4.50	0.1	190.05
0.1	5.00	0.1	139.94
0.1	5.50	0.1	179.51
0.1	6.00	0.1	201.23
0.1	7.00	0.1	141.21
0.1	8.00	0.1	193.23
0.15	0.50	0.1	87.25
0.15	1.00	0.1	61.20
0.15	1.50	0.1	84.72
0.15	2.00	0.1	94.52
0.15	3.00	0.1	63.58
0.15	4.00	0.1	90.31

Pitch of Helix (rad)	Wave Number	Core Size	Max Divergence Rate
0.10	0.25	0.10	332.56
0.10	0.50	0.10	315.78
0.10	0.75	0.10	288.09
0.10	1.00	0.10	250.72
0.10	1.25	0.10	219.68
0.10	1.50	0.10	252.93
0.10	1.75	0.10	282.58
0.10	2.00	0.10	307.43
0.10	2.50	0.10	340.74
0.10	3.00	0.10	311.15
0.10	3.50	0.10	256.42
0.10	3.75	0.10	220.27
0.10	4.00	0.10	242.70
0.10	4.50	0.10	302.72
0.10	5.00	0.10	327.21
0.10	5.50	0.10	307.83
0.10	6.00	0.10	253.02
0.10	6.25	0.10	220.94
0.10	7.00	0.10	290.84
0.10	7.50	0.10	316.34
0.10	8.00	0.10	298.76

TABLE IX.   MAXIMUM DIVERGENCE RATES FOR FIVE-BLADED ROTOR

TABLE X. MAXIMUM DIVERGENCE RATES FOR SIX-BLADED ROTOR			
Pitch of Helix (rad)	Wave Number	Core Size	Max Divergence Rate
0.10	0.25	0.10	483.43
0.10	0.50	0.10	465.33
0.10	0.75	0.10	435.62
0.10	1.00	0.10	395.08
0.10	1.25	0.10	358.51
0.10	1.50	0.10	318.15
0.10	1.75	0.10	353.64
0.10	2.00	0.10	390.09
0.10	2.50	0.10	459.22
0.10	3.00	0.10	485.01
0.10	3.50	0.10	462.12
0.10	4.00	0.10	396.97
0.10	4.50	0.10	318.72
0.10	5.00	0.10	381.72
0.10	5.50	0.10	445.94
0.10	6.00	0.10	472.46
0.10	7.00	0.10	394.10
0.10	8.00	0.10	370.54

In short, peak values of divergence rate occur at wave numbers, ω, equal to integer multiples times one-half the number of blades, and in all cases the magnitude of the peak divergence rate decreases with wave number.

Enveloping curves can be drawn through maximum and minimum divergence rate points in all cases. There is some absolute maximum divergence rate which occurs at the maximum of the enveloping curve through the maximum divergence rate points. For two-, four- and six-bladed rotors this absolute maximum rate occurs at wave number 0.0, i.e., for the dilatational mode. For three- and five-bladed rotors the dilatational mode is still highly unstable, but the absolute maximum divergence rate occurs at wave numbers 1.5 and 2.5 respectively, i.e., where the wave number is one-half the number of blades ($\omega = n/2$).

To assess the effect of helix pitch angle, some variations in this parameter were run for two-, three-, and four-bladed rotors. For the higher pitch angles the divergence rate drops considerably, even though the characteristic variations with wave number remain. For example, an increase in pitch of helix from 0.10 to 0.15 reduces the divergence rate by a factor of almost 2. Note that the curves for pitch = 0.15 must be read on the right scales, as also pointed out in Figures 15 through 17. Physically, this behavior can be explained in terms of interaction between the neighboring coils of the helices. For higher pitch angles the neighboring helix coils are farther apart, and distortions that tend to cause neighboring coils to approach each other therefore result in lesser interactions. Absolute maximum divergence rates for different rotors are plotted against pitch in Figure 22 and are tabulated in Table XI.

The nondimensional divergence rate of multiple-bladed rotors would seem to increase with the number of blades for the same sort of reason that it increases with decreasing pitch; namely, there is a decreased separation between successive lines of vorticity. Figure 22 shows that for a helix pitch angle of .05, for example, a two-bladed rotor has a maximum divergence rate of 200 and a four-bladed rotor has a maximum divergence rate of 850. It must be noted that these rates are nondimensionalized by total vortex strength Γ, as shown in the equation for λ on pages 27 and 37. If the sum of the blades in each rotor produced the same lift (which is the case in comparing alternate designs for the same aircraft), the vortex strength, Γ, in the two-bladed case would be twice that of the four-bladed case, so that the dimensional rates would then compare as 400 to 850. Thus, in terms of the stability of the vortices in the far wake for rotors of equal lifting capacity, the fewer blades the better.

The effect of core size on stability is not so noticeable for multiple rotors. When the core size was increased from 0.1 to

Pitch of Helix (rad)	Number of Blades	Wave Number	Absolute Maximum Divergence Rates
0.05	2	0.0	199.89
0.10			50.05
0.15			22.34
0.20			12.65
0.05	3	1.5	492.11
0.10			123.71
0.15			54.67
0.20			30.47
0.05	4	0.0	853.90
0.10			214.57
0.15			96.17
0.20			54.70
0.05	5	2.5	1363.00
0.10			340.74
0.15			150.64
0.20			84.26
0.05	6	0.0	1940.50
0.10			489.65
0.15			219.78
0.20			125.26

TABLE XI. ABSOLUTE MAXIMUM DIVERGENCE RATES FOR MULTIBLADED ROTORS OF VARYING PITCH

0.33, the amplification rate dropped only about 2% for the wave numbers with highest divergence rates in all cases where $n = 1$. Core size does appear to be an important influence on stability of a single helix, i.e., where $n = 1$, as shown in Figure 14.. Its reduced effect on the stability of multiple-bladed rotors does not seem unreasonable, since the mutual inductance between different helices is a relatively important influence on the stability of interdigitated vortex systems, whereas variations in core size are felt most in self-induction effects.

4.8 COMMENTS ON ABSOLUTE MAXIMUM WAKE DIVERGENCE RATES FOR MULTIBLADED ROTORS WITH ODD AND EVEN NUMBERS OF BLADES

This section deals with a qualitative physical explanation of absolute maximum divergence rates for multibladed rotors. First, as seen in Figures 15 through 19, these absolute maxima are associated with the $\omega = 0$ and $\omega = n/2$ modes for rotors with even and odd numbers of blades respectively. Comments in most cases will be restricted to axial perturbation displacements since the effect on induced velocities of such motions is one order of magnitude higher than either radial or circumferential perturbation displacements insofar as the mutual inductance between neighboring coils is concerned. This can be explained more explicitly as follows:

The Biot-Savart law reveals that the maximum interaction occurs between those vortex elements which are nearest to each other. For helix pitch angles less than 0.20, the parallel elements which are closest to each other are on two neighboring coils at the same circumferential position, i.e., located on the same line parallel to the axial direction. This axial distance shall be denoted by d. A radial perturbation of in the radial direction will replace d by $\sqrt{d^2 + e^2}$, and the integrand in the Biot-Savart law will be modified from d^{-3} to $d^{-3}[1 + 3e^2/d + \cdots]$,

contributing a second-order term to the perturbation integrand. However, an axial perturbation of ϵ will modify the minimum interaction distance d to $(d - \epsilon)$, contributing $(d-\epsilon)^{-3}$ in the perturbation integrand. This corresponds to a change from

d^{-3} to $d^{-3}[1 + 3\epsilon/d + \cdots]$ and is a first-order contribution. Therefore, the axial perturbation is the dominant factor in the interactions between the nearest parallel vortex elements. It follows that the divergence rate of a given deformation mode will be greater than another, if the normalized axial displacements which reduce the separation between vortex elements adjacent to their counterparts on neighboring coils take place over more of the arc lengths of the helix than the other deformation mode.

61

For the purpose of evaluating this intuitive notion pertaining to the absolute maximum wake instability of multibladed hovering rotors, an average distortion factor will be defined. This "average relative distortion" will be calculated for two- and three-bladed rotors for axial perturbations at the wave numbers where maximum instabilities occur. Subsequently, it will be used to explain why absolute maximum instability occurs at wave numbers 0.0 for rotors with an even number of blades, and at wave numbers 1.5 and 2.5 for rotors with an odd number of blades, i.e., three- and five-bladed rotors, respectively.

For the case of the three-bladed rotor, maximum instabilities occur at wave numbers 0.0 and 1.5. Eigenfunctions for the most unstable eigenvalues at these wave numbers are tabulated in Table XII, and the elevation views of the perturbed vortex system for only axial perturbations are sketched in Figures 23 and 24.

For a wave number of 0.0, eigenfunctions for helices 1, 2 and 3 are
$$\delta \hat{z}_1 = +1 \quad ; \quad \delta \hat{z}_2 = 0 \quad ; \quad \delta \hat{z}_3 = -1$$

The "average relative distortion" is defined as a line integral of the reduction in the axial displacement between vortex elements at the same circumferential position on neighboring coils evaluated around the azimuth.

Thus, the average relative distortion between the 1st and 3rd helices for period π is
$$\int_0^\pi d\theta + \int_0^\pi d\theta = 2\pi$$

The average relative distortion between the 3rd and 2nd helices for period π is
$$\int_0^\pi d\theta = \pi$$

and finally, the average relative distortion between the 2nd and 1st helices for period π is
$$\int_0^\pi d\theta = \pi$$

The total average relative distortion factor, therefore, is $4\pi = 12.57$.

For a wave number of 1.5, eigenfunctions for helices 1, 2 and 3 are
$$\delta \hat{z}_1 = +1 \quad ; \quad \delta \hat{z}_2 = -0.25 \quad ; \quad \delta \hat{z}_3 = +1$$

TABLE XII.	EIGENFUNCTIONS FOR THE MOST UNSTABLE EIGENVALUES OF A THREE-BLADED ROTOR AT WAVE NUMBERS 0.0 AND 1.5, PITCH = 0.1 AND CORE SIZE = 0.1

Eigenfunction for Wave Number 0.0			Eigenfunction for Wave Number 1.5		
Label	Real	Imaginary	Label	Real	Imaginary
$\delta\hat{r}_1$	-1.000	0.000	$\delta\hat{r}_1$	-0.981	-0.005
$r\delta\hat{\phi}_1$	-0.076	0.000	$r\delta\hat{\phi}_1$	-0.073	-0.012
$\delta\hat{z}_1$	+0.996	0.000	$\delta\hat{z}_1$	+0.996	+0.004
$\delta\hat{r}_2$	0.000	0.000	$\delta\hat{r}_2$	+0.210	0.000
$r\delta\hat{\phi}_2$	0.000	0.000	$r\delta\hat{\phi}_2$	+0.016	+0.002
$\delta\hat{z}_2$	0.000	0.000	$\delta\hat{z}_2$	-0.248	+0.000
$\delta\hat{r}_3$	1.000	0.000	$\delta\hat{r}_3$	-0.981	-0.005
$r\delta\hat{\phi}_3$	0.076	0.000	$r\delta\hat{\phi}_3$	-0.073	-0.012
$\delta\hat{z}_3$	-0.996	0.000	$\delta\hat{z}_3$	+0.996	+0.004

Referring to Figure 24, the following distortion factors can be calculated.

The average relative distortion between 1st and 3rd helices for period π is

$$\int_0^{\pi/3} [\,|\sin(1.5\theta)| + |\cos(1.5\theta)|\,]\,d\theta + i\int_0^{\pi/3} [\,|\cos(1.5\theta)| + |\sin(1.5\theta)|\,]\,d\theta$$

$$+ \int_0^{\pi/3} [\,|\cos(1.5\theta)| - |\sin(1.5\theta)|\,]\,d\theta + i\int_0^{\pi/3} [\,|\cos(1.5\theta)| - |\sin(1.5\theta)|\,]\,d\theta$$

$$+ \int_0^{\pi/3} [\,|\cos(1.5\theta)| + |\sin(1.5\theta)|\,]\,d\theta + i\int_0^{\pi/3} [\,|\cos(1.5\theta)| + |\sin(1.5\theta)|\,]\,d\theta$$

$$= 4 + 4i$$

Similarly, the average relative distortion between 3rd and 2nd helices for period π is

$$\int_0^{\pi/3} [\,|\cos(1.5\theta)| + 0.25\,|\sin(1.5\theta)|\,]\,d\theta + i\int_0^{\pi/3} [\,|\cos(1.5\theta)| + 0.25\,|\sin(1.5\theta)|\,]\,d\theta$$

$$+ \int_0^{\pi/3} [\,|\sin(1.5\theta)| - 0.25\,|\cos(1.5\theta)|\,]\,d\theta + i\int_0^{\pi/3} [\,|\sin(1.5\theta)| - 0.25\,|\cos(1.5\theta)|\,]\,d\theta$$

$$+ \int_0^{\pi/3} [\,|\cos(1.5\theta)| + 0.25\,|\sin(1.5\theta)|\,]\,d\theta + i\int_0^{\pi/3} [\,|\cos(1.5\theta)| + 0.25\,|\sin(1.5\theta)|\,]\,d\theta$$

$$= 3.25 + 3.25\,i$$

Finally, the average relative distortion between 2nd and 1st helices for period π is

$$\int_0^{\pi/3} [\,0.25\,|\sin(1.5\theta)| + |\sin(1.5\theta)|\,]\,d\theta + i\int_0^{\pi/3} [\,0.25\,|\sin(1.5\theta)| + |\sin(1.5\theta)|\,]\,d\theta$$

$$+ \int_0^{\pi/3} [\,|\cos(1.5\theta)| + 0.25\,|\cos(1.5\theta)|\,]\,d\theta + i\int_0^{\pi/3} [\,|\cos(1.5\theta)| + 0.25\,|\cos(1.5\theta)|\,]\,d\theta$$

$$+ \int_0^{\pi/3} [\,0.25\,|\sin(1.5\theta)| + |\sin(1.5\theta)|\,]\,d\theta + i\int_0^{\pi/3} [\,0.25\,|\sin(1.5\theta)| + |\sin(1.5\theta)|\,]\,d\theta$$

$$= 3.75 + 3.75\,i$$

Thus, the total average relative distortion factor is $11 + 11i$, and its magnitude is approximately 15.5.

Consider the case of a two-bladed rotor; maximum instabilities occur at wave numbers 0.0 and 1.0. Eigenfunctions for the most unstable eigenvalues at these wave numbers are tabulated in Table XIII.

For a wave number of 0.0, the axial distortion amplitudes for helices 1 and 2 are

$$\delta \hat{e}_1 \cong -1.00 \qquad ; \qquad \delta \hat{e}_2 \cong +1.00$$

The average relative distortion factor over a period π is

$$\int_0^\pi d\theta + \int_0^\pi d\theta = 2\pi \cong 6.28$$

For a wave number of 1.0, the axial distortion amplitudes for helices 1 and 2 are

$$\delta \hat{e}_1 \cong 0.812 \qquad ; \qquad \delta \hat{e}_2 = 0.812$$

Referring to Figure 21, the average relative distortion factor over a period π is

$$2(0.812) \int_0^{\pi/2} |\cos(\theta)| \, d\theta + 2(0.812) \int_0^{\pi/2} |\cos(\theta)| \, d\theta$$
$$+ i \left[2(0.812) \int_0^{\pi/2} |\sin(\theta)| \, d\theta + 2(0.812) \int_0^{\pi/2} |\sin(\theta)| \, d\theta \right]$$
$$= 3.25 + 3.25 i$$

Thus the magnitude of the average relative distortion factor is approximately 4.60.

Results of the above calculations are tabulated in Table XIV. This shows that the relative axial displacements do, in fact, determine the stability and that those modes which have the highest average reduction of axial separation between adjacent coils around the circumference of the helix will be the most highly divergent.

65

TABLE XIII.	EIGENFUNCTIONS FOR THE MOST UNSTABLE EIGENVALUES OF A TWO-BLADED ROTOR AT WAVE NUMBERS 0.0 AND 1.0, PITCH = 0.1 AND CORE SIZE = 0.1

Eigenfunction for Wave Number 0.0			Eigenfunction for Wave Number 1.0		
Label	Real	Imaginary	Label	Real	Imaginary
$\delta\hat{r}_1$	+0.998	0.002	$\delta\hat{r}_1$	-0.784	-0.215
$r\delta\hat{\phi}_1$	+0.065	0.000	$r\delta\hat{\phi}_1$	-0.043	-0.034
$\delta\hat{z}_1$	-0.998	-0.002	$\delta\hat{z}_1$	+0.783	+0.212
$\delta\hat{r}_2$	-0.998	-0.002	$\delta\hat{r}_2$	-0.784	-0.215
$r\delta\hat{\phi}_2$	-0.065	-0.000	$r\delta\hat{\phi}_2$	-0.043	-0.034
$\delta\hat{z}_2$	+0.998	+0.002	$\delta\hat{z}_2$	+0.783	+0.212

66

TABLE XIV.		COMPARISON OF MAXIMUM INSTABILITY FOR TWO- AND THREE-BLADED ROTORS		
Number of Blades	Wave Numbers	Amplitude of Average Distortion Factor	Max Divergence Rate	Conclusion
2	0.0	6.28	50.05	Perturbations for the wave number 0.0 are more unstable
	1.0	4.60	49.80	
3	0.0	12.57	118.42	Perturbations for the wave number 1.5 are more unstable
	1.5	15.50	123.71	

CHAPTER 5

CONCLUSIONS

1. The small-perturbation stability analysis of a doubly infinite array of interdigitated right circular helical vortices formulated here shows reasonable agreement with the recent work of Widnall [Reference 16] where vortex core to helix diameter ratios are 0.1 or less and when the number of blades is set equal to unity. The larger differences which appear in a comparison with the Reference 16 results at larger core ratios (e.g., 0.33) are attributed to differences in the methods for eliminating the self-induction singularity. While the method works best for small pitch angles, it has been shown to be the equivalent of the formulations developed by S.C. Crow and Parks [References 17 and 20] dealing with the infinite straight vortices such as trail from the tips of fixed-wing aircraft, when the pitch angle is made to approach infinity for a two-bladed rotor.

2. A continuum of instability modes has been found associated with all values of wave numbers; only modes with wave numbers 0 and 1 are so much as neutrally stable, and only for the case of a single helix. The most unstable modes involve the most axial motion of adjacent vortex segments relative to each other. By "adjacent segments" is meant vortex segments above and below each other (i.e., at the same azimuthal location) on adjacent coils of the same or neighboring helices. Furthermore, the larger the percentage of the helical arc length involved in such motion, the more rapidly the distortion will diverge. Maximum divergence rates in the unstable modes increase as the helix pitch decreases, increase as the number of helices increases, and decrease as the number of cycles of deformations in one turn of the helix (i.e., wave number) increases.

3. The effect of increasing helix filament core diameter is to make the analysis more sensitive to the means by which the singularity is eliminated. Increasing the number of blades appears to make the core diameter less influencial in determining the rates of divergence. Although it has not been demonstrated here, one would expect that reduced pitch would also reduce the dependence of the calculation on the vortex core size. Finally, a larger core diameter ratio also appears to reduce the difference between peak and minimum divergence rates as a function of wave number.

CHAPTER 6

RECOMMENDATIONS

In view of the instability of helical vortex arrays observed
(a) in tests and (b) in iterative distorted wake geometry
calculations and which now have been confirmed in this study,
it is recommended that the stability of a semi-infinite vortex
array, together with the bound vortices which generate it, be
studied in a manner similar to the analyses reported here.
The purpose of such a study would be twofold: first, to
examine the effect of the bound vortex on helical vortex
stability and the associted unstable divergence rates, and
second, to develop analytical and realistic perturbation
quantities to be used as forcing functions for the unstable
modes of the semi-infinite vortex array typical of lifting
rotors.   In such a "forced" calculation, one would expect
to predict the actual distorted geometry of the wake beneath
lifting rotors which must be known to perform more accurate
airloads analyses, for all purposes.
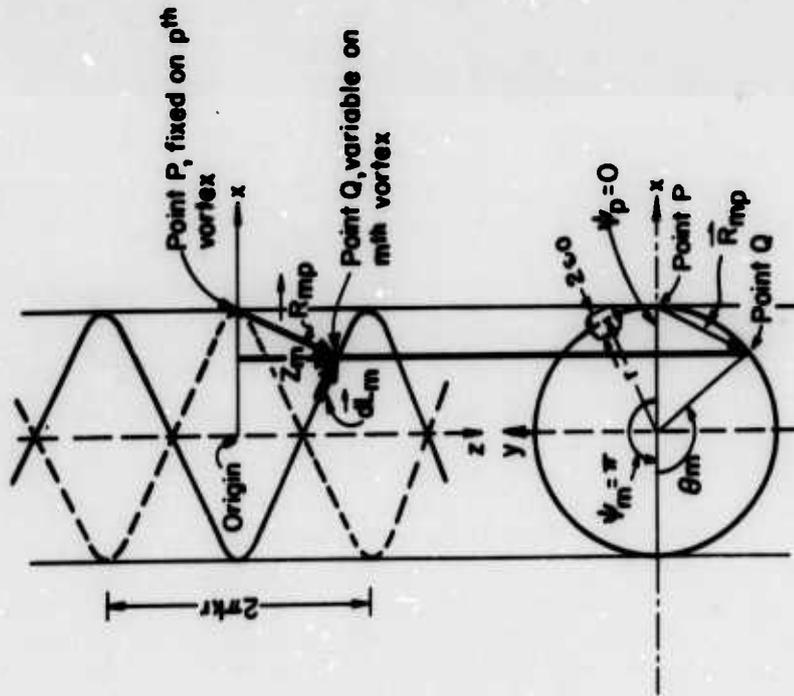
b. Isometric

a. Plan and Elevation
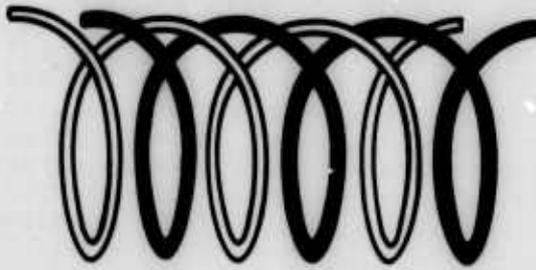
Figure 1.   Undistorted p^{th} and m^{th} Vortex Helices of Radius r, Pitch R, and Vortex Core Diameter $2\epsilon_o$.

70
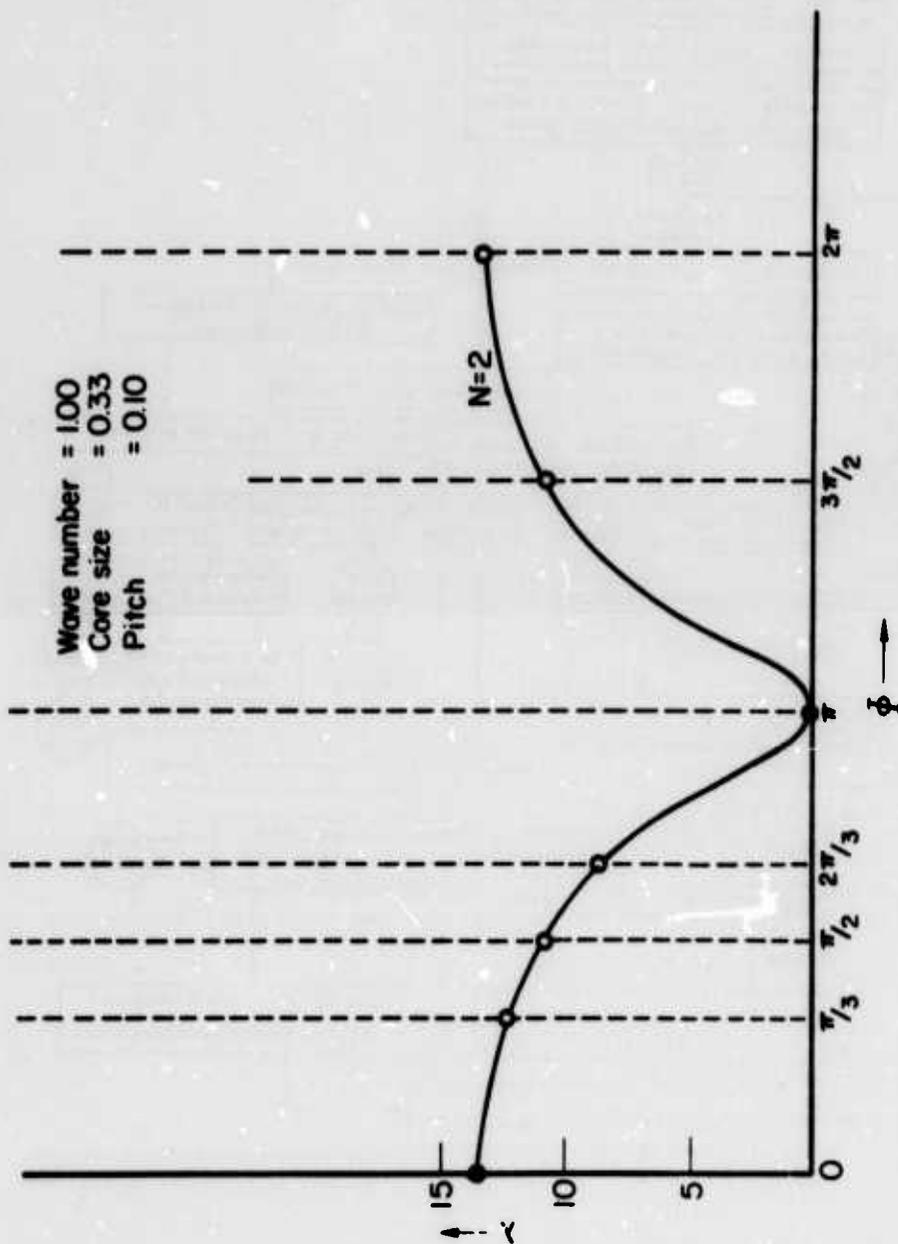
Figure 2. Plot of Divergence Rate Against Phase Difference for a Two-Bladed Rotor.

71

START

INPUT: Pitch, Wave Number, Core Size, Number of blades

Set upper limit on analytical integrals

Compute analytical integrals

Set overall cutoff limit on infinite integrals depending on pitch

K = 1

K = K+1

Variable of integration ≤ 14π ? — Yes → K=N? — Yes

No

Calculate integrals for limits from 14π to upper cutoff

SUB QG9

SUB INTG

Self-Induction Integral EPS = Core Size

Mutual Induction Integral

Calculate integrals for variable range 0 to 14π

SUB DSIM9

SUB INTG

Add two partial sums of integrals

variable of integration ≤ 2π ?

No — Calculate integrals for variable limit 2π to 14π

SUB DSIM9

SUB INTG

Yes — Modify the integrand

Calculate Modified Integrals

SUB DSIM9

SUB INTG

Add analytically calculated Integrals

Add two partial sums of integrals

Evaluate the perturbation integrals which are elements of a 3x3 matrix

Add Integrated Values

No

K=N? — Yes

Form 3n x 3n Complex eigenmatrix

SUB ALLMAT

N=2? — Yes — Form possible 3x3 symmetry eigenmatrix Combination — SUB ALLMAT

No

OUTPUT: Set of eigenvalues and eigenfunctions

OUTPUT: Set of decoupled eigenvalues and eigenfunctions

No

INPUT CARD = LAST CARD, N=0 ?

Yes

STOP

END

Figure 3. Major Steps in the Computer Program.

72
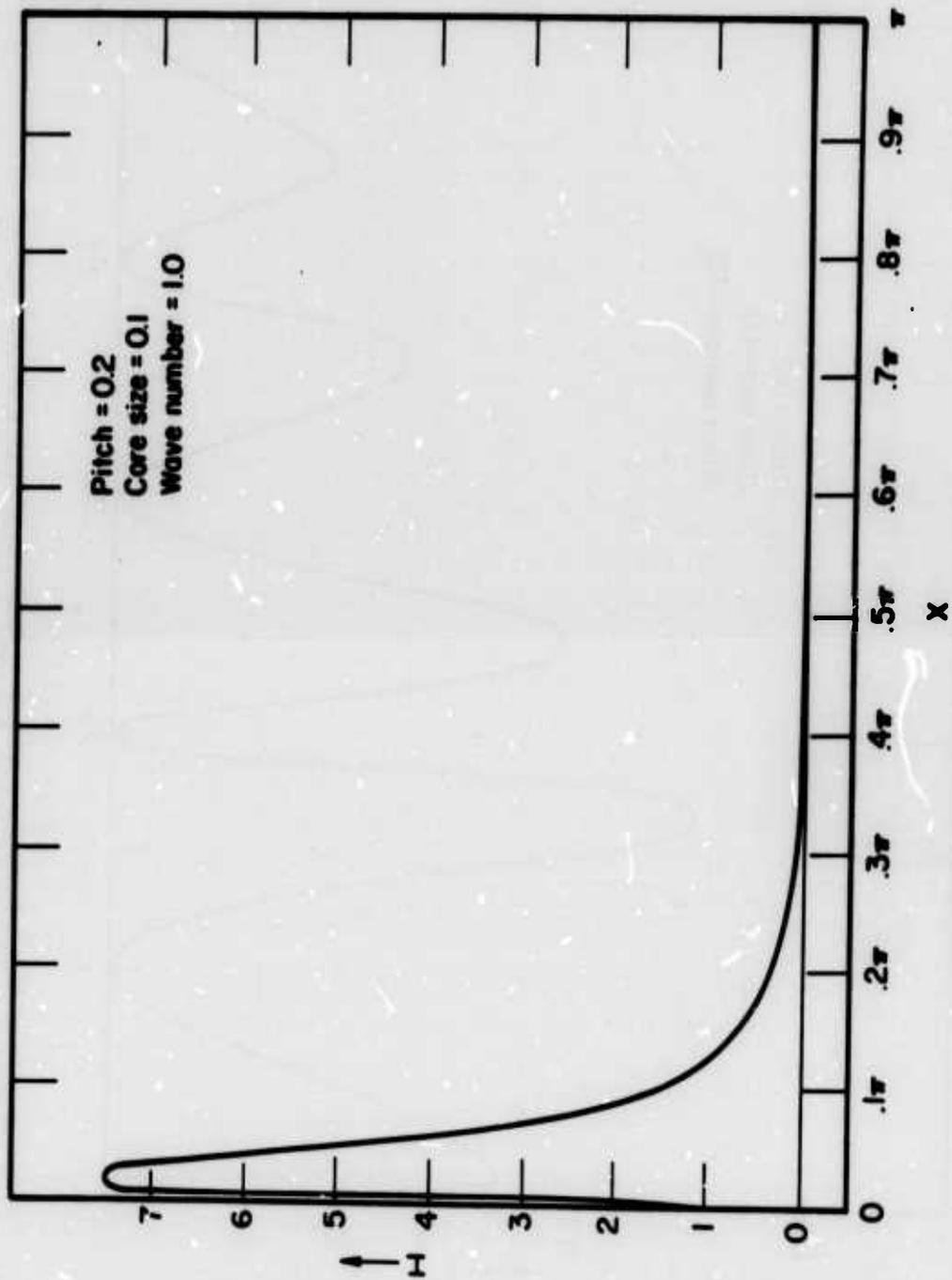
Figure 4. Perturbation Integrand $I = [bJ^{-3/2} \sin x \cos(\omega x)]$.

Pitch = 0.2
Core size = 0.1
Wave number = 1.0

73

Figure 5. Perturbation Integrand $I = [KJ^{-3/2} x \sin x \sin(\omega x)]$.

Pitch = 0.2
Core size = 0.1
Wave number = 1.0

74
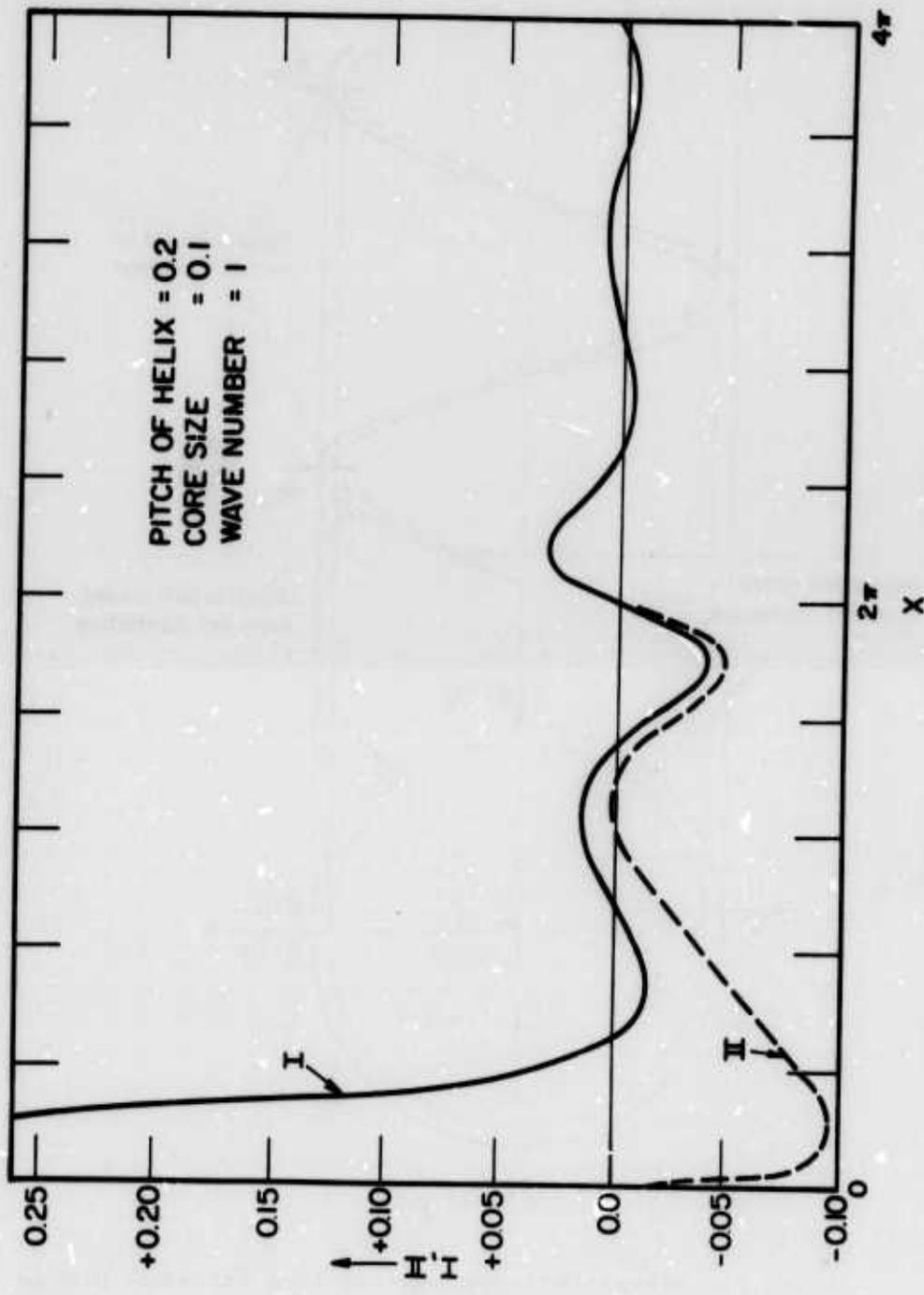
Figure 6. Plot I: I = $(k_1 J^{3/2} \sin x \cos x)$ Against x ;
Plot II: II = $[(k_1 J^{1/2} \sin x \cos x) - k_1 x \{(1+k^2) x^2 + \epsilon^2\}^{-3/2}]$ Against x .

75
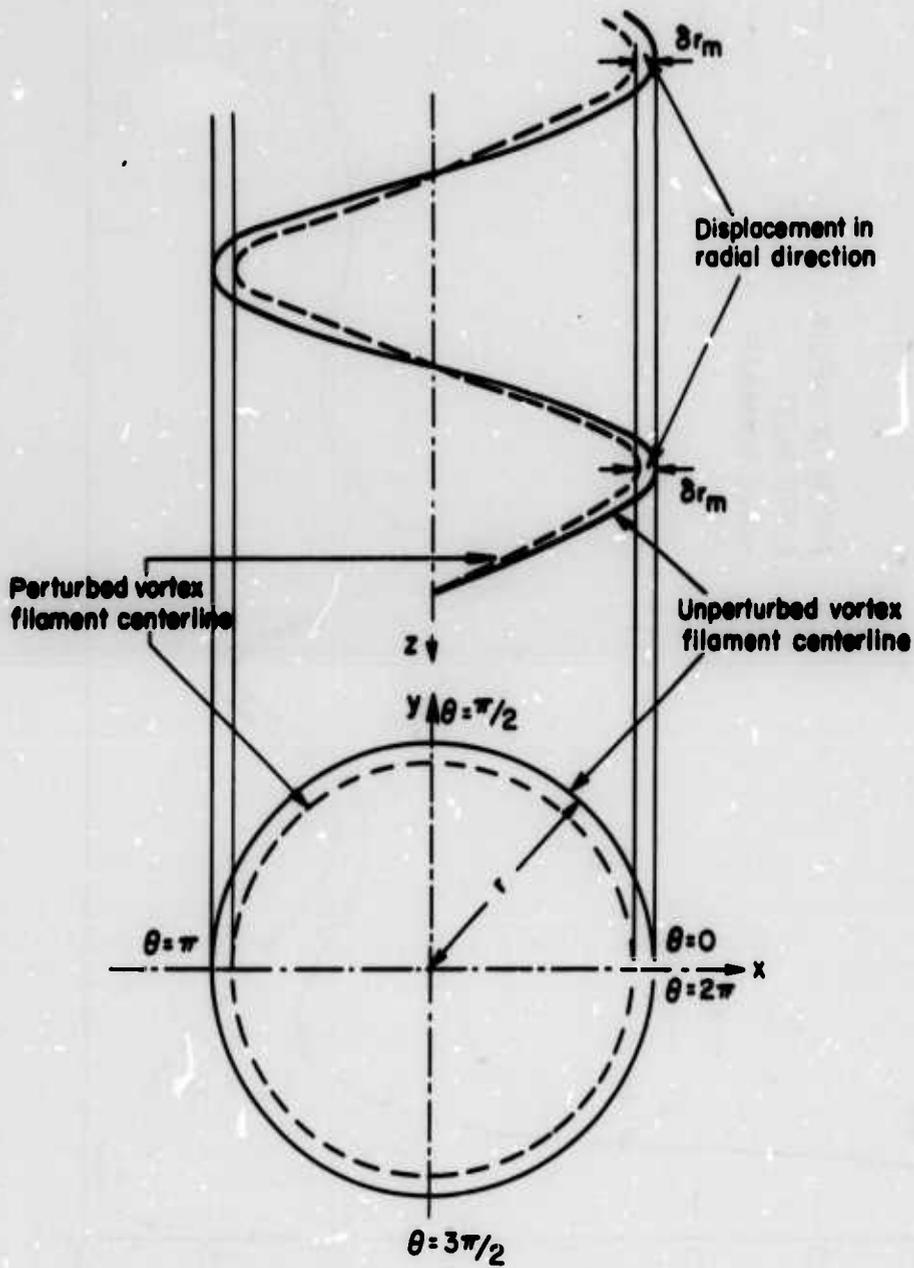
Figure 7.   Radial Perturbations in Wave Number = 0 Mode
(Dilatational).
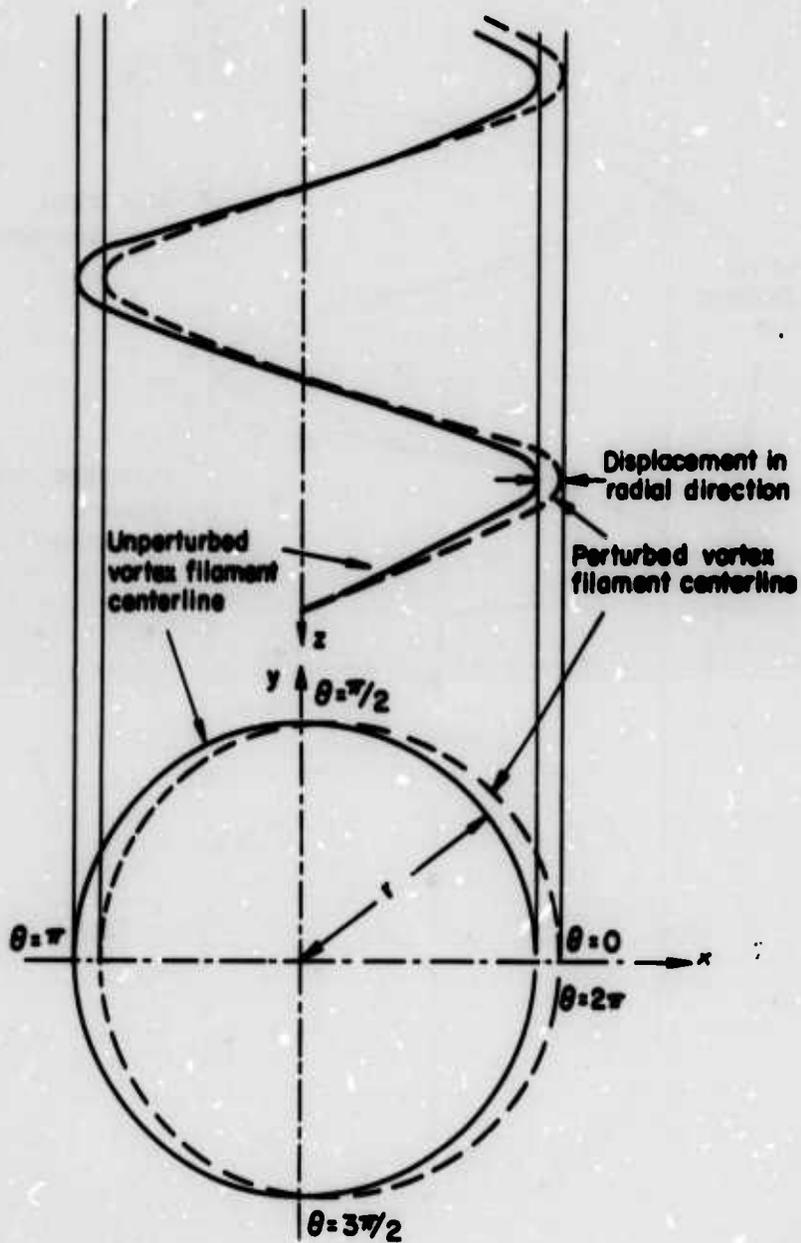
Figure 8. Radial Perturbations in Wave Number = 1 Mode.

77
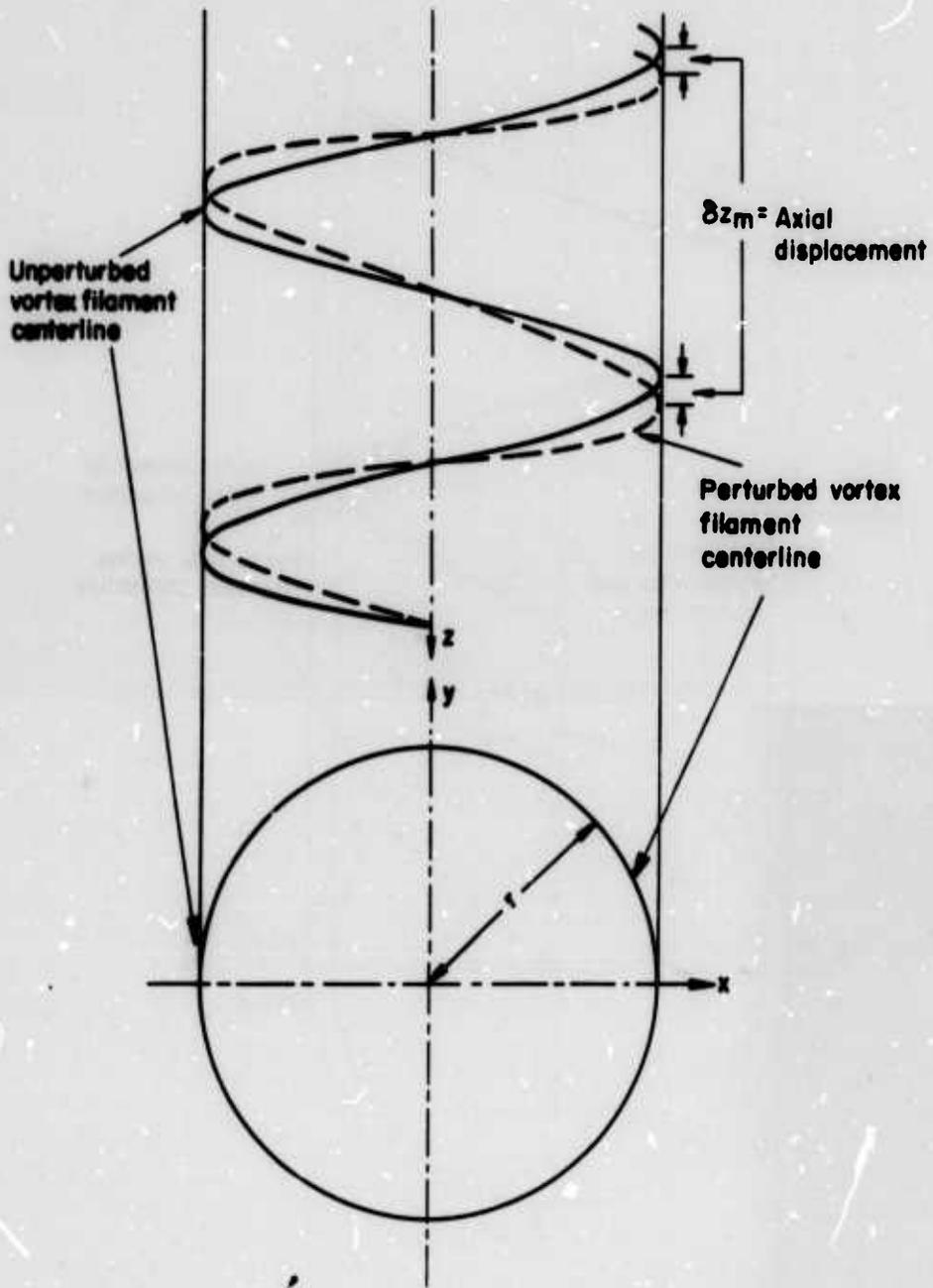
Figure 9.   Axial Perturbations in Wave Number = 1 Mode.

78
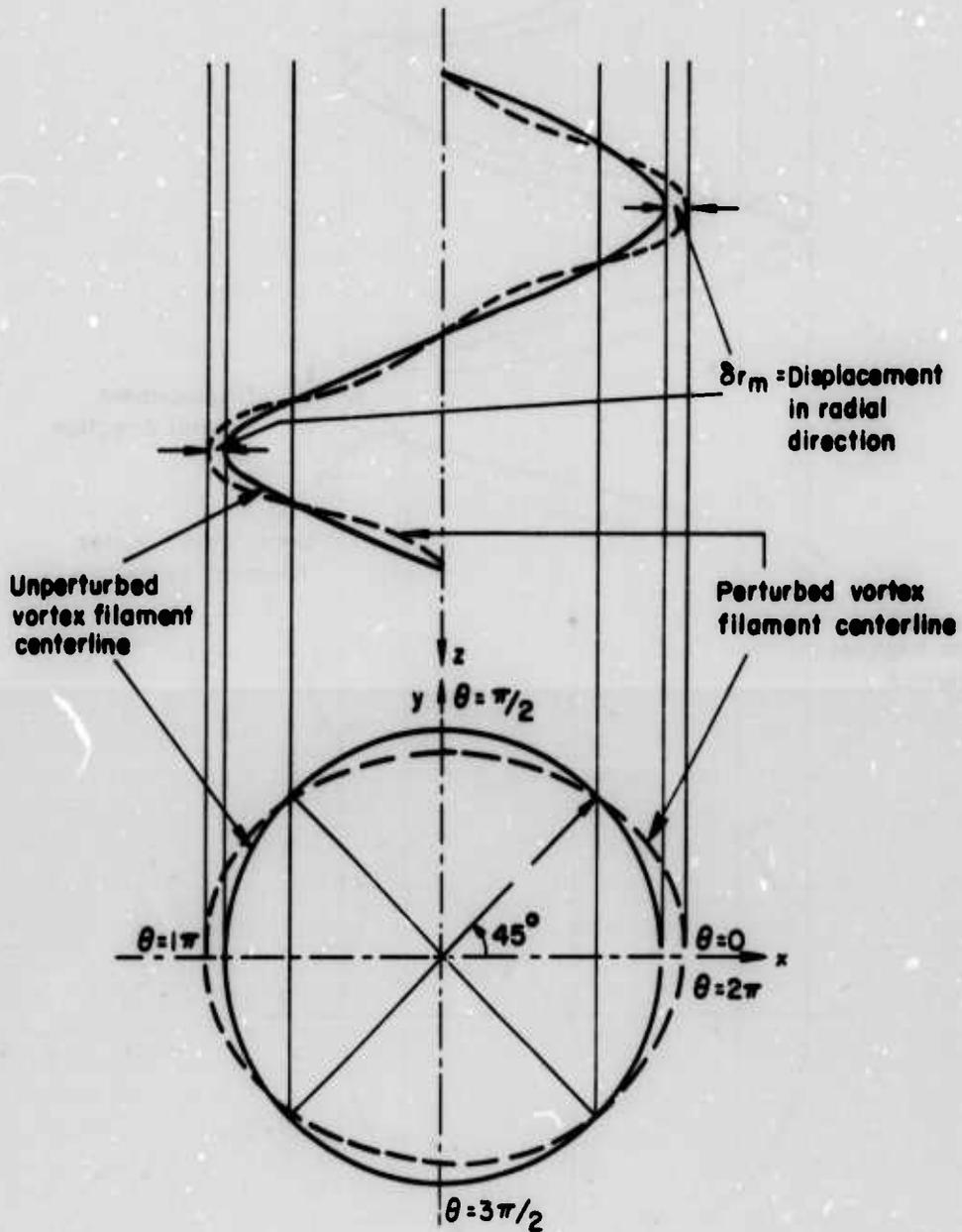
Figure 10. Radial Perturbations in Wave Number = 2 Mode.
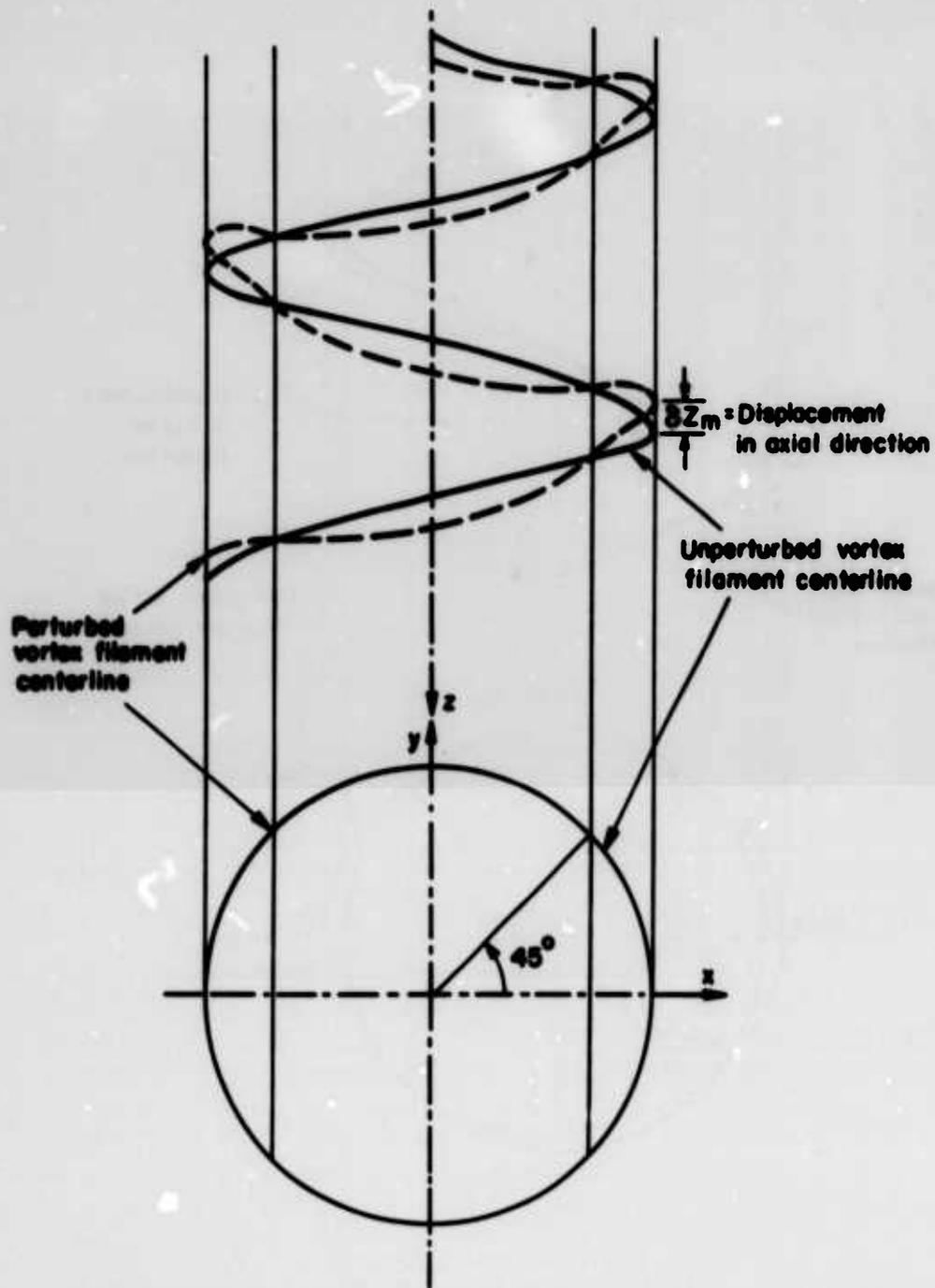
Figure 11. Axial Perturbations in Wave Number = 2 Mode.
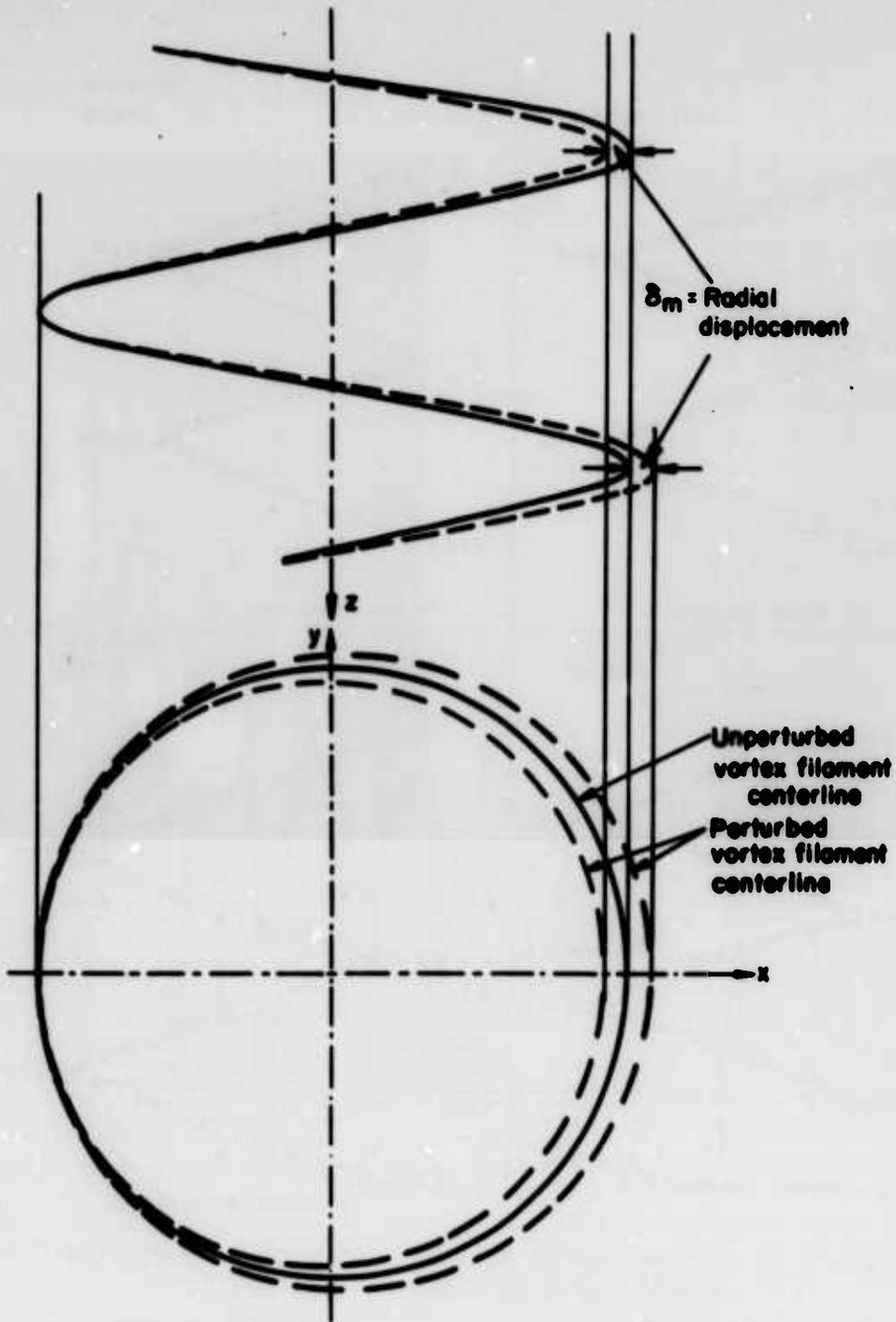
Figure 12.   Radial Perturbations in Wave Number = 1/2 Mode.
81
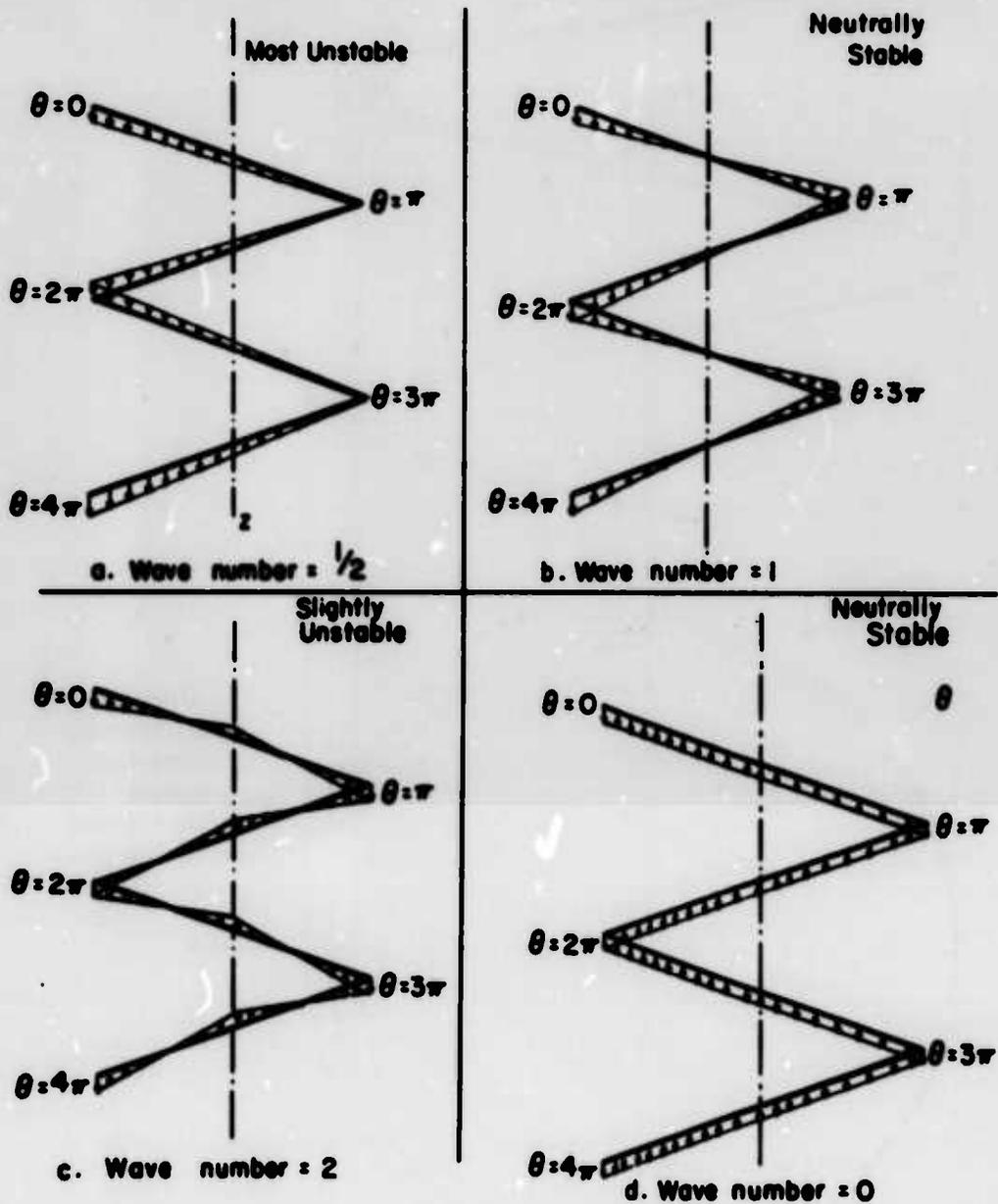
Figure 13. Comparison of Various Perturbation Modes for Single Helix in Axial Direction.
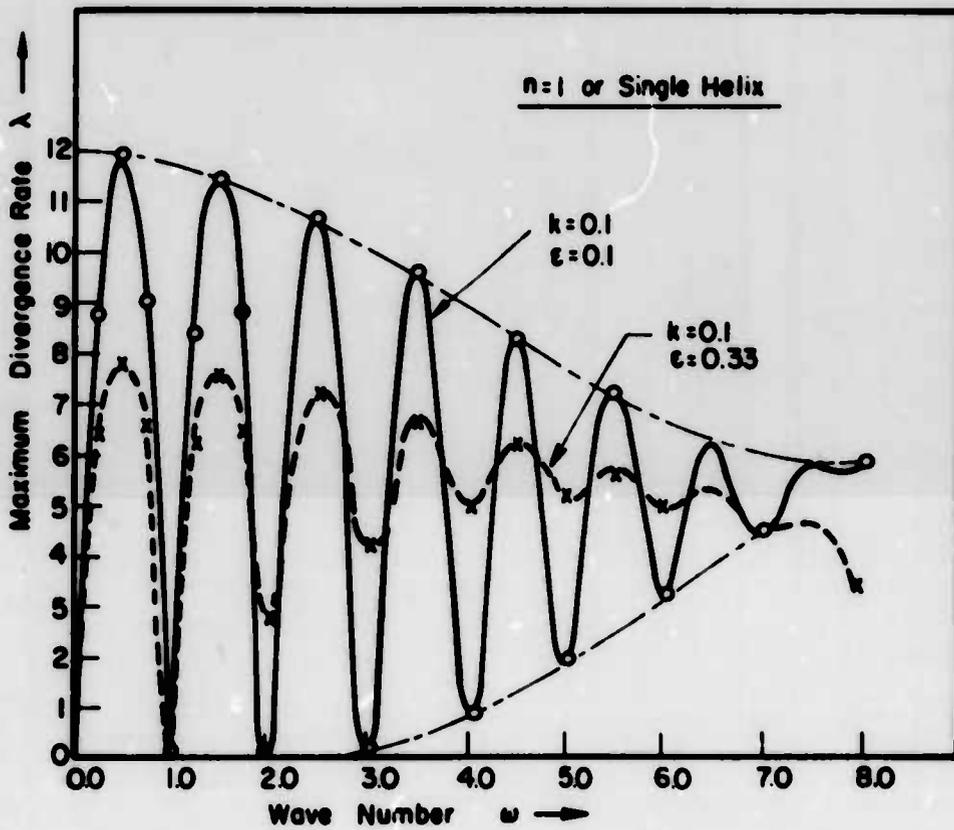
Figure 14. Plot of Maximum Divergence Rate vs Wave Number for Single Helix.

83
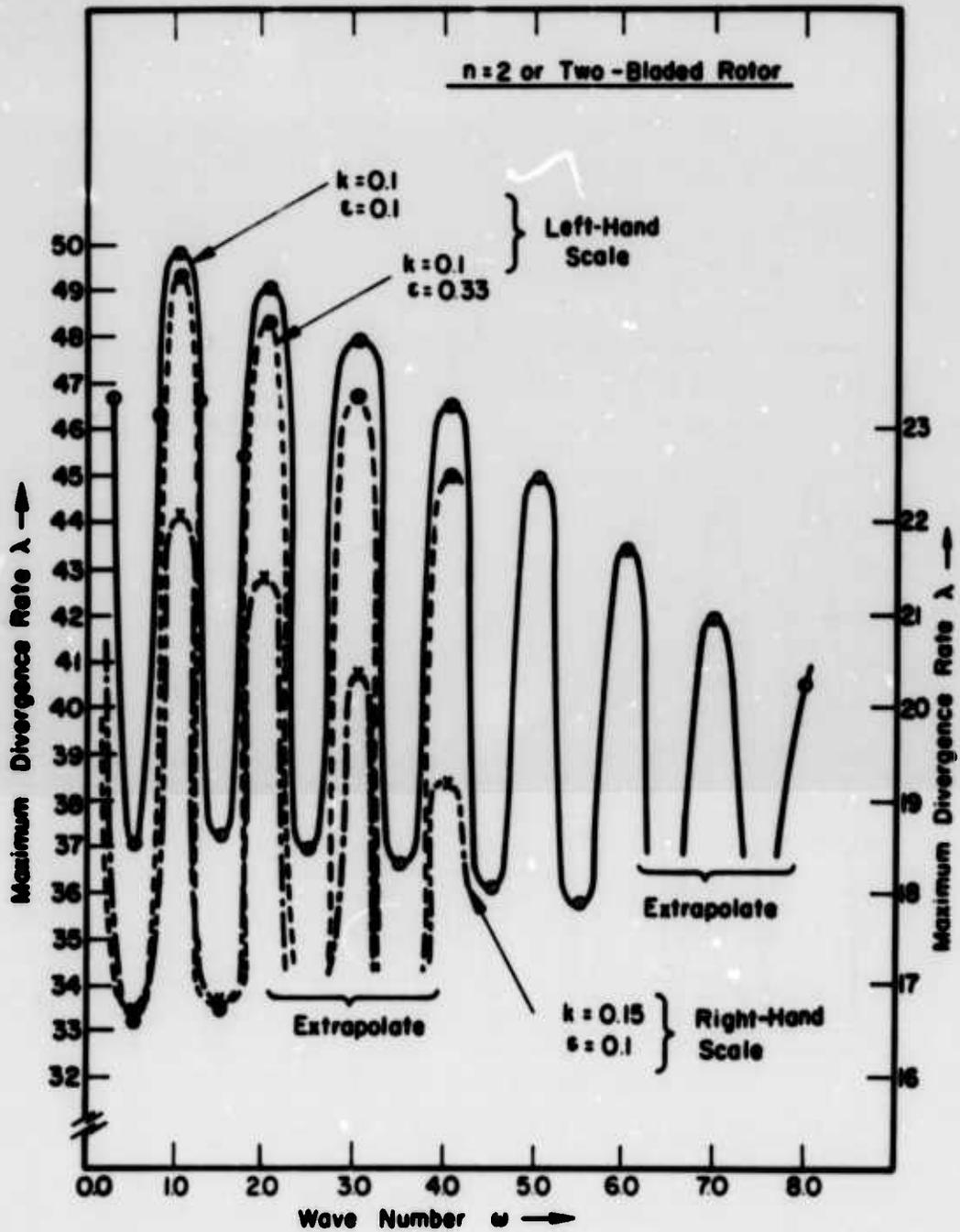
Figure 15. Plot of Maximum Divergence Rate vs Wave
Number for Two-Bladed Rotor.

84
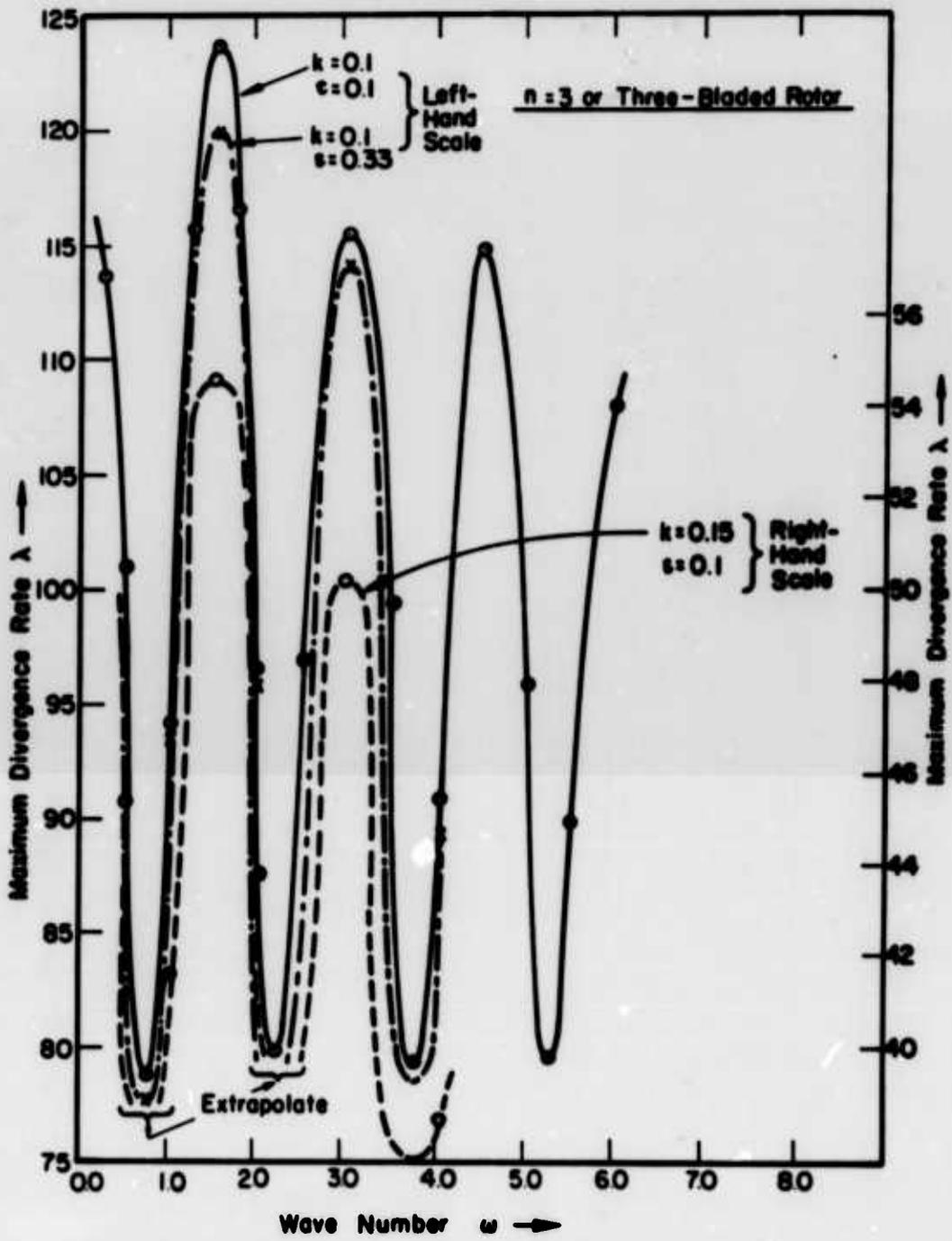
Figure 16. Plot of Maximum Divergence Rate vs Wave Number for Three-Bladed Rotor.

85
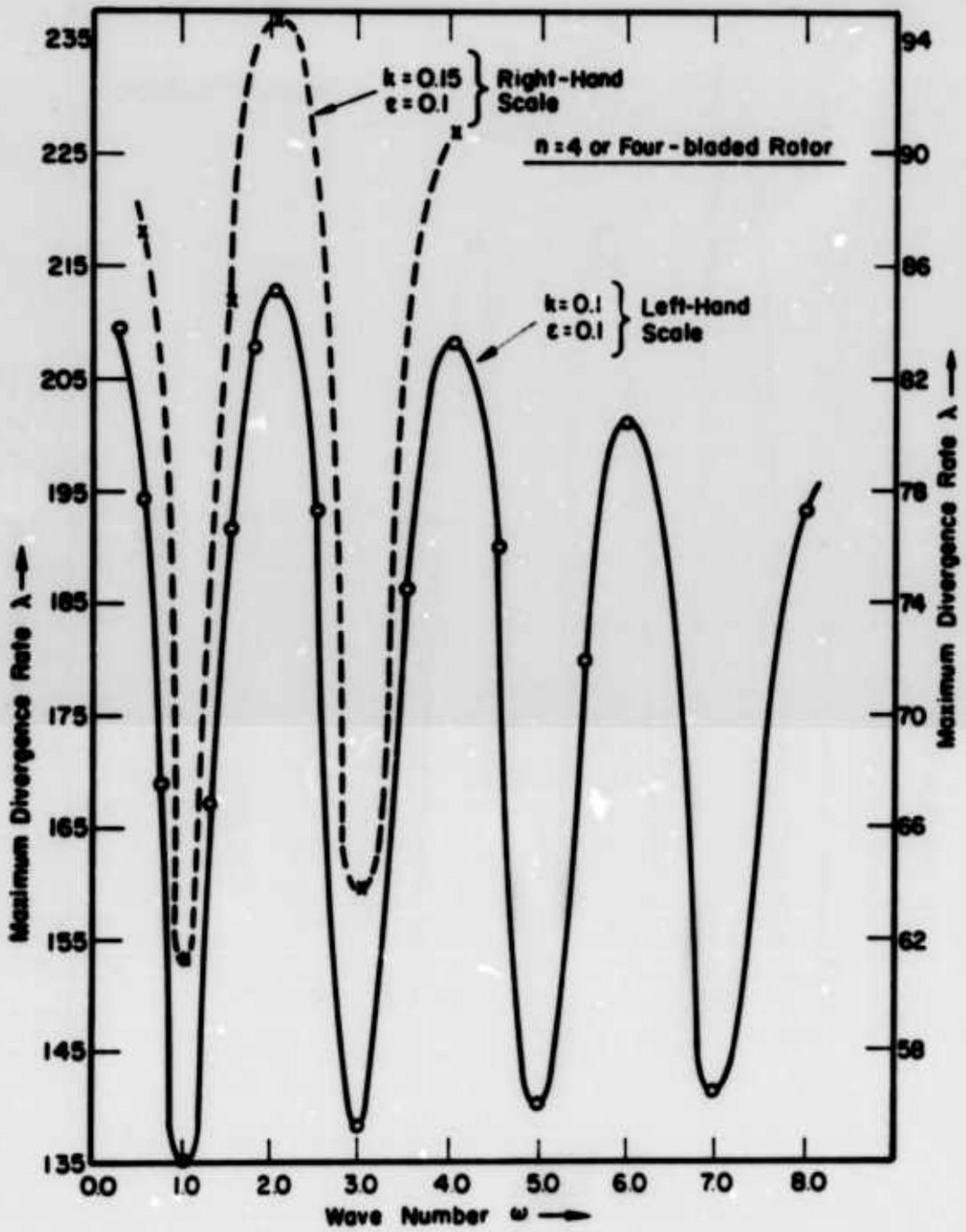
Figure 17. Plot of Maximum Divergence Rate vs Wave
Number for Four-Bladed Rotor.
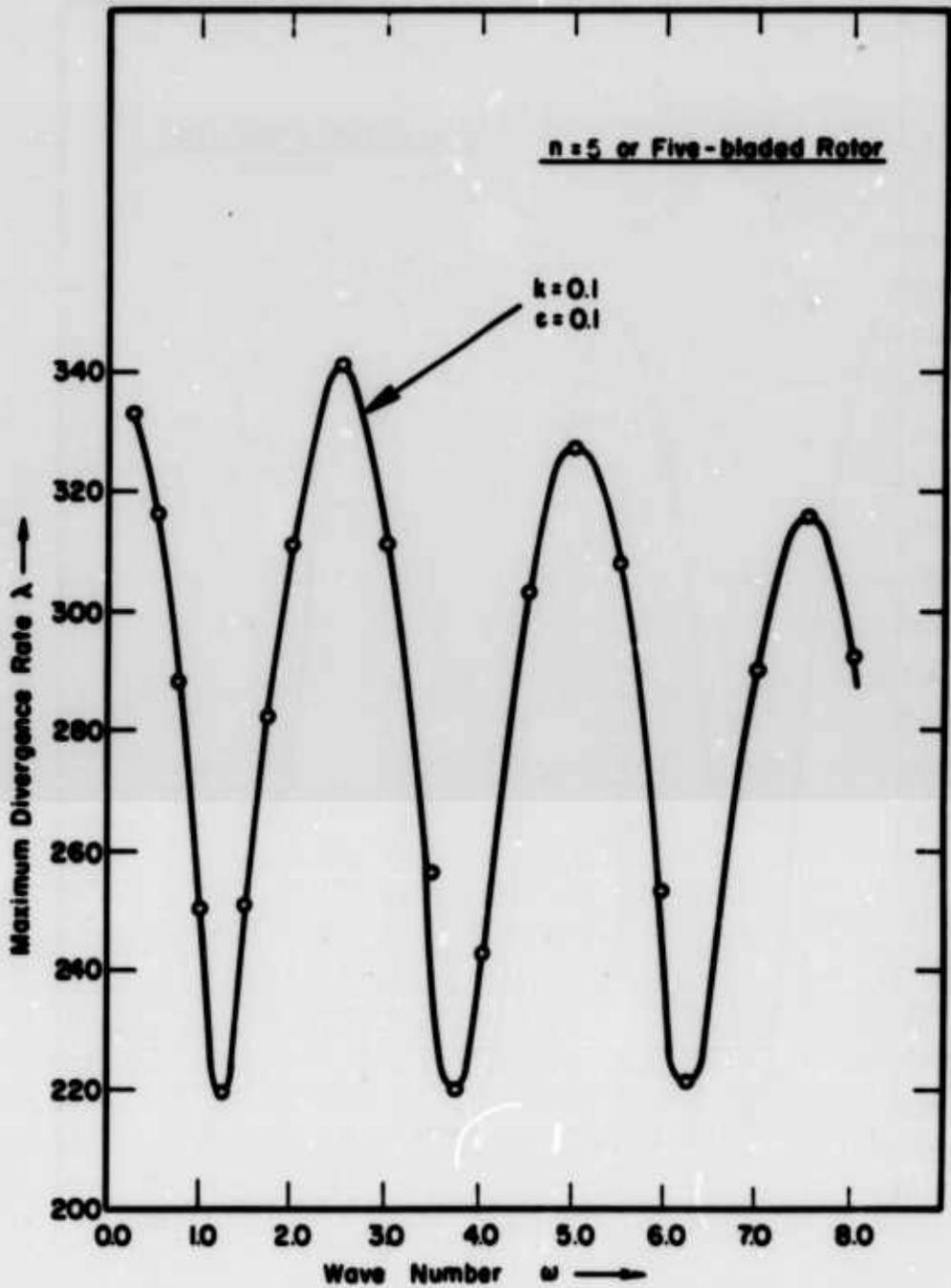
Figure 18. Plot of Maximum Divergence Rate vs Wave
Number for Five-Bladed Rotor.
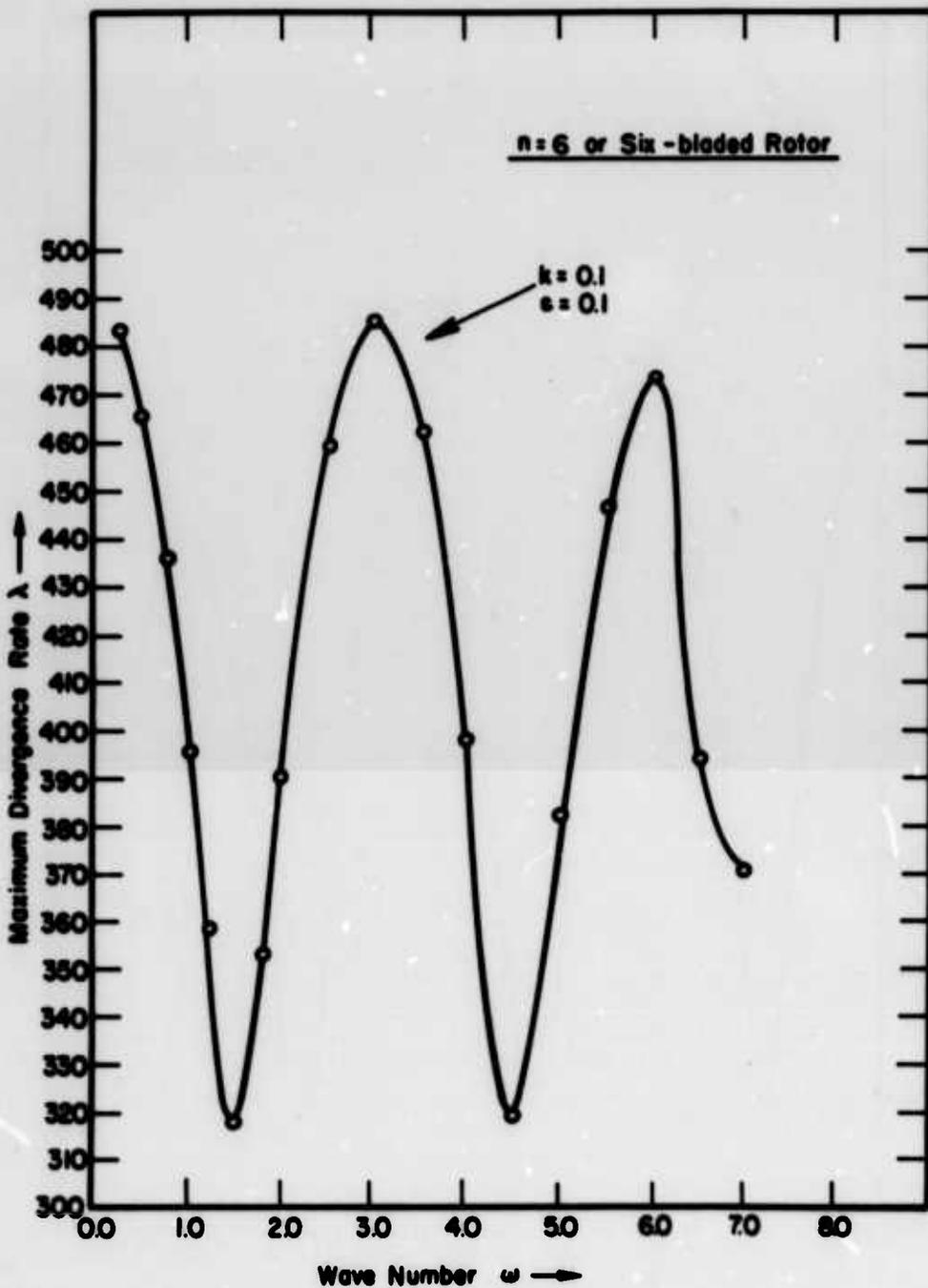
Figure 19. Plot of Maximum Divergence Rate vs Wave Number for Six-Bladed Rotor.
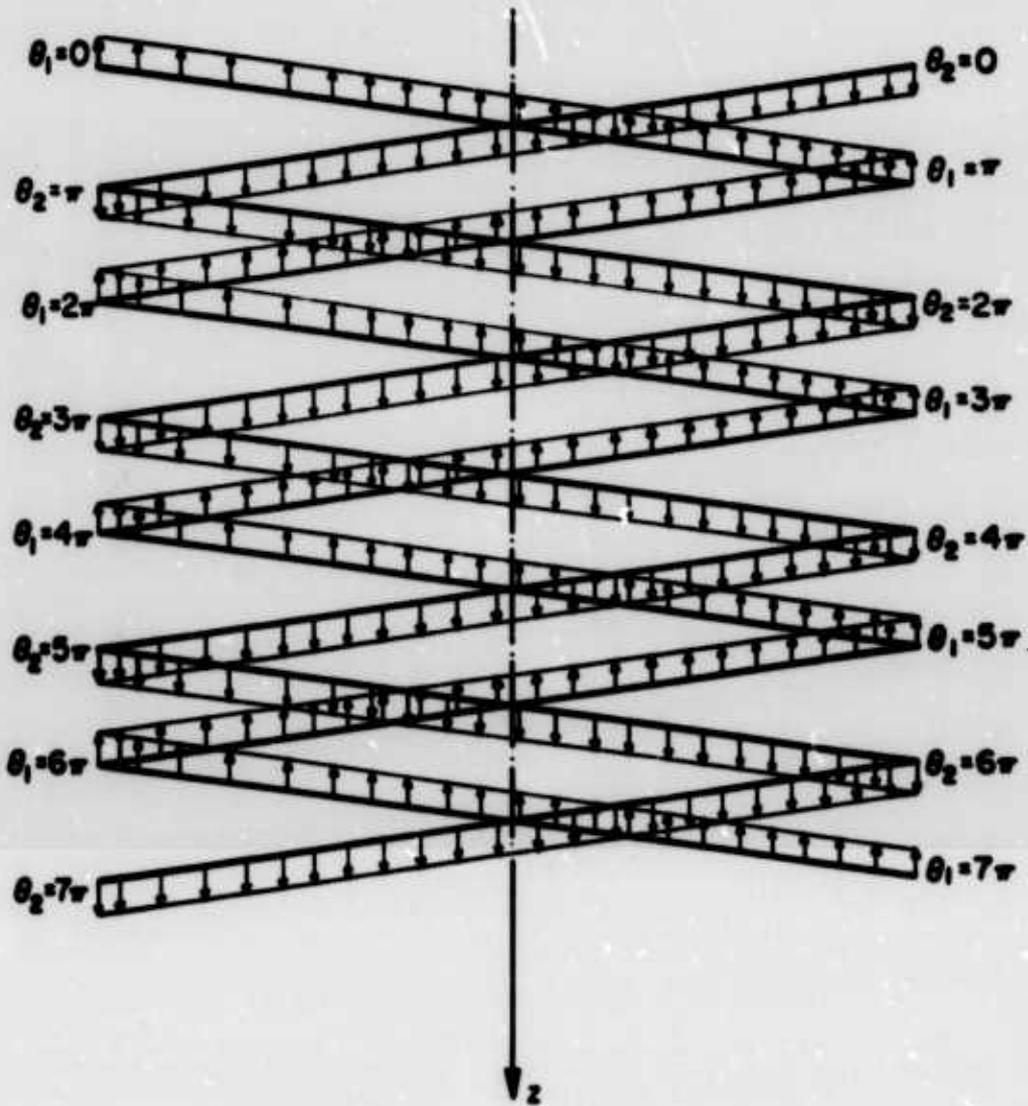
Figure 20. Real Component of Axial Perturbations for a Two-Bladed Rotor at Wave Number 0.0.

89
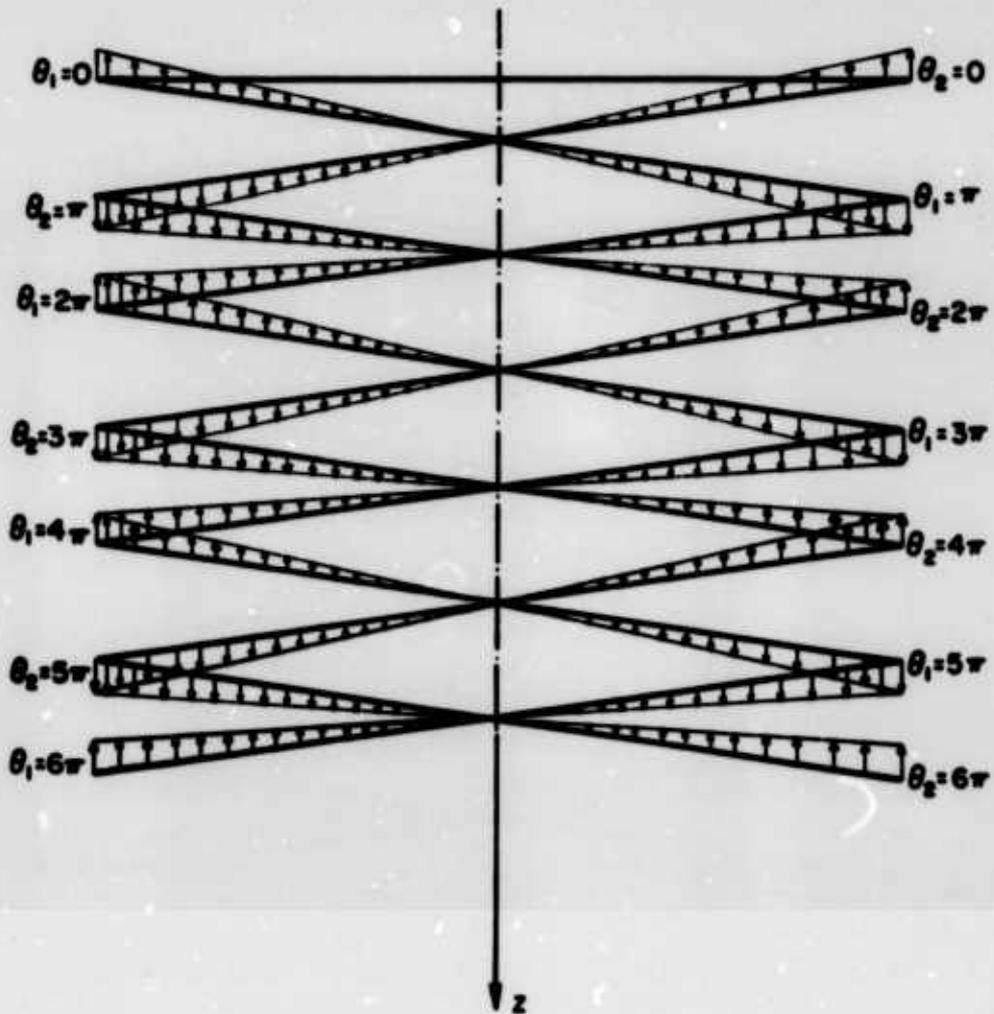
Figure 21.   Real Component of Axial Perturbations for a
Two-Bladed Rotor at Wave Number 1.0.
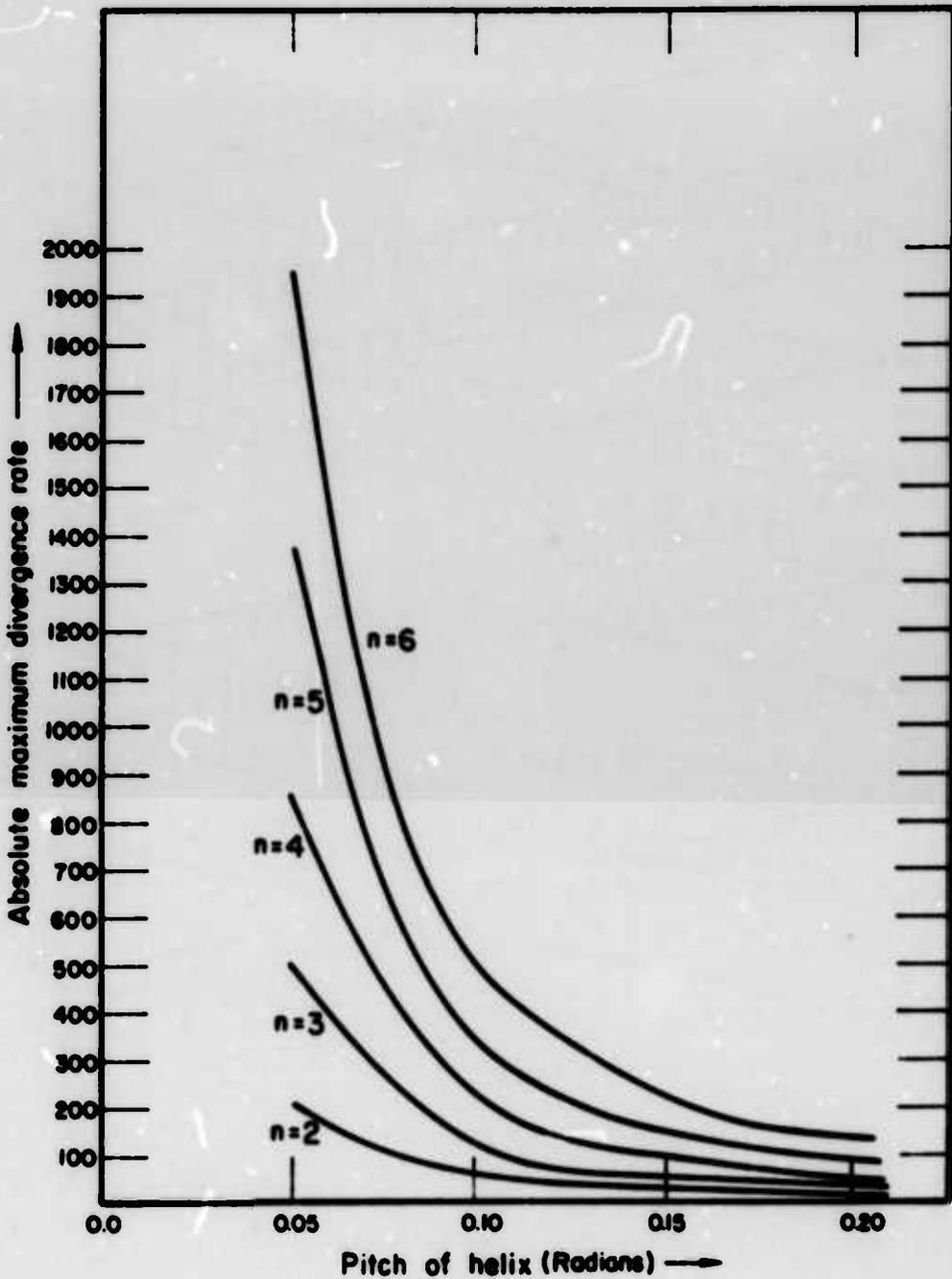
Figure 22.   Absolute Maximum Divergence Rates for
             Multibladed Rotors of Varying Pitch.

91
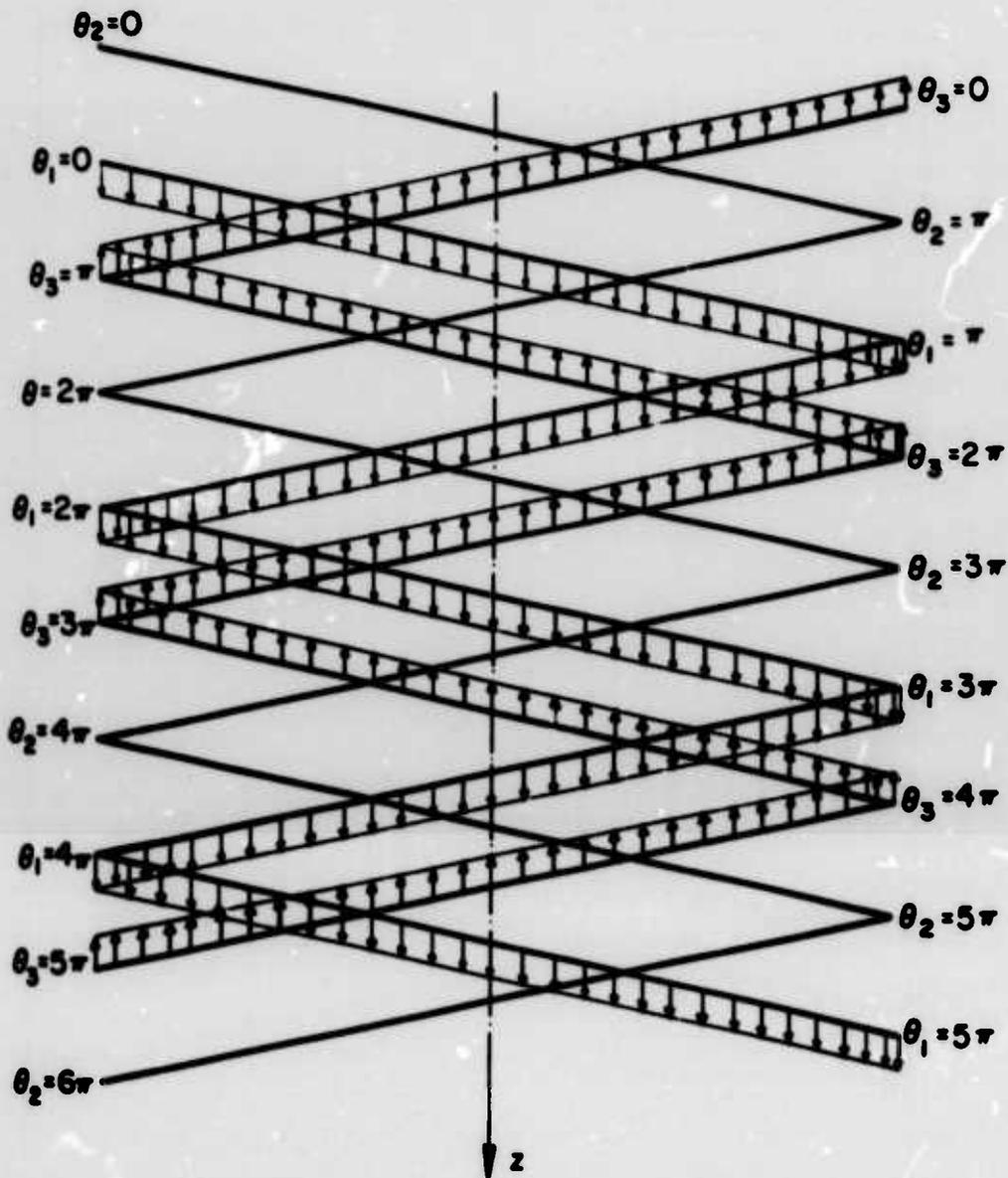
Figure 23. Real Component of Axial Perturbations for a
Three-Bladed Rotor at Wave Number 0.0.

92
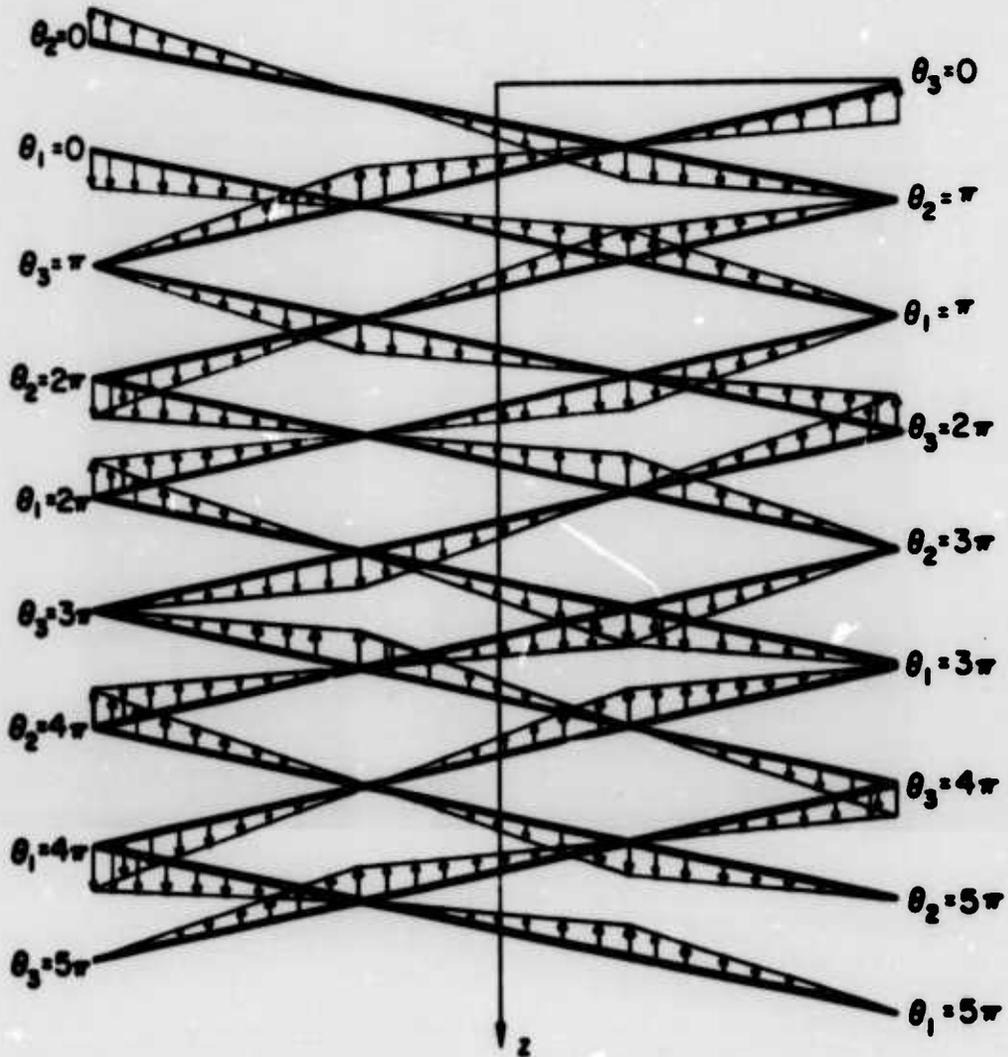
Figure 24.   Real Component of Axial Perturbations for a
Three-Bladed Rotor at Wave Number 1.5.

93

LITERATURE CITED

1. Glauert, H., AIRPLANE PROPELLERS, Aerodynamic Theory,
edited by W. F. Durand, Dover Publications, New York, 1935,
Chapter X, Division L, Vol. IV.

2. Shapiro, Jacob, PRINCIPLES OF HELICOPTER ENGINEERING, New
York, McGraw-Hill Book Co., Inc., 1956, pp. 70-73.

3. Gessow, A.,and Myers, G. C. Jr., AERODYNAMICS OF THE HELI-
COPTER, New York, The MacMillan Company, 1952, pp. 46-47.

4. Mangler, K. W., CALCULATION OF INDUCED VELOCITY FIELD OF A
ROTOR, Royal Aircraft Establishment Report, No. Aero.2247,
1948.

5. Loewy, R.,and Joglekar, M., AN ACTUATOR DISC ANALYSIS OF
HELICOPTER WAKE GEOMETRY AND THE CORRESPONDING BLADE RESPONSE,
University of Rochester; USAAVLABS Technical Report 69-66,
U. S. Army Aviation Materiel Laboratories, Fort Eustis,
Virginia, December 1970, AD 891981.

6. Goldstein, S., ON THE VORTEX THEORY OF SCREW PROPELLERS,
Proceedings - Royal Society of London, Vol. A123, No. A792,
1929.

7. Jenny, D., Olson, J., and Landgrebe, A., A REASSESSMENT OF
ROTOR HOVERING PERFORMANCE PREDICTION METHODS, Journal of the
American Helicopter Society, Vol. 13, No. 2, April 1968,
pp. 1-26.

8. Miller, R. H., ON THE COMPUTATION OF AIRLOADS ACTING ON
ROTOR BLADES IN FORWARD FLIGHT, Journal of the American Heli-
copter Society, Vol. 7, No. 2, April 1962.

9. DuWaldt, F. A., Piziali, R. A., A METHOD FOR COMPUTING
ROTARY WING AIRLOAD DISTRIBUTIONS IN FORWARD FLIGHT, U. S.
Army TRECOM Report No. TCREC TR 62-44, November 1962.

10. Tarrarine, S., EXPERIMENTAL AND THEORETICAL STUDY OF LOCAL
INDUCED VELOCITIES OVER A ROTOR DISC FOR ANALYTICAL EVALUATION
OF THE PRIMARY LOADS ACTING ON HELICOPTER ROTOR BLADES, Euro-
pean Research Office, U. S. Army Contract, October 1960.

11. Landgrebe, A. J., AN ANALYTICAL AND EXPERIMENTAL INVESTI-
GATION OF HELICOPTER ROTOR HOVER PERFORMANCE AND WAKE GEOMETRY
CHARACTERISTICS, United Aircraft Corporation; USAAMRDL Tech-
nical Report 71-24, U. S. Air Mobility Research and Develop-
ment Laboratory, Fort Eustis, Virginia, June 1971, AD 728835.

12. Crimi, P., PREDICTION OF ROTOR WAKE FLOWS, presented at CAL/USAAVLABS symposium, Buffalo, New York, June 1966.

13. Sadler, Gene S., MAIN ROTOR FREE WAKE GEOMETRY EFFECTS ON BLADE AIR LOADS AND RESPONSE FOR HELICOPTERS IN STEADY MANEUVERS, Rochester Applied Science Associates, Inc., NASA CR-2110, National Aeronautics and Space Administration, Washington, D. C., September 1972.

14. Kármán, Theodore von, AERODYNAMICS, Ithaca, N. Y., Cornell University Press, 1954, Chapter II, pp. 31-59.

15. Levy, M. A., and Forsdyke, A. G., THE STEADY MOTION AND STABILITY OF A HELICAL VORTEX, Royal Society - Proceedings, Vol. 120, No. A786, October 1, 1928, pp. 670-690.

16. Widnall, S. E., THE STABILITY OF A HELICAL VORTEX FILAMENT, Journal of Fluid Mechanics, Vol. 54, Part 4, 1972, pp. 641-663.

17. Crow, S. C., STABILITY THEORY FOR A PAIR OF TRAILING VORTICES, American Institute of Aeronautics and Astronautics Journal, Vol. 8, No. 12, Dec. 1970, pp. 2172-2179.

18. Hama, F. R., PROGRESSIVE DEFORMATION OF A CURVED VORTEX FILAMENT BY ITS OWN INDUCTION, The Physics of Fluids, Vol. 5, No. 10, October 1962, pp. 1156-1162.

19. Hama, F. R., PROGRESSIVE DEFORMATION OF A PERTURBED LINE VORTEX FILAMENT, The Physics of Fluids, Vol. 6, No. 4, April 1963, pp. 526-534.

20. Parks, P. C., A NEW LOOK AT THE DYNAMICS OF VORTICES WITH FINITE CORES: Proceedings of Symposium on Aircraft Wake Turbulence held in Seattle, Washington, September 1970 (Included in the book AIRCRAFT WAKE TURBULENCE AND ITS DETECTION, editors, Olson, J. H., Goldberg, A., and Rogers, M., New York, Plenum Press, 1971, pp. 355-388).

21. Batchelor, G. K., AN INTRODUCTION TO FLUID DYNAMICS, Cambridge University Press, Cambridge, England, 1967, p. 264.

22. Hildebrand, F. B., INTRODUCTION TO NUMERICAL ANALYSIS, New York, McGraw-Hill Book Company, 1956, pp. 73, 141, 146.

23. Krylov, V. I., APPROXIMATE CALCULATION OF INTEGRALS, New York, The Macmillan Company, 1962, pp. 338-339.

24. Ralston, A., A FIRST COURSE IN NUMERICAL ANALYSIS, New York, McGraw-Hill Book Company, 1965, pp. 516-519.

25. Acton, F. S., NUMERICAL METHODS THAT WORK, New York, Harper and Row, 1970, p. 347.

26. Payne, P. R., HELICOPTER DYNAMICS AND AERODYNAMICS, New York, The Macmillan Company, 1959, p. 32.

27. Thomson, W., ON THE VIBRATIONS OF A COLUMNAR VORTEX, Philosophical Magazine, Serial 5, Volume 10, No. 61, Sept. 1880, pp. 155-168.

28. Widnall, S. E., and Sullivan, J., ON THE STABILITY OF VORTEX RINGS, Proceedings - Royal Society of London, Vol. A332, 1973, pp. 335-353.

29. Betchov, R., ON THE CURVATURE AND TORSION OF AN ISOLATED VORTEX FILAMENT, Journal of Fluid Mechanics, Vol. 22, Part 3, 1965, pp. 471-479.

30. Spreiter, J. R., and Sacks, A. H., THE ROLLING UP OF THE TRAILING VORTEX SHEET AND ITS EFFECT ON THE DOWNWASH BEHIND WINGS, Journal of the Aeronautical Sciences, Vol. 18, No. 1, Jan. 1951, pp. 21-32.

APPENDIX I
LIMITS FOR S. C. CROW'S CASE

The equivalence of the special case of the present work with
that of Crow and Parks can be seen by noting that the direc-
tion z in the present study corresponds to the axial direction
of the aircraft trailing vortex, and that the directions r and
± of the present study in the limit will correspond to the y
and ± directions, respectively, in S. C. Crow's theory. All the
nondimensional parameters in Crow's work must be defined in
terms of the parameters of the present study to demonstrate the
correspondence. The r perturbation equation in the present
study with above-mentioned restrictions can be written as

$$\alpha \, \delta \hat{r}_p = \sum_{m=1}^{n} \frac{\Gamma_s}{2\pi} \int_{-\infty}^{\infty} J_{mp}^{-3/2} \left[kr \, \delta \hat{r}_m \left\{ \omega \, x_{mp} \, \text{Sin}(x_{mp} + \psi_{mp}) \, \text{Sin} \, \omega \, x_{mp} \right. \right.$$

$$\left. - x_{mp} \, \text{Cos}(x_{mp} + \psi_{mp}) \, \text{Cos} \, \omega \, x_{mp} + \text{Sin}(x_{mp} + \psi_{mp}) \, \text{Cos} \, \omega \, x_{mp} \right\}$$

$$+ i \, kr \, \delta \hat{r}_m \left\{ -\omega \, x_{mp} \, \text{Sin}(x_{mp} + \psi_{mp}) \, \text{Cos} \, \omega \, x_{mp} - x_{mp} \, \text{Cos}(x_{mp} + \psi_{mp}) \, \text{Sin} \, \omega \, x_{mp} \right.$$

$$\left. + \text{Sin}(x_{mp} + \psi_{mp}) \, \text{Sin} \, \omega \, x_{mp} \right\} + kr^2 \, \delta \hat{\phi}_m \left\{ \text{Cos}(x_{mp} + \psi_{mp}) \, \text{Cos}(\omega \, x_{mp}) \right.$$

$$+ x_{mp} \, \text{Sin}(x_{mp} + \psi_{mp}) \, \text{Cos} \, \omega \, x_{mp}$$

$$\left. + \omega \, x_{mp} \, \text{Cos}(x_{mp} + \psi_{mp}) \, \text{Sin} \, \omega \, x_{mp} \right\} + i \, kr^2 \, \delta \hat{\phi}_m$$

$$\left\{ + \text{Cos}(x_{mp} + \psi_{mp}) \, \text{Sin} \, \omega \, x_{mp} + x_{mp} \, \text{Sin}(x_{mp} + \psi_{mp}) \, \text{Sin} \, \omega \, x_{mp} \right.$$

$$\left. - \omega \, x_{mp} \, \text{Cos}(x_{mp} + \psi_{mp}) \, \text{Cos} \, \omega \, x_{mp} \right\} + kr^2 \, \delta \hat{\phi}_p \left\{ -\text{Cos}(x_{mp} + \psi_{mp}) \right.$$

$$\left. \left. - x_{mp} \, \text{Sin}(x_{mp} + \psi_{mp}) \right\} \right] d x_{mp}$$

$$- 3 \sum_{m=1}^{n} \frac{\Gamma_m}{4\pi} \int_{-\infty}^{\infty} J_{mp}^{-5/2} \left[kr^2 \left\{ \text{Sin}(x_{mp} + \psi_{mp}) - x_{mp} \, \text{Cos}(x_{mp} + \psi_{mp}) \right\} \right] K_{mp} \, d x_{mp}$$

where J_{mp} and K_{mp} are defined in Section 2.6.

First the variables of the present theory will be transformed
into corresponding variables used in S. C. Crow's analysis,
and then the limit will be taken as helix pitch tends to
infinity. All of S. C. Crow's parameters will carry the
subscript 's' to avoid confusion.

From the definition of axial coordinate, $kr x = x_s$.

The perturbations in the present study are of the type $e^{\alpha t + i \omega x_{mp}}$,

97

and if the wave number in S. C. Crow's theory is expressed as $k_s = \frac{\omega}{kr}$, the form of the perturbations is transformed to $e^{ik_s x_s + \alpha t}$ and the nondimensional wave number becomes $\beta_s = k_s \cdot 2r = k_s b$.

Applying the transformation described above, the self-induction term can be written as

$$\alpha \hat{\delta r_1} = \frac{\Gamma}{2\pi} \int_0^\infty J_{11}^{-3/2} kr\hat{\delta r_1} \left[i \left\{ -\frac{\omega}{kr}x_s \sin\left(\frac{x_s}{kr}\right) \cos\left(\frac{\omega x_s}{kr}\right) - \frac{x_s}{kr} \cos\left(\frac{x_s}{kr}\right) \sin\left(\frac{\omega x_s}{kr}\right) \right.\right.$$

$$\left.\left. - \frac{x_s}{kr} \cos\left(\frac{x_s}{kr}\right) \sin\left(\frac{\omega x_s}{kr}\right) + \sin\left(\frac{x_s}{kr}\right) \sin\left(\frac{\omega x_s}{kr}\right) \right\} \right] \frac{dx_s}{kr}$$

$$+ \frac{\Gamma}{2\pi} \int_0^\infty J_{11}^{-3/2} kr^2 \hat{\delta \phi_1} \left[\cos\left(\frac{x_s}{kr}\right) \cos\left(\frac{\omega x_s}{kr}\right) + \frac{x_s}{kr} \sin\left(\frac{x_s}{kr}\right) \cos\left(\frac{\omega x_s}{kr}\right) \right.$$

$$\left. + \frac{\omega x_s}{kr} \cos\left(\frac{x_s}{kr}\right) \sin\left(\frac{\omega x_s}{kr}\right) \right] \frac{dx_s}{kr}$$

$$+ \frac{\Gamma}{4\pi} \int_{-\infty}^\infty J_{11}^{-3/2} kr^2 \hat{\delta \phi_1} \left[-\cos\left(\frac{x_s}{kr}\right) - \frac{x_s}{kr} \sin\left(\frac{x_s}{kr}\right) \right] \frac{dx_s}{kr}$$

. . . . plus terms involving $J_{11}^{-5/2}$

Now, $\frac{x_s}{kr} = x \ll \Theta \to 0$ as helix pitch $\to \infty$, and one can approximate

$$\cos\left(\frac{x_s}{kr}\right) \to 1$$

$$\sin\left(\frac{x_s}{kr}\right) \to \frac{x_s}{kr}$$

Neglecting $\left(\frac{x_s}{kr}\right)^2$ terms and noting that $\frac{\omega}{kr} \cong k_s$, it follows that $J_{11}^{-3/2} = \left[2r^2 - 2r^2 \cos\left(\frac{x_s}{kr}\right) + \frac{k^2 x_s^2}{k^2} + \epsilon_0^2 \right] = \left[x_s^2 + \epsilon_0^2 \right]^{-3/2}$

and $\alpha \hat{\delta r_1} = \frac{\Gamma}{2\pi} \int_0^\infty r\hat{\delta \phi_1} \left[\frac{\cos(k_s x_s) + k_s x_s \sin(k_s x_s) - 1}{(x_s^2 + \epsilon^2)^{3/2}} \right] dx_s$.

Similarly, mutual-inductance terms can be written as

$$\alpha \hat{\delta r_1} = \frac{\Gamma}{2\pi} \int_0^\infty J_{12}^{-3/2} \left[kr\hat{\delta r_2} \left\{ -\frac{\omega i x_s}{kr} \sin\left(\frac{x_s}{kr} + \pi\right) \cos\left(\frac{\omega x_s}{kr}\right) \right.\right.$$

$$\left.\left. + i \sin\left(\frac{x_s}{kr} + \pi\right) \sin\left(\frac{\omega x_s}{kr}\right) - \frac{i x_s}{kr} \cos\left(\frac{x_s}{kr} + \pi\right) \sin\left(\frac{\omega x_s}{kr}\right) \right\} \right] \frac{dx_s}{kr}$$

98

$$+ \frac{\Gamma_2}{2\pi} \int_0^\infty J_{12}^{-3/2} \, k r^2 \, \delta\hat{\phi}_2 \left[\cos\left(\frac{x_s}{Rr} + \pi\right) \cos(k_s x_s) + \frac{x_s}{Rr} \sin\left(\frac{x_s}{Rr} + \pi\right) \cos(k_s x_s) \right.$$

$$\left. + k_s x_s \cos\left(\frac{x_s}{Rr} + \pi\right) \sin k_s x_s \right] \frac{dx_s}{Rr}$$

$$+ \frac{\Gamma_2}{2\pi} \int_0^\infty J_{12}^{-3/2} \, k r^2 \, \delta\hat{\phi}_1 \left[-\cos\left(\frac{x_s}{Rr} + \pi\right) - \frac{x_s}{Rr} \sin\left(\frac{x_s}{Rr} + \pi\right) \right] \frac{dx_s}{Rr}$$

$$J_{12}^{-3/2} = \left[2r^2 - 2r^2 \cos\left(\frac{x_s}{Rr} + \pi\right) + \frac{k^2 r^2 x_s^2}{R^2 r^2} \right]^{-3/2}$$

Taking the limits again yields $J_{12}^{-3/2} = \left[x_s^2 + 4r^2 \right]^{-3/2} = \left[x_s^2 + b^2 \right]^{-3/2}$

and $\propto \delta\hat{r}_1 = -\frac{\Gamma_2}{2\pi} \int_0^\infty r\delta\hat{\phi}_2 \left[\frac{\cos k_s x_s + k_s x_s \sin k_s x_s}{(x_s^2 + b^2)^{3/2}} \right] dx_s + \frac{\Gamma_2}{2\pi} \int_0^\infty \frac{r\delta\hat{\phi}_1 \, dx_s}{(x_s^2 + b^2)^{3/}}$

Writing $\delta\hat{r}_1 = \hat{y}_{1s}$, $r\delta\hat{\phi}_1 = \hat{z}_{1s}$, $\delta\hat{r}_2 = \hat{y}_{2s}$ and $r\delta\hat{\phi}_2 = \hat{z}_{2s}$, and remembering that $\delta\hat{r}$ is positive outward, while $\hat{y}_1$ and $\hat{y}_2$ are parallel (thereby changing sign of either the self- or mutual-inductance terms),

$$\propto \hat{y}_{1s} = \frac{\Gamma_1}{2\pi} \int_0^\infty \hat{z}_{1s} \, \frac{\cos k_s x_s + k_s x_s \sin k_s x_s - 1}{(x_s^2 + \varepsilon_0^2)^{3/2}} \, dx_s$$

$$- \frac{\Gamma_2}{2\pi} \int_0^\infty \hat{z}_{1s} \, \frac{1}{(x_s^2 + b^2)^{3/2}} \, dx_s + \frac{\Gamma_2}{2\pi} \int_0^\infty \hat{z}_{2s} \, \frac{\cos(k_s x_s) + k_s x_s \sin(k_s x_s)}{(x_s^2 + b^2)^{3/2}} \, dx_s$$

This is the same equation that results when Parks' modification is applied to Crow's theory. The one remaining equation relating $\hat{z}_{1s}$ with $\hat{y}_{1s}$ and $\hat{y}_{2s}$ can be obtained by following the same process for $r\delta\hat{\phi}_1$ perturbation equation.

APPENDIX II
FORTRAN IV SOURCE LISTING

```
C     * * * * * * * * * * * *                                   MAIN0001
C     *    MAIN PROGRAM     *                                   MAIN0002
C     * * * * * * * * * * * *                                   MAIN0003
      IMPLICIT REAL*8 (A-H,O-Z)                                 MAIN0004
      REAL*4 PK                                                 MAIN0005
      REAL*4 CP(27)                                             MAIN0006
      REAL*4 P1,P2,P3,P1,P2,D3,DELTA                            MAIN0007
      CCMPLEX*8 A(1P,1P),CMPLX                                  MAIN0008
      CCMPLEX*8 COMPA(3,3),COMPR(3,3)                           MAIN0009
      CCMPLEX*8 LAMFDA(3),LAMBDB(3)                             MAIN0010
      CCMPLEX*8 ACC(3,3)                                        MAIN0011
      CCMPLEX*8 LAMBC(18)                                       MAIN0012
      DIMENSICN Y(61),VA(61),R(27)                              MAIN0013
      DIMENSICN FC(61,51),CC(61),Z(61),C(51)                    MAIN0014
      CCMMCN B,AK,EPS                                           MAIN0015
C     INPUT NUMBER OF BLADES                                    MAIN0016
 100  READ(5,110) N,P                                           MAIN0017
 110  FCRMAT(I3,I3)                                             MAIN0018
      IF(N.EC.C) GO TO 680                                      MAIN0019
C     INPUT PITCH-WAVE NUMBER  AND CORE SIZE                    MAIN0020
 120  READ(5,130)BK,b,EPS                                       MAIN0021
 130  FCRMAT(F8.3,2X,DIC-3,1CX,DIC-3)                           MAIN0022
      IF(BK.EC.C.O)GO TO 100                                    MAIN0023
      AK=B*61.CCO                                               MAIN0024
      A2=304                                                    MAIN0025
      J1=61                                                     MAIN0026
      DO 140 I=1,N2                                             MAIN0027
      DO 140 J=1,N2                                             MAIN0028
 140  A(I,J)=CMPLX(C.C.C.C)                                     MAIN0029
      PI=3.141592653589793200                                  MAIN0030
      XU=2.CC*PI                                                MAIN0031
      AAV=(1.CC*AK*AK)                                          MAIN0032
                                                                MAIN0033
```

101

```
      AA=EPS/DSQRT(AAK)
      ZZ=XU/AA
      ZI=FLOG(ZZ+(ZZ**7+1.CC)**(.5D0))
      TANYZI=CTANH(ZI)
      CEN=AAK+XU*XU+EPS*EPS
C     CALCULATION OF ANALYTICALLY KNOWN  INTEGRALS FCR MODIFICATION CF
C     SINGULAR SELF INDUCTICN PERTURBATION INTEGRALS
      CC(1)=TANYZI/(EPS*EPS*DSQRT(AAK))
      CC(2)=((1.CC/EPS)-(1.DC/DSQRT(DEN)))/AAK
      CC(3)=(ZI-TANYZI/(AAK*DSQRT(AAK))
      CC(4)=(TANYZI-(TANYZI*TANYZI*TANHZI)/3.DC)/(3A**(4.D0))
      CC(5)=((1.DC/(EPS*EPS)/(EPS*EPS))-(1.DG/(CEN*DSQRT(DEN))))/(3.CO*AAK)
      CC(6)=(TANHZI*TANHZI*TANYZI)/(3.CO*EPS*EPS*DSQRT(AAK))
      CC(7)=((7.DC/(3.CO*EPS))-1.DC/DSQRT(CEN))+(EPS*EPS)/(3.CO*(CEN*
     1 DSQRT(DEN))))/(AAK*AAK)
      CC(8)=(ZI-TANYZI-(TANYZI*TANYZI*TANHZI)/3.CC)/(AAK*AAK*DSQRT(AAK))
     1 )
      IF(P.NE.2) GC TO 150
      CC(2)=0.CD0
      CC(5)=C.CDC
      CC(7)=C.CD0
15C   WRITE(6,160)(CC(I),I=1,8)
16C   FCRMAT(5X,8D12.5,2X))
      KL=2*N-1
      IF(P.EC.2) KL=N
CC 450 K=1,KU
CC 170 I=1,J1
      Y(I)=C.CD0
      Z(I)=C.CD0
17C   YA(I)=C.CD0
CC 18C I=1,27
18C   ZI(I)=C.CDC
      LLI=1
```

102

```
C     SET LL1=2 FCR SELF INDUCTICN INTEGRALS                              MAIN0067
      IF(K.EQ.N)LL1=2                                                     MAIN0068
C     CORE SIZE FACTOR EPS IS SET ZERC IN MUTUAL INDUCTICN INTEGRALS      MAIN0069
      EPS1=EPS                                                            MAIN0070
      IF(K.NE.N)EPS=C.GC0                                                 MAIN0071
      IF(K.EC.1)EPS=EPS1                                                  MAIN0072
      CK=K                                                                MAIN0073
      CN=N                                                                MAIN0074
      THETA=2.GC*PI*(1.CC-CK/CN)                                          MAIN0075
C     SET UPPER CUT CFF LIMIT CR INFINITE INTEGRALS DEPENDING UPCN PITCH  MAIN0076
      IF(CK.LF.C.1)GC TC 22C                                             MAIN0077
      IF(HK.LE.C.2) GC TC 21C                                            MAIN0078
      IF(HK.LT.C.4) GC TC 7CO                                            MAIN0079
      IF(HK.LT.1.0) GC TC 19C                                            MAIN0080
      J2=4C                                                               MAIN0081
      CC TC 23C                                                           MAIN0082
19C   J2=50                                                               MAIN0083
      CC TC 23C                                                           MAIN0084
2CC   J2=7C                                                               MAIN0085
      CC TC 23C                                                           MAIN0086
21C   J2=1C0                                                              MAIN0087
      CC TC 23C                                                           MAIN0088
22C   J2=2CC                                                              MAIN0089
C     INTEGRATE USING CSIMP UP TO AN UPPER LIMIT CF 14*PI                MAIN0090
23C   CC 22C J=1,J2                                                      MAIN0091
      XL=(J-1)*(PI/3.GC)                                                 MAIN0092
      IF(J.LF.42)GC TO 25C                                              MAIN0093
      L1=2                                                                MAIN0094
C     INTEGRATE USING QUADRATURE BEYCNC 14*PI UP TC UPPER CUT CFF LIMIT   MAIN0095
C     AT AN INTERVAL CF PI                                               MAIN0096
      YL=(J-2G)*PI                                                       MAIN0097
      XL=(J-29)*PI                                                       MAIN0098
      CALL GGS(IXL,XU,YA)                                                MAIN0099
```

103

```
      CC 24C KT=1,J1                                              MAIN0100
24C   Z(KT)=Z(KT)+YA(KT)                                         MAIN0101
      GC TC 320                                                  MAIN0102
25C   L1=1                                                       MAIN0103
      IF(J.GT.6)L1=2                                             MAIN0104
      P=PI/15C.CC                                                MAIN0105
26C   CC 2P0 I=1,51                                              MAIN0106
      X=XL+(I-1)*P                                               MAIN0107
      CALL INTG(X,YA)                                            MAIN0108
27C   CC 27C KR=1,J1                                             MAIN0109
      BC(KR,I)=YA(KR)                                            MAIN0110
28C   CCATINUE                                                   MAIN0111
      CC 3CC KS=1,J1                                             MAIN0112
29C   CC 29C I=1,51                                              MAIN0113
      C(I)=BE(KS,I)                                              MAIN0114
      Y(KS)=DSIPP(H,1,51,C)                                      MAIN0115
3C0   CCATINUE                                                   MAIN0116
      CC 31C I=1,J1                                              MAIN0117
31C   Z(I)=Z(I)+V(I)                                             MAIN0118
32C   CCATINUE                                                   MAIN0119
      IF(LL1.NF.2)GO TC 33C                                      MAIN0120
C     ACC ANALYTICALLY FVALUATED INTEGRAL VALUES TC THE MODIFIED MAIN0121
C     SELF INCLCTICA INTEGRALS                                   MAIN0122
      Z(1)=Z(1)+CC(1)                                            MAIN0123
      Z(2)=Z(2)+CC(1)                                            MAIN0124
      Z(3)=Z(3)+CC(2)                                            MAIN0125
      Z(4)=Z(4)+CC(2)                                            MAIN0126
      Z(5)=Z(5)+CC(3)                                            MAIN0127
      Z(6)=Z(6)+CC(1)                                            MAIN0128
      Z(7)=Z(7)+CC(2)                                            MAIN0129
      Z(8)=Z(8)+CC(1)                                            MAIN0130
      Z(9)=Z(9)+CC(2)                                            MAIN0131
      Z(1C)=Z(10)+CC(2)                                          MAIN0132
```

104

```fortran
C     SET LL1=2 FCR SELF INCUCTICN INTEGRALS                            MAIN0067
      IF(K.FG.N)LL1=2                                                   MAIN0068
C     CCRE SIZE FACTCR EPS IS SET ZERC IN MUTUAL INDUCTICN INTEGRALS    MAIN0069
      EPS1=EPS                                                          MAIN0070
      IF(K.NE.N)EPS=C.0C0                                               MAIN0071
      IF(N.EC.1)EPS=EPS1                                                MAIN0072
      CK=K                                                              MAIN0073
      CN=N                                                              MAIN0074
      THETA=2.FC*PI*(1.CC-CK/CN)                                        MAIN0075
C     SET UPPER CUT CFF LIMIT CN INFINITE INTEGRALS DEPENDING UPCN PITCHMAIN0076
      IF(EK.LF.C.5))GC TC 22C                                           MAIN0077
      IF(CK.LE.C.2) GC TC 21C                                           MAIN0078
      IF(CHK.LT.C.4) GC TC 2C0                                          MAIN0079
      IF(CHK.LT.1.0) GC TC 19C                                          MAIN0080
      J2=4C                                                             MAIN0081
      GC TC 23C                                                         MAIN0082
19C   J2=5C                                                             MAIN0083
      GC TC 73C                                                         MAIN0084
2CC   J2=7C                                                             MAIN0085
      GC TC 23D                                                         MAIN0086
21C   J2=1C0                                                            MAIN0087
      GC TC 23C                                                         MAIN0088
22C   J2=2CC                                                            MAIN0089
C     INTEGRATE USING CSIMP UP TO AN UPPER LIMIT CF 14*PI               MAIN0090
23C   CC 32C J=1,J2                                                     MAIN0091
      XL=(J-1)*(PI/3.0C0)                                               MAIN0092
      IF(J.LF.42)GC TO 25C                                              MAIN0093
      LL=2                                                              MAIN0094
C     INTEGRATE USING CUACRATURE REYCNE 14*PI LP TC UPPER CUT CFF LIMIT MAIN0095
C     AT AN INTERVAL CF PI                                              MAIN0096
      YL=(J-2S)*PI                                                      MAIN0097
      XL=(J-29)*PI                                                      MAIN0098
      CALL GCS(XL,XU,YA)                                                MAIN0099
```

103

```
MAINO133    Z(11)=Z(11)+CC(3)
MAINO134    Z(12)=Z(12)+CC(2)
MAINO135    Z(13)=Z(13)+CC(3)
MAINO136    Z(14)=Z(14)+CC(3)
MAINO137    Z(16)=Z(16)+CC(4)
MAINO138    Z(17)=Z(17)+CC(5)
MAINO139    Z(1C)=Z(1e)+CC(4)
MAINO140    Z(19)=Z(19)+CC(5)
MAINO141    Z(2C)=Z(2C)+CC(5)
MAINO142    Z(21)=Z(21)+CC(6)
MAINO143    Z(22)=Z(22)+CC(4)
MAINO144    Z(23)=Z(23)+CC(5)
MAINO145    Z(24)=Z(24)+CC(6)
MAINO146    Z(25)=Z(25)+CC(5)
MAINO147    Z(26)=Z(26)+CC(6)
MAINO148    Z(27)=Z(27)+CC(7)
MAINO149    Z(2e)=Z(2e)+CC(6)
MAINO150    Z(29)=Z(29)+CC(7)
MAINO151    Z(3C)=Z(3C)+CC(4)
MAINO152    Z(31)=Z(31)+CC(5)
MAINO153    Z(32)=Z(32)+CC(6)
MAINO154    Z(33)=Z(33)+CC(5)
MAINO155    Z(34)=Z(34)+CC(6)
MAINO156    Z(35)=Z(35)+CC(7)
MAINO157    Z(36)=Z(36)+CC(6)
MAINO158    Z(37)=Z(37)+CC(6)
MAINO159    Z(38)=Z(38)+CC(7)
MAINO160    Z(39)=Z(39)+CC(6)
MAINO161    Z(4C)=Z(4C)+CC(7)
MAINO162    Z(41)=Z(41)+CC(P)
MAINO163    Z(42)=Z(42)+CC(6)
MAINO164    Z(43)=Z(43)+CC(7)
MAINO165    Z(44)=Z(44)+CC(7)
```

105

```
Z(45)=Z(45)+CC(8)                                                    MAIN0166
Z(46)=Z(46)+CC(4)                                                    MAIN0167
Z(47)=Z(47)+CC(5)                                                    MAIN0168
Z(48)=Z(48)+CC(4)                                                    MAIN0169
Z(49)=Z(49)+CC(5)                                                    MAIN0170
Z(5C)=Z(5C)+CC(5)                                                    MAIN0171
Z(51)=Z(51)+CC(6)                                                    MAIN0172
Z(52)=Z(52)+CC(5)                                                    MAIN0173
Z(53)=Z(53)+CC(6)                                                    MAIN0174
Z(54)=Z(54)+CC(4)                                                    MAIN0175
Z(55)=Z(55)+CC(7)                                                    MAIN0176
Z(56)=Z(56)+CC(6)                                                    MAIN0177
Z(57)=Z(57)+CC(7)                                                    MAIN0178
Z(5E)=Z(54)+CC(7)                                                    MAIN0179
Z(59)=Z(59)+CC(8)                                                    MAIN0180
Z(6C)=Z(6C)+CC(5)                                                    MAIN0181
Z(61)=Z(61)+CC(6)                                                    MAIN0182
33C  CC 34C J=1,J1                                                   MAIN0183
34C  Y(J)=Y(J)                                                       MAIN0184
EPS=EPS1                                                             MAIN0185
CC=3.CDC                                                            MAIN0186
CE=2.CDC                                                            MAIN0187
C   FCRM THE 3*3 COMPLEX SELF CR MUTUAL INDUCTICN MATRIX            MAIN0188
B(1)=AK*(W+Y(5)+Y(1C)-V(12))-CC+AK*(Y(45)-Y(52)-Y(31)+Y(36))        MAIN0189
B(2)=AK*(-W+Y(14)+Y(11)-Y(13))-CD+AK*(Y(51)-Y(34)-Y(54)+Y(39))      MAIN0190
B(3)=AK*(W+Y(13)+Y(8)+Y(14))-CC+AK*(Y(32)-Y(37))                    MAIN0191
P(4)=AK*(-W+Y(12)+Y(9)+Y(15))-CC+AK*(Y(35)-Y(40))                   MAIN0192
E(5)=-W+Y(11)-Y(8)-CC+AK+AK*(Y(53)-Y(56))                           MAIN0193
P(6)=W+Y(10)-Y(9)-CC+AK+AK*(Y(55)-Y(58))                            MAIN0194
P(7)=AK*(-W+Y(7)-Y(8)-V(14))-CC+AK*(Y(46)-CE+Y(48)-Y(53))+          MAIN0195
1 Y(3C)+Y(37))                                                      MAIN0196
P(8)=AK*(W+Y(7)-Y(9)-V(15))-CC+AK*(Y(47)-CE+Y(50)-Y(55)+Y(33))      MAIN0197
1 +Y(46C))                                                          MAIN0198
```

106

```
P(5)=AK*(h*V(15)+V(1C)-CD+AK*(V(45)-V(31)-V(38))                    MAIN0199
F(1C)=AK*(-h*V(14)+V(11)-V(13))-CD+AK*(V(51)-V(34)-V(41))          MAIN0200
P(11)=-V(10)-CF*AF*AK*( V(6C)-V(52)-V(57))-h*V(7)+h*V(9)           MAIN0201
2C(12)=-V(11)-CC+AK+AK*(V(61)-V(54)-V(55))+h*V(6)-h*V(8)           MAIN0202
P(13)=CF+V(6)-V(9)-h*V(1)-CD*(V(46)-CE*V(3C))                     MAIN0203
P(14)=CF+V(7)-V(5)-h*V(7C)-CD*(V(47)-CE*V(45)+V(31))              MAIN0204
P(15)=V(1C)-h*V(7D+h*V(6)-CC*(V(45)-V(31))                        MAIN0205
P(16)=V(11)+h*V(6)-h*V(2)-CD*(V(51)-V(34))                        MAIN0206
P(17)=-CF+AK*(V((C)-V(52))                                        MAIN0207
P(18)=-CF+AK*(V(61)-V(54))                                        MAIN0208
P(19)=-CC+AK*(V(19)+V(75)-Y(23))-V(2C))                           MAIN0209
P(21)=CC+AK+AK*(V(21)-V(24))+V(2)                                 MAIN0210
P(24)=CF+AK+AV*(V(17)-Y(2S)-Y(2S))+V(3)                           MAIN0211
P(25)=-CF+V(11C)-CE*(V(18)+V(22))-V(2)                            MAIN0212
F(26)=CC*(V(15)-Y(73))-V(2C)                                      MAIN0213
P(27)=CC+AK+AK*(V(17)-V(2C))                                      MAIN0214
35C  E(2C)=CF*AK*(Y(24)-V(2C))-hK+(Y(2)+V(5))                     MAIN0215
     E(22)=-CF+AV*(V(16)-CF+V(1C)-Y(21)+V(22)+V(26))+AK*(Y(2C)+V(26.)+AK*(Y(2))+V(5)) MAIN0216
     E(23)=CC+AK*(Y(19)-V(23)-Y(27))+AK*(V(4)-V(3))             MAIN0217
36C  hRITE(6,37C) J7,AK                                           MAIN0218
37C  FCRMAT(5X,///,5X,13,5X,*K=*,F5.2)                            MAIN0219
     hRITE(6,38C) (h(I),I=1,9)                                    MAIN0220
     hRITE(6,38C) (F(I),I=1C,18)                                  MAIN0221
     hRITE(6,38C) (F(I),I=19,27)                                  MAIN0222
38C  FCRMAT(2V,S(1P5,C12.5))                                      MAIN0223
     CALL NOUMFL                                                  MAIN0224
C    FCRM THE COMPLETE EIGENMATRIX AFTER CALCULATING ALL THE SELF AND MAIN0225
C    MUICAL INCUCTION MATRICES AND BY USING THE SYMMETRY CONSIDERATIONS MAIN0226
     IF(K.GT.A.)GC TC 39C                                         MAIN0227
     IJ1=1                                                        MAIN0228
     IJ2=K                                                        MAIN0229
     MJ1=N+1-K                                                    MAIN0230
     MJ2=N                                                        MAIN0231
```

107

```
      GC TC 40C                                                     MAIN0232
350   IJ1=K-N+1                                                     MAIN0233
      IJ2=N                                                         MAIN0234
      PJ1=1                                                         MAIN0235
      PJ2=2*N-K                                                     MAIN0236
400   IJU=IJ2-IJ1+1                                                 MAIN0237
      IF(IJ1.NF.PJ1) GC TC 42C                                      MAIN0238
CC 41C L=1,18,2                                                     MAIN0239
      L2=(L+1)/2+18                                                 MAIN0240
410   P(L)=B(L)+B(L2)                                               MAIN0241
420   CC 430 I=1,77                                                 MAIN0242
430   CE(I)=B(I)                                                    MAIN0243
44C   CC 480 IJ=1,IJU                                               MAIN0244
      IF(K.GT.1)GO TC 46C                                           MAIN0245
      P1=CB(2)+CH(1C)+CF(18)                                        MAIN0246
      P2=CE(12)+CB(16)-CR(1C)*CR(18)-CE(2)*CE(10)-CR(2)*CB(18)      MAIN0247
     1 -CP(3)*CR(7)-CR(5)*CB(13)                                    MAIN0248
      P3=CR(2)*CE(12)*CF(16)*CR(3)*CB(13)*CR(12)*CR(5)*CR(7)*CB(16)- MAIN0249
     1CE(2)*CR(1C)*CR(18)-CR(3)*CR(7)*CE(18)-CR(5)*CB(1C)*CB(13)    MAIN0250
      P1=P1/3                                                       MAIN0251
      P2=-P2/3                                                      MAIN0252
      P3=-P3                                                        MAIN0253
      CELTA=3.*R1*R2*P1*P2*6.*(R1*R2*R3)-R3*C3*R3-4.*P2*P2*P2       MAIN0254
     1 -4.*P3*P1*R1*R1                                              MAIN0255
45C   WRITE(6,450) P1,P2,P3,CELTA                                   MAIN0256
46C   FCRPAT(5X,E12.5,5X,F12.5,5X,F12.5,5X,'CELTA=',E12.5)          MAIN0257
      I2=3*(IJ+IJ1-1)                                               MAIN0258
      P2=3*(IJ+PJ1-1)                                               MAIN0259
      A(I2-2,P2-2)=C*PLX(CP(1),CR(2))+A(I2-2,P2-2)                  MAIN0260
      A(I2-2,P2-1)=C*PLX(CF(3),CR(4))+A(I2-2,P2-1)                  MAIN0261
      A(I2-2,P2)=C*PLX(CF(5),CR(6))+A(I2-2,P2)                      MAIN0262
      A(I2-1,P2-2)=C*PLX(CR(7),CR(8))+A(I2-1,P2-2)                  MAIN0263
      A(I2-1,P2-1)=C*PLX(CR(9),CC(1C))+A(I2-1,P2-1)                 MAIN0264
```

108

```
      A(I2-1,M2)=CMPLX(CH(11),CR(12))+A(I2-1,M2)
      A(I2,M2-2)=CMPLX(CP(13),CE(14))+A(I2,M2-2)
      A(I2,M2-1)=CMPLX(CP(15),CH(16))+A(I2,M2-1)
      A(I2,M2)=CMPLX(CB(17),CH(18))+A(I2,M2)
      IF(I2.EC.M2) GO TO 48C
      ACC(1,1)=CMPLX(CP(19),C.C)
      ACC(1,2)=CMPLX(CC(2C),C.C)
      ACC(1,3)=CMPLX(CP(21),C.C)
      ACC(2,1)=CMPLX(CP(22),C.C)
      ACC(2,2)=CMPLX(CH(23),C.C)
      ACC(2,3)=CMPLX(CH(24),C.C)
      ACC(3,1)=CMPLX(CP(25),C.C)
      ACC(3,2)=CMPLX(CH(26),C.C)
      ACC(3,3)=CMPLX(CH(27),C.C)
      CC 47C I=1,3
      CC 470 J=1,3
      A(I2-3+I,I2-3+J)=A(I2-3+I,I2-3+J)+ACD(I,J)
      IF(M.NE.2)GC TC 47C
      A(M2-3+I,M2-3+J)=A(M2-3+I,M2-3+J)+ACC(I,J)
 47C  CCNTINUE
 48C  CCNTINUE
      IF(N.EC.1)GO TO 53C
      IF(M.NE.2)GC TC 53C
      IPL=N-1
      CC 5CC IPI=1,IPL
      IP2=IPI+1
      CC 5CO IPJ=IP2,N
      CC 49C I=1,3
      CC 49C J=1,3
      A(3+IPJ-3+I,3+IPI-3+J)=A(3+IPI-3+I,3+IPJ-3+J)
 49C  CCNTINUE
 5CC  CCNTINUE
C     EXAMINE SPECIAL POSSIBLE SYMMETRY COMBINATIONS OF SYMMETRIC AND
```

```
C      ANTI-SYMMETRIC MODES GIVING RISE TO MAX. AND MIN. DIVERGENCE     MAIN0298
C      RATES FCR THE CASE CF A THC BLADEC RCTCR                         MAIN0299
       IF(N.NE.2)GC TC 530                                              MAIN0300
       CC 510 I=1,3                                                     MAIN0301
       CC 51C J=1,3                                                     MAIN0302
       CCPRA(I,J)=A(I,J)+A(I,J+3)                                       MAIN0303
       CCPMP(I,J)=A(I,J)-A(I,J+3)                                       MAIN0304
510    CCNTINUE                                                         MAIN0305
       WRITE(6,520)                                                     MAIN0306
520    FCRMAT(////)                                                     MAIN0307
530    WRITE(6,540)AK,A,EPS,N,M                                         MAIN0308
540    FCRMAT(5X,'PITCH=',FP.3,5X,'WAVE NUMBER=',G1C.3,5X,'CCRE SIZE=', MAIN0309
      1  G1C.3,5X,//,5X,'NUMBER CF BLADES=',I3,5X,'M=',I3,//)           MAIN0310
       WRITE(6,520)                                                     MAIN0311
550    WRITE(6,560)                                                     MAIN0312
560    FCRMAT(5X,'MATRIX BEFCRE CIAGONALISATICN',//)                    MAIN0313
       CC 570 I=1,N7                                                    MAIN0314
       CC 57C J=1,N2                                                    MAIN0315
570    WRITE(6,580) A(I,J),I,J                                          MAIN0316
5AC    FCRMAT(5X,F12.5,5X,F12.5,5X,I3,5X,I3)                            MAIN0317
       KVEC=1                                                           MAIN0318
C      EIGENVALUE ANALYSIS PERFCRMEC RY CALLING ALLMAT                  MAIN0319
       CALL ALLMAT(A,LAMND,N2,IR,ACAL,KVEC)                             MAIN0320
       WRITE(6,520)                                                     MAIN0321
       WRITE(6,590)                                                     MAIN0322
590    FCRMAT(5X,'EIGENFUNCTICNS',//)                                   MAIN0323
       CC 6CC I=1,N2                                                    MAIN0324
       CC 6CC J=1,N2                                                    MAIN0325
6CC    WRITE(6,580) A(I,J),I,J                                          MAIN0326
       WRITE(C,61C)                                                     MAIN0327
C      PRINT CUT REAL AND IMACINARY PARTS CF EIGENVALUES                MAIN0328
610    FCRMAT(5X,//,5X,'EIGENVALUES',//,19X,'REAL',11X,'IMAGINARY')     MAIN0329
       CC 62C I=1,N2                                                    MAIN0330
```

110

```
620   WRITE(6,630) I,LAMPR(I)                                              MAIN0331
630   FORMAT(5X,I3,5X,E12.5,5X,E12.5)                                      MAIN0332
      IF(N.NE.2) GO TO 670                                                 MAIN0333
C     PRINT CUT SYMMETRIC AND ANTI-SYMMETRIC EIGENVALUES FOR THE CASE OF   MAIN0334
C     TWO PLACED ROTOR                                                     MAIN0335
      CALL ALLMAT (COEFFA,LAMHTA,3,3,NCAL,KVEC)                            MAIN0336
      CALL ALLMAT(COEFF,LAMFFB,3,3,NCAL,KVEC)                              MAIN0337
      WRITE(6,640)                                                         MAIN0338
640   FORMAT(5X,//,5X,'SPECIAL POSSIBLE SYMMETRY COMBINATIONS GIVING       MAIN0339
     1 RISE TO MAX. DIVERGENCE RATE',//,5X,'EIGENVALUES',//,17X,'REAL',    MAIN0340
     2 ,11X,'IMAGINARY',14X,'REAL',11X,'IMAGINARY',//)                     MAIN0341
      DO 650 I=1,3                                                         MAIN0342
650   WRITE(6,660)LAMPCA(I),LAMPRB(I),I                                    MAIN0343
660   FORMAT(13X,E12.5,5X,E12.5,10X,E12.5,5X,E12.5,5X,I3)                  MAIN0344
670   GO TO 120                                                           MAIN0345
680   STOP                                                                MAIN0346
      END                                                                 MAIN0347
```

111

```
C      * * * * * * * * * * * * * *                              ALMT0001
C      *      SUBROUTINE ALLMAT      *                          ALMT0002
C      * * * * * * * * * * * * * *                              ALMT0003
C                                                               ALMT0004
       SUBROUTINE ALLMAT(A,LAMBDA,M,IA,NCAL,KVEC)               ALMT0005
C                                                               ALMT0006
C  UNIVERSITY OF ROCHESTER FILE NO. 31C.2.5CB.                  ALMT0007
C  A FORTRAN IV SUBROUTINE TO CALCULATE THE RIGHT EIGENVALUES AND/OR  ALMT0008
C  EIGENVECTORS OF ARBITRARY COMPLEX MATRICES BY USE OF THE     ALMT0009
C  OR ALGORITHM AND WIELANDT INVERSE POWER METHOD FOR VECTORS.  ALMT0010
C  ALLMAT WAS WRITTEN BY R.E. FUNDERLIC AND J. KENZEL FOR THE   ALMT0011
C  IBM 7C9C COMPUTER AT OAK RIDGE AND SUBMITTED TO THE SHARE    ALMT0012
C  PROGRAM LIBRARY (OR APMAT).                                  ALMT0013
C                                                               ALMT0014
C  ALLMAT IS ADOPTED FROM THE 7C9C FORTRAN IV PROGRAM OR APMAT FROM  ALMT0015
C  THE SHARE PROGRAM LIBRARY                                    ALMT0016
C                                                               ALMT0017
C  THE MAXIMUM ORDER OF MATRIX A IS 6C@6C                       ALMT0018
C                                                               ALMT0019
C  THE SUBPROGRAM IS CALLED BY THE STATEMENT .                  ALMT0020
C                                                               ALMT0021
C      CALL ALLMAT(A,LAMBDA,M,IA,NCAL,KVEC)                     ALMT0022
C                                                               ALMT0023
C               DESCRIPTION OF ARGUMENTS                        ALMT0024
C                                                               ALMT0025
C  A      = COMPLEX*8,INPUT MATRIX. ON RETURN CONTAINS THE COMPLEX  ALMT0026
C           EIGENVECTORS OF THE ORIGINAL MATRIX AS COLUMNS, IF  ALMT0027
C           REQUESTED                                           ALMT0028
C  LAMBDA = COMPLEX*8,ARRAY OF EIGENVALUES OF MATRIX A UPON RETURN  ALMT0029
C  M      = INTEGER*4,ORDER OF MATRIX A                         ALMT0030
C  IA     = INTEGER*4, THE ROW DIMENSION OF MATRIX A            ALMT0031
C  NCAL   = INTEGER*4, NUMBER OF EIGENVALUES CALCULATED UPON RETURN.  ALMT0032
C  KVEC   = INTEGER*4, KVEC = C NO EIGENVECTORS CALCULATED, OTHERWISE ALMT0033
C           EIGENVECTORS RETURNED AS COLUMNS OF A
```

112

```
C
      CCPPLEX A(IA,IA),H(6C,6C),PL(6C,6C),LAPECLA(IA),VECT(60),     ALMT0034
     1PLLT(6C),SHIFT(3),TEMP,SOM,CIS,TEPP1,TEPP2                     ALMT0035
      CCPPLEX*16 SUMT                                                ALMT0036
      CCPPLEX*16 CP1,CP2                                             ALMT0037
      CCPPLEX CSCRT,CCAJG                                            ALMT0038
      LCCICAL INT-(6C),TWICE                                         ALMT0039
      INTEGER INT(6C),R,RP1,RP2                                      ALMT0040
      N=P                                                            ALMT0041
      ACAL=N                                                         ALMT0042
      IF(R.NE.1)GC TO 10C                                            ALMT0043
      LAPECA(1)=A(1,1)                                               ALMT0044
      A(1,1)=1.                                                      ALMT0045
      GC TC 67C                                                      ALMT0046
  1CC ICCUNT=C                                                       ALMT0047
      SHIFT(1)=(C.,0.)                                               ALMT0048
      SHIFT(2)=(C.,C.)                                               ALMT0049
      SHIFT(3)=(C.,0.)                                               ALMT0050
      IF(R.NE.2)GO TC 13C                                            ALMT0051
  11C TEPP=(A(1,1)+A(2,2)+CSCRT((A(1,1)+A(2,2))**2-                  ALMT0052
     14.*(A(2,2)*A(1,1)-A(2,1)+A(1,2))))/2.                          ALMT0053
      IF(REAL(TEPP).NE.C..CR.AIMAG(TEPP).NE.C.)GO TC 120             ALMT0054
      LAPECCA(P)=SHIFT(1)                                            ALMT0055
      LAPECA(P-1)=A(1,1)+A(2,2)+SHIFT(1)                             ALMT0056
      GC TC 470                                                      ALMT0057
  12C LAPCCA(P)=TEPP+SHIFT(1)                                        ALMT0058
      LAPECA(P-1)=(A(2,7)+A(1,1)-A(2,1)+A(1,2))/(LAMBCA(P)-SHIFT(1))+SHI ALMT0059
     1FT(1)                                                      ALMT0060
      GC TC 470                                                      ALMT0061
C                                                                    ALMT0062
C     RECLCE MATRIX A TC HESSENBERG FORP                             ALMT0063
C                                                                    ALMT0064
  13C NP2=N-2                                                        ALMTC065
                                                                     ALMTC066
```

113

```
       CC 24C R=1,NP2                                              ALMTO067
       RF1=R+1                                                     ALPTO068
       RP2=R+2                                                     ALMTO069
       APIC=C.                                                     ALMTO070
       IAT(R)=RP1                                                  ALMTO071
       CC 14C I=RP1,N                                              ALMTO072
       ABSSC=REAL(A(I,R))**2+AIMAG(A(I,R))**2                      ALMTO073
       IF(APSSC.LE.APIC)GO TO 14C                                  ALMTO074
       IAT(R)=I                                                    ALMTO075
       APIC=ABSSC                                                  ALMTO076
  14C  CCNTINUE                                                    ALMTO077
       INTER=IAT(R)                                                ALMTO078
       IF(ABS(APIC).LT.1.E-5C) GO TO 24C                           ALMTO079
       IF(INTER.EC.RP1)GO TO 17C                                   ALMTO080
       CC 15C I=R,N                                                ALMTO081
       TEMP=A(RP1,I)                                               ALMTO082
       A(RP1,I)=A(INTER,I)                                         ALMTO083
  15C  A(INTER,I)=TEMP                                             ALMTO084
       CC 16C I=1,N                                                ALMTO085
       TEPP=A(I,RP1)                                               ALMTO086
       A(I,RP1)=A(I,INTER)                                         ALMTO087
  16C  A(I,INTER)=A(I,INTER)                                       ALMTO088
  17C  CC 18C I=RP2,N                                              ALMTO089
       MULT(I) = A(I,R)/A(RP1,R)                                   ALMTO090
  18C  A(I,R)=MULT(I)                                              ALMTO091
       CC 2CC I=1,RP1                                              ALMTO092
       SUPT=C.C                                                    ALMTO093
       CC 19C J=RP2,N                                              ALMTO094
       CP1=A(I,J)                                                  ALMTO095
       CP2=MULT(J)                                                 ALMTO096
  19C  SUPT=SUPT+CP1*CP2                                           ALMTO097
  2CC  A(I,RP1)=A(I,RP1)+SUPT                                      ALMTO098
       CC 22C I=RP2,N                                              ALMTO099
```

114

```
      SLPT=C.C                                                      ALMT0100
      DC 21C J=KP2,N                                                ALMT0101
      CP1=A(1,J)                                                    ALMT0102
      CP2=PLL(T(J)                                                  ALMT0103
210   SLPT=SLPT+CP1*CP2                                             ALMT0104
220   A(1,KP1)=A(1,KP1)-SLPT-WLT(I)*A(RP1,RP1)                      ALMT0105
      DC 22C I=KP2,N                                                ALMT0106
      DC 23C J=KP2,N                                                ALMT0107
230   A(1,J)=A(1,J)-PLLT(I)*A(RP1,J)                                ALMT0108
240   CCATINUE                                                      ALMT0109
C                                                                   ALMT0110
C     CALCULATE FPSILCN                                             ALMT0111
C                                                                   ALMT0112
      EPS=C.                                                        ALMT0113
      DC 25C I=1,N                                                  ALMT0114
250   EPS=EPS+CABS(A(1,I))                                          ALMT0115
      DC 27C I=2,N                                                  ALMT0116
      SUP=C.                                                        ALMT0117
      IP1=I-1                                                       ALMT0118
      DC 26C J=IP1,N                                                ALMT0119
260   SUP=SUP+CAPS(A(1,J))                                          ALMT0120
27C   IF(SLP.GT.EPS)EPS=SLP                                         ALMT0121
      EPS=SCRT(FLCAT(A,1))*EPS*1.E-12                               ALMT0122
      IF(EPS.EC.C.)EPS=1.F-12                                       ALMT0123
      DC 2PC I=1,N                                                  ALMT0124
      DC 2FC J=1,N                                                  ALMT0125
      A(1,J)=A(1,J)                                                 ALMT0126
25C   IF(A.NE-1)GC TC 3CC                                           ALMT0127
      LAPEGA(W)=A(1,1)+SHIFT(1)                                     ALMT0128
      GC TC 47C                                                     ALMT0129
3CC   IF(A.EC.7)CO TC 11C                                           ALMT0130
31C   M(1=M-Nc1                                                     ALMT0131
      IF(REAL(A(K,N)).NE.C..CR.AIPAG(A(K,N)).NE.G.)                 ALMT0132
```

115

```
    1 IF(ABS(REAL(A(N,N-1)/A(K,K)))*ABS(AIMAG(A(N,N-1)/A(N,N)))-1.E-7)   ALMTO133
    2 320,330,320                                                          ALMTO134
320 IF(ABS(REAL(A(K,K-1)))+ABS(AIMAG(A(K,K-1))).GE.EPS)GO TO 340          ALMTO135
330 LAMBDA(IPN1)=A(N,N)+SHIFT(1)                                          ALMTO136
    ICOUNT=C                                                              ALMTO137
    N=N-1                                                                 ALMTO138
    GO TO 300                                                             ALMTO139
C                                                                         ALMTO140
C                                                                         ALMTO141
C   DETERMINE SHIFT                                                       ALMTO142
C                                                                         ALMTO143
340 SHIFT(2)=(A(N-1,N-1)+A(N,N))+CSQRT((A(N-1,N-1)+A(N,N))**2             ALMTO144
   1 -4.*(A(N,N)*A(N-1,N-1)-A(N,N-1)*A(N-1,N))))/2.                       ALMTO145
    IF(REAL(SHIFT(2)).NE.C..OR.AIMAG(SHIFT(2)).NE.C.)GO TO 350            ALMTO146
    SHIFT(3)=A(N-1,N-1)+A(N,N)                                           ALMTO147
    GO TO 360                                                             ALMTO148
350 SHIFT(3)=(A(N,N)+A(N-1,N-1)-A(N,N-1)*A(N-1,N))/SHIFT(2)               ALMTO149
360 IF(CABS(SHIFT(2)-A(N,N)).LT.CABS(SHIFT(3)-A(N,N)))GO TO 370           ALMTO150
    INDEX=3                                                               ALMTO151
    GO TO 380                                                             ALMTO152
370 INDEX=2                                                               ALMTO153
380 IF(CABS((A(N-1,N-2)).GE.EPS)GO TO 390                                 ALMTO154
    LAMBDA(IPN1)=SHIFT(2)+SHIFT(1)                                        ALMTO155
    LAMBDA(IPN1+1)=SHIFT(3)+SHIFT(1)                                      ALMTO156
    ICOUNT=0                                                              ALMTO157
    N=N-2                                                                 ALMTO158
    GO TO 290                                                             ALMTO159
390 SHIFT(1)=SHIFT(1)+SHIFT(INDEX)                                        ALMTO160
    DO 400 I=1,N                                                          ALMTO161
400 A(I,I)=A(I,I)-SHIFT(INDEX)                                            ALMTO162
C                                                                         ALMTO163
C   PERFORM GIVENS ROTATIONS, OR ITERATES                                 ALMTO164
C                                                                         ALMTO165
    IF(ICOUNT.LE.10)GO TO 410
```

116

```
      NCAL=N-K                                                          ALMT0166
      GC TC 470                                                         ALMT0167
41C   AP1=A-1                                                           ALMT0168
      TEPP1=A(1,1)                                                      ALMT0169
      TEPP2=A(2,1)                                                      ALMT0170
      CC 46C R=1,AP1                                                    ALMT0171
      RP1=R+1                                                           ALMT0172
      R+C=SCRT(REAL(TEPP1)**2+AIPAG(TEPP1)**2+                          ALMT0173
     1 REAL(TEPP2)**2+AIPAG(TEPP2)**2)                                  ALMT0174
      IF(R+C.EC.C.)GC TC 46C                                            ALMT0175
      CIS=TEPP1/RHO                                                     ALMT0176
      SCN=TFPP2/R+C                                                     ALMT0177
      INCEX=PAXC(R-1,1)                                                 ALMT0178
      CC 42C I=INCEX,N                                                  ALMT0179
      TEPP=CCNJG(CIS)*A(R,I)+CONJG(SCN)*A(RP1,I)                        ALMT0180
      A(RP1,I)=-SCN*A(R,I)+CIS*A(RP1,I)                                 ALMT0181
42U   A(R,I)=TEPP                                                       ALMT0182
      TEPP1=A(RP1,RP1)                                                  ALMT0183
      IF(R+2.GT-N)GC TC 43C                                             ALMT0184
      TEPP2=A(R+2,R+1)                                                  ALMT0185
43C   CC 44C I=1,R                                                      ALMT0186
      TEPP=CIS*A(I,R)+SCN*A(I,RP1)                                      ALMT0187
      A(I,RP1)=-CCNJG(SCN)*A(I,R)+CONJG(CIS)*A(I,RP1)                   ALMT0188
44C   A(I,R)=TEPP                                                       ALMT0189
      INCEX=MIMC(R+2,N)                                                 ALMT0190
      CC 45C I=RP1,INCEX                                                ALMT0191
      A(I,R)=SCN*A(I,RP1)                                               ALMT0192
45C   A(I,RP1)=CCNJG(CIS)*A(I,RP1)                                      ALMT0193
46C   CCNTINUE                                                          ALMT0194
      ICCLAT=ICCUNT+1                                                   ALMT0195
      GC TC 31C                                                         ALMT0196
C                                                                       ALMT0197
C     CALCULATE VECTORS                                                 ALMT0198
```

117

```fortran
C
  47C IF(ACAL.FC.C)GC TO 67C
      IF(RVEC.FC.0)GC TO 67C
      N=P
      NP1=N-1
      IF(A.NF.2)GC TO 42C
      EPS=AMAX1(CABS(LAMBCA(1)),CABS(LAMBCA(2)))*1.E-8
      IF(EPS.EC.C.)EPS=1.E-12
      H(1,1)=A(1,1)
      H(1,2)=A(1,2)
      H(2,1)=A(2,1)
      H(2,2)=A(2,2)
  48C  CC 66C L=1,ACAL
       CC 5CO I=1,A
       CC 49C J=1,A
  490  HL(I,J)=H(I,J)
  5CC  HL(I,I)=HL(I,I)-LAMBCA(L)
       CC 54C I=1,AP1
       MLLT(I)=C.
       INTH(I)=.FALSE.
       IP1=I+1
       IF(CABS(HL(I+1,I)).LE.CABS(HL(I,I)))GC TO 520
       INTH(I)=.TRUE.
       CC 51C J=I,A
       TEMP=HL(I+1,J)
       HL(I+1,J)=HL(I,J)
  51C  HL(I,J)=TEMP
  52C  IF(REAL(HL(I,I)).FC.C..ANC.AIPAG(HL(I,I)).EC.C.)GC TO 54C
       MULT(I)=-HL(I+1,I))/HL(I,I)
       CC 53C J=IP1,N
       HL(I+1,J)=HL(I+1,J)+MLLT(I)*HL(I,J)
  530  CCNTINUE
  54C  CCNTINUE
       CC 55C I=1,N
```

```
55C   VECT(I)=1.
      THICE=.FALSE.
56C   IF(REAL(HL(N,N)).EC.C..AND.AIMAG(HL(N,N)).EC.O.)HL(N,N)=EPS
      VECT(N)=VECT(N)/HL(N,N)
      CC 58C I=1,NP1
      K=N-I
      CC 57C J=K,NP1
57C   VECT(K)=VECT(K)-HL(K,J+1)*VECT(J+1)
58C   IF(REAL(HL(K,K)).EC.C..AND.AIMAG(HL(K,K)).EC.O.)HL(K,K)=EPS
5FC   VECT(K)=VECT(K)/HL(K,K)
      BIG=C.
      CC 59C I=1,N
      SUP=AMS(REAL(VECT(I)))+ABS(AIMAG(VECT(I)))
59C   IF(SUP.GT.PIG)PIG=SUP
      CC 6CC I=1,N
6CC   VECT(I)=VECT(I)/BIG
      IF(THICE)GC TC 62C
      CC 61C I=1,NP1
      IF(.NCT.INTH(I))GC TC 61C
      TEPP=VECT(I)
      VECT(I)=VECT(I+1)
      VECT(I+1)=TEMP
61C   VECT(I+1)=VECT(I+1)+MULT(I)*VECT(I)
      THICE=.TRUE.
      CC TC 56C
62C   IF(N.EC.2)GC TC 65C
      N2=N-2
      CC 64C I=1,AM2
      N11=A-1-I
      N11=A-I+1
      CC 63C J=N11,A
63C   VECT(J)=+(J,K11)*VECT(K11+1)+VECT(J)
      INCEX=INTH(I)
```

ALMT0232
ALMT0233
ALMT0234
ALMT0235
ALMT0236
ALMT0237
ALMT0238
ALMT0239
ALMT0240
ALMT0241
ALMT0242
ALMT0243
ALMT0244
ALMT0245
ALMT0246
ALMT0247
ALMT0248
ALMT0249
ALMT0250
ALMT0251
ALMT0252
ALMT0253
ALMT0254
ALMT0255
ALMT0256
ALMT0257
ALMT0258
ALMT0259
ALMT0260
ALMT0261
ALMT0262
ALMT0263
ALMT0264

119

```
      TEMP=VECT(N1+1)                                          ALMT0265
      VECT(N1+1)=VECT(INDEX)                                   ALMT0266
  640 VECT(INDEX)=TEMP                                         ALMT0267
  650 CC 663 I=1,N                                             ALMT0268
  660 A(I,L)=VECT(I)                                           ALMT0269
  670 RETURN                                                   ALMT0270
      END                                                      ALMT0271
```

120

```
C     * * * * * * * * * * * *                                            CG90001
C     *    SUBROUTINE CG9    *                                           CG90002
C     * * * * * * * * * * * *                                            CG90003
C                                                                        CG90004
C     SUBROUTINE CG9 EVALUATES THE INTEGRALS BY MEANS OF A 12-POINT     CG90005
C     GAUSS CLADRATURE FORMULA.THE NODES AND COEFFICIENTS ARE TAKEN FROM CG90006
C     KRYLCVINSI.,IEJANC IPF PUBLICATION SYSTEM/360 SCIENTIFIC SUBROUTINE CG90007
C     PACKAGE .SUBROUTINE INTG SUPPLIES THE INTEGRAND FUNCTIONS TO BE    CG90008
C     INTEGRATED                                                         CG90009
C                                                                        CG90010
C     THE SUBROUTINE IS CALLED BY THE STATEMENT.                         CG90011
C                                                                        CG90012
C            CALL CG9(XL,XU,Y)                                           CG90013
C                                                                        CG90014
C     WHERE                                                              CG90015
C     XL=REAL*8,LOWER LIMIT ON THE INTEGRAL                              CG90016
C     XU=REAL*8,UPPER LIMIT ON THE INTEGRAL                              CG90017
C     Y=REAL*8,ARRAY OF INTEGRATED VALUES BETWEEN THE LIMITS XL AND XU   CG90018
      SUBROUTINE CG9(XL,XU,Y)                                           CG90019
      IMPLICIT REAL*8 (A-H,O-Z)                                          CG90020
      DIMENSION Y(61),ZA(61),ZB(61)                                      CG90021
      J1=61                                                              CG90022
      A=.5CC*(XU+XL)                                                     CG90023
      B=XU-XL                                                            CG90024
      C=.4967203171233596EC.C*B                                          CG90025
      CALL INTG(A+C,ZA)                                                  CG90026
      CALL INTG(A-C,ZP)                                                  CG90027
      DC 1CC I=1,J1                                                      CG90028
  1CC Y(I)=-.2354766819375591C-1*(ZA(I)+ZB(I))                          CG90029
      C=.452C5PE281852374CC*B                                           CG90030
      CALL INTG(A+C,ZA)                                                  CG90031
      CALL INTG(A-C,ZP)                                                  CG90032
      DC 11C I=1,J1                                                      CG90033
  11C Y(I)=Y(I)+.534+96+2957659220-1*(ZA(I)+ZB(I))
```

121

```
      C=.38465133705715236CC+A
      CALL INTG(A+C,ZA)
      CALL INTG(A-C,ZB)
      DO 12C I=1,J1
 12C  Y(I)=V(I)+.8CC3516427167310-1*(ZA(I)+ZB(I))
      C=.29365R5771433687CC+B
      CALL INTG(A+C,ZA)
      CALL INTG(A-C,ZB)
      DO 13C I=1,J1
 13O  Y(I)=Y(I)+.1C15R37133615360S+(ZA(I)+ZB(I))
      C=.1R391574545SC901CC+B
      CALL INTG(A+C,ZA)
      CALL INTG(A-C,ZB)
      DO 14C I=1,J1
 14O  Y(I)=Y(I)+.11674626P26S1770C+(ZA(I)+ZB(I))
      C=.62C16.7C425573446D-1+B
      CALL INTG(A+C,ZA)
      CALL INTG(A-C,ZA)
      DO 15C I=1,J1
 15C  Y(I)=B+(V(I)+.17457352290670140S+(ZA(I)+ZB(I)))
      RETURN
      ENC
```

122

```
C      * * * * * * * * * * * * *                                    INTG0001
C      *      SUBROUTINE INTG      *                                INTG0002
C      * * * * * * * * * * * * *                                    INTG0003
C                                                                   INTG0004
C   THIS SUBPROGRAM SUPPLIES THE INTEGRAND FUNCTIONS FOR A GIVEN VALUE INTG0005
C   OF THE ARGUMENT EITHER TO THE MAIN PROGRAM OR TO SUBROUTINE GG)  INTG0006
C                                                                   INTG0007
C   THE CALLING STATEMENT IS .                                      INTG0008
C         CALL INTG(X,Z)                                            INTG0009
C                                                                   INTG0010
C   WHERE                                                           INTG0011
C   X=REAL*. VARIABLE OF INTEGRATION                                INTG0012
C   Z=REAL*8 ARRAY OF INTEGRAND FUNCTIONS FOR GIVEN VALUE OF X      INTG0013
C   UPON RETURN                                                     INTG0014
      SUBROUTINE INTG(X,Z)                                          INTG0015
      IMPLICIT REAL*8 (A-H,O-Z)                                     INTG0016
      DIMENSION Z(61)                                               INTG0017
      DIMENSION CC(8)                                               INTG0018
      COMMON CC(8)                                                  INTG0019
      COMMON B,AK,EPS                                               INTG0020
      COMMON P,LL,THETA,LL1                                         INTG0021
      I=L1                                                          INTG0022
      DO 100 J=1,61                                                 INTG0023
  100 Z(J)=C.CC0                                                    INTG0024
      A1=CCCS(X+THETA)                                              INTG0025
      A2=CSIN(X+THETA)                                              INTG0026
      A3=CCOS(W+X)                                                  INTG0027
      A4=CSIN(W+X)                                                  INTG0028
      AJ=2.CFC-2.CCS+A1+AK+AK+X+X+EPS+EPS                           INTG0029
      AP=AJ++(-1.5CC)                                               INTG0030
      AP=AJ++(-2.5CC)                                               INTG0031
      Z(1)=A1+AP                                                    INTG0032
      Z(2)=A2+AP                                                    INTG0033
      Z(3)=A2+AM
      Z(4)=X+A1+AP
```

123

```
Z(5)=X*A7*AP                              INTG0034
Z(6)=A3*AP                                INTG0035
Z(7)=A4*AP                                INTG0036
Z(8)=A1*A3*AP                             INTG0037
Z(9)=A1*A7(7)                             INTG0038
Z(10)=A2*Z(6)                             INTG0039
Z(11)=A2*Z(7)                             INTG0040
Z(12)=X*7(8)                              INTG0041
Z(13)=X*7(9)                              INTG0042
Z(14)=X*7(10)                             INTG0043
Z(15)=X*7(11)                             INTG0044
Z(16)=AP                                  INTG0045
Z(17)=X*AP                                INTG0046
Z(18)=A1*AP                               INTG0047
Z(19)=A2*AP                               INTG0048
Z(20)=X*7(18)                             INTG0049
Z(21)=X*7(19)                             INTG0050
Z(22)=A1*7(18)                            INTG0051
Z(23)=A2*7(18)                            INTG0052
Z(24)= *7(19)                             INTG0053
Z(25)= *7(22)                             INTG0054
Z(26)=X*7(23)                             INTG0055
Z(27)=X*7(24)                             INTG0056
Z(28)=X*7(20)                             INTG0057
Z(29)=X*7(21)                             INTG0058
Z(30)=A3*7(22)                            INTG0059
Z(31)=A4*7(23)                            INTG0060
Z(32)=A3*7(24)                            INTG0061
Z(33)=A4*7(22)                            INTG0062
Z(34)=A4*7(23)                            INTG0063
Z(35)=A4*7(24)                            INTG0064
Z(36)=X*7(30)                             INTG0065
Z(37)=X*7(31)                             INTG0066
```

124

```
Z(38)=X*Z(32)                                                      INTG0067
Z(39)=X*Z(33)                                                      INTG0068
Z(40)=X*Z(34)                                                      INTG0069
Z(41)=X*Z(35)                                                      INTG0070
Z(42)=A3*Z(28)                                                     INTG0071
Z(43)=A3*Z(29)                                                     INTG0072
Z(44)=A4*Z(28)                                                     INTG0073
Z(45)=A4*Z(29)                                                     INTG0074
Z(46)=A3*AP                                                        INTG0075
Z(47)=A4*AP                                                        INTG0076
Z(48)=A1*Z(46)                                                     INTG0077
Z(49)=A2*Z(46)                                                     INTG0078
Z(50)=A1*Z(47)                                                     INTG0079
Z(51)=A2*Z(47)                                                     INTG0080
Z(52)=X*Z(48)                                                      INTG0081
Z(53)=X*Z(49)                                                      INTG0082
Z(54)=X*Z(50)                                                      INTG0083
Z(55)=X*Z(51)                                                      INTG0084
Z(56)=X*Z(52)                                                      INTG0085
Z(57)=X*Z(53)                                                      INTG0086
Z(58)=X*Z(54)                                                      INTG0087
Z(59)=X*Z(55)                                                      INTG0088
Z(60)=X*Z(46)                                                      INTG0089
Z(61)=X*Z(47)                                                      INTG0090
C     LL1 IS SET EQUAL TO 2 FOR CALCULATION OF SELF INDUCED INTEGRAL .  INTG0091
C     IN THIS SITUATION THE PERTURBATION INTEGRAL BECOMES SINGULAR      INTG0092
C     AND INTEGRALS ARE TO BE MODIFIED FOR NUMERICAL INTEGRATION        INTG0093
      IF(LL1.NE.2)GO TO 110                                            INTG0094
C     L1 IS SET EQUAL TO 2 FOR INTEGRATION LIMIT BEYOND 2*PI AFTER WHICHINTG0095
C     THE SELF INDUCTION INTEGRALS ARE NO MORE MODIFIED                 INTG0096
      IF(I1.EC.2)GO TO 110                                            INTG0097
      A1=(AK*AK+1)*X*X+EPS*EPS                                         INTG0098
      AN=A1**(-1.5C00)                                                INTG0099
```

125

```
AC=A100(-7.5CC)
CC(1)=AK
CC(2)=X*CC(1)
CC(3)=X*CC(2)
CC(4)=AC
CC(5)=X*CC(4)
CC(6)=X*CC(5)
CC(7)=X*CC(6)
CC(8)=X*CC(7)
Z(1)=Z(1)-CC(1)
Z(2)=Z(2)-CC(1)
Z(3)=Z(3)-CC(2)
Z(4)=Z(4)-CC(2)
Z(5)=Z(5)-CC(3)
Z(6)=Z(6)-CC(1)
Z(7)=Z(7)-CC(2)
Z(8)=Z(8)-CC(1)
Z(9)=Z(9)-CC(2)
Z(10)=Z(10)-CC(2)
Z(11)=Z(11)-CC(3)
Z(12)=Z(12)-CC(2)
Z(13)=Z(13)-CC(3)
Z(14)=Z(14)-CC(3)
Z(16)=Z(16)-CC(4)
Z(17)=Z(17)-CC(5)
Z(18)=Z(18)-CC(4)
Z(19)=Z(19)-CC(5)
Z(20)=Z(20)-CC(5)
Z(21)=Z(21)-CC(6)
Z(22)=Z(22)-CC(4)
Z(23)=Z(23)-CC(5)
Z(24)=Z(24)-CC(6)
Z(25)=Z(25)-CC(5)
```

```
INTG0100
INTG0101
INTG0102
INTG0103
INTG0104
INTG0105
INTG0106
INTG0107
INTG0108
INTG0109
INTG0110
INTG0111
INTG0112
INTG0113
INTG0114
INTG0115
INTG0116
INTG0117
INTG0118
INTG0119
INTG0120
INTG0121
INTG0122
INTG0123
INTG0124
INTG0125
INTG0126
INTG0127
INTG0128
INTG0129
INTG0130
INTG0131
INTG0132
```

```
Z(126)=Z(76)-CC(6)        INTG0133
Z(127)=Z(77)-CC(7)        INTG0134
Z(129)=Z(28)-CC(6)        INTG0135
Z(129)=Z(79)-CC(7)        INTG0136
Z(130)=Z(30)-CC(4)        INTG0137
Z(131)=Z(31)-CC(5)        INTG0138
Z(132)=Z(32)-CC(6)        INTG0139
Z(133)=Z(33)-CC(5)        INTG0140
Z(134)=Z(34)-CC(6)        INTG0141
Z(135)=Z(35)-CC(7)        INTG0142
Z(136)=Z(36)-CC(5)        INTG0143
Z(137)=Z(77)-CC(6)        INTG0144
Z(138)=Z(38)-CC(7)        INTG0145
Z(139)=Z(39)-CC(6)        INTG0146
Z(140)=Z(40)-CC(7)        INTG0147
Z(141)=Z(41)-CC(8)        INTG0148
Z(142)=Z(42)-CC(6)        INTG0149
Z(143)=Z(43)-CC(7)        INTG0150
Z(144)=Z(44)-CC(7)        INTG0151
Z(145)=Z(45)-CC(8)        INTG0152
Z(146)=Z(46)-CC(4)        INTG0153
Z(147)=Z(47)-CC(5)        INTG0154
Z(149)=Z(49)-CC(4)        INTG0155
Z(149)=Z(49)-CC(5)        INTG0156
Z(150)=Z(50)-CC(5)        INTG0157
Z(152)=Z(52)-CC(5)        INTG0158
Z(153)=Z(53)-CC(6)        INTG0159
Z(154)=Z(54)-CC(6)        INTG0160
Z(155)=Z(55)-CC(7)        INTG0161
Z(156)=Z(56)-CC(6)        INTG0162
Z(157)=Z(57)-CC(7)        INTG0163
Z(158)=Z(58)-CC(7)        INTG0164
                          INTG0165
```

```
                              Z(59)=Z(59)-CO(8)                    INTG0166
                              Z(60)=Z(60)-CC(5)                    INTG0167
                              Z(61)=Z(61)-CC(6)                    INTG0168
C   M IS READ AS EQUAL TO 2 FOR FAR WAKE STABILITY                 INTG0169
110 IF(M.EQ.2) GO TO 120                                           INTG0170
    RETURN                                                         INTG0171
120 Z(3)=0.0C3                                                     INTG0172
    Z(4)=0.CDC                                                     INTG0173
    Z(7)=0.CC0                                                     INTG0174
    Z(5)=C.CC0.                                                    INTG0175
    Z(1C)=G.CCC                                                    INTG0176
    Z(12)=C.CDC                                                    INTG0177
    Z(15)=C.CD0                                                    INTG0178
    Z(17)=C.CD0                                                    INTG0179
    Z(19)=0.CN0                                                    INTG0180
    Z(2C)=C.CUC                                                    INTGJ181
    Z(23)=C.CC0                                                    INTGJ182
    Z(25)=C.CE0                                                    INTGJ183
    Z(27)=0.CDC                                                    INTG0184
    Z(29)=C.CDC                                                    INTG0185
    Z(31)=C.CCC                                                    INTG0186
    Z(23)=C.CC0                                                    INTG0187
    Z(35)=C.CD8                                                    INTGJ188
    Z(36)=C.CCC                                                    INTG0189
    Z(38)=C.CC0                                                    INTG0190
    Z(4C)=C.C00                                                    INTG0191
    Z(43)=C.CCC                                                    INTGJ192
    Z(44)=0.C00                                                    INTG0193
    Z(47)=0.CCC                                                    INTG0194
    Z(49)=C.CCC                                                    INTG0195
    Z(5C)=C.CC0                                                    INTGJ196
    Z(52)=0.CC0                                                    INTG0197
    Z(55)=C.CC0                                                    INTG0198
```

128

```
INTG0199
INTG0200
INTGC201
INTGC202
INTGC203
```

```
Z(157)=C.CDC
Z(58)=G.CCO
Z(60)=C.CDC
RETURN
EAL
```

```
C     * * * * * * * * * * * * *              CSIMP0001
C     *                       *              CSIMP0002
C     *    FUNCTION CSIMP      *              CSIMP0003
C     *                       *              CSIMP0004
C     * * * * * * * * * * * * *              CSIMP0005
C                                            CSIMP0006
C     FUNCTION SUBPROGRAM CSIMP EVALUATES THE INTEGRAL OF  F(X) OVER AN   CSIMP0007
C     INTERVAL FROM THE POINT A TO THE POINT B USING SIMPSON'S RULE AND   CSIMP0008
C     THE THREE-EIGHTS RULE. THE TOTAL NUMBER OF POINTS OVER THE RANGE    CSIMP0009
C     OF INTEGRATION MAY BE EVEN OR ODD .THE ABSCISSAE OF THE POINTS      CSIMP0010
C     MUST BE EVENLY SPACED                                              CSIMP0011
C                                                                        CSIMP0012
C     THE FUNCTION IS CALLED BY THE FOLLOWING STATEMENT,                 CSIMP0013
C          Z=CSIMP(H,IS,IE,FUNC)                                        CSIMP0014
C     WHERE                                                              CSIMP0015
C                                                                        CSIMP0016
C     H    = REAL*8,VARIABLE OR CONSTANT NAMING THE INTERVAL BETWEEN      CSIMP0017
C            POINTS OF INTEGRATION                                       CSIMP0018
C     IS   = INTEGER*4,CONSTANT OR VARIABLE , SPECIFYING THE SUBSCRIPT OF CSIMP0019
C            THE FIRST VALUE OF THE ARRAY,FUNC.                          CSIMP0020
C     IE   = INTEGER*4, CONSTANT OR VARIABLE,SPECIFYING THE SUBSCRIPT OF  CSIMP0021
C            THE LAST VALUE OF THE ARRAY,FUNC.                           CSIMP0022
C     FUNC = REAL*8, ONE-DIMENSIONAL ARRAY CONTAINING THE VALUES OF THE   CSIMP0023
C            FUNCTION TO BE INTEGRATED, EVALUATED AT INTERVALS OF H OVER  CSIMP0024
C            THE RANGE OF THE DESIRED INTEGRATION.                       CSIMP0025
      FUNCTION CSIMP(H,IS,IE,FUNC)                                       CSIMP0026
      IMPLICIT REAL*8(A-H,O-Z)                                           CSIMP0027
      DIMENSION FUNC(1C1)                                                CSIMP0028
      TOT=C.CCC                                                          CSIMP0029
      IT=IE-IS+1                                                         CSIMP0030
      IF(IT-7)1CC,11C,12C                                               CSIMP0031
C          ONLY ONE POINT --NC INTERVAL                                 CSIMP0032
  1CC CSIMP=C.CCC                                                        CSIMP0033
      RETURN
C          ONE INTERVAL
```

```
11C   CSIPP=(FUNC(IS)+FUNC(IE))*H*.5DC
      RETURN
12C   IF(IT-4)190,14C,15C
C        THC INTERVAL
13C   CSIPP=H/3.CCG*(FUNC(IS)+4.CCC*FUNC(IS+1)+FUNC(IE))
      RETURN
C        CNLY THREE INTERVALS CR LAST THREE INTERVALS
14C   CSIPP=TCT+(3.CCC/8.CDC)*H*(FUNC(IE-3)+3.CCC*FUNC(IE-2)+3.CCC*
     1 FUNC(IE-1)+FUNC(IE))
      RETURN
C        CLC NUMBER CF INTERVALS
15C   IREV=IT-(IT/2)*2
      IF(IREV.GT.C) GO TO 17C
16C   IL=IE-3
      GC TO 18C
C        EVEN NO. CF INTERVALS
17C   IL=IE
18C   TCT=FUNC(IS)+FUNC(IL)
      LA=IS+1
      LB=IL-1
      KA=LA+1
      KP=LP-1
      SUP=C.CCC
      CC 19C I=LA,LB,2
19C   SUP=SUP+FUNC(I)
      TCT=TCT+4.CCC*SUP
      SUP=C.CCC
      CC 2CC I=KA,KB,2
2CC   SUY=SUP+FUNC(I)
      TCT=TCT+2.CCC*SUP
      TCT=TCT+(1.CCC/3.CCC)*H
      IF(IREV.LE.C) GC TO 14C
210   CSIPP=TCT
```

```
CSIMC034
USIMC035
LSIMC036
CSIMC037
CSIM0038
LSIP0039
USIPC040
LSIM0041
LSIP-0042
LSIP-C043
LSIM0044
LSIMCC45
LSIPCC46
USIMC047
USIM0048
LSIM0049
CSIM0050
DSIPC051
LSIMC052
LSIMC053
LSIPC054
USIPC055
LSIM0056
CSIP0057
CSIMC058
USIP0059
LSIP0060
LSIP0061
USIM0062
CSIP0063
LSIMC064
LSIM0065
990C4I5J
```

132